University of Southampton

Faculty of Engineering and Physical Sciences

School of Chemistry

Development of a miniaturised system for the high throughput investigations of biofilm responses to antimicrobial agents.

by

Jelena Pisaruka

Thesis for the degree of Doctor of Philosophy

February 2023

University of Southampton

Abstract

Faculty of Engineering and Physical Sciences

School of Chemistry

Doctor of Philosophy

Development of a miniaturised system for the high throughput investigations of biofilm responses to antimicrobial agents.

by

Jelena Pisaruka

This thesis describes the development of a high throughput device for biofilm studies. The device generates reproducible results and can operate in several modes for different research purposes related to biofilms. The fabrication procedure is quick, easy, and cheap. The final product is robust and easy to operate. The design, production, and assembly of the device are presented, followed by physical validation of the device's performance and ability to grow *E. coli* biofilms. Production of a dynamic system that will aid biofilm studies with parallel readout is critical to enable the acquisition of many data points per unit of time. The performance of current systems is the main barrier to achieving high throughput studies of biofilms with reliable results. Consequently, a new device has been developed that implements 3D printing technologies. This approach has enabled the device's production with a transparent area for non-destructive biofilm observations, consisting of three parallel channels with separate growth compartments for biological repeats. The small size of the device grants extensive control over factors involved in biofilm formation and minimises the consumption of reagents. Uniformity of flow rate via separate parallel channels was achieved and provides even distribution of biofilm within the device and uniform delivery of reagents. The performance of the fabricated device was compared to static and dynamic systems widely used in biofilm research. These studies showed that the new device could be used for complex dynamic studies of biofilms and static experiments. Further validation of the fabricated device and comparing its performance against existing techniques was performed using two sterilising agents. The effect of antimicrobial properties of plant-derived compounds was studied to demonstrate the feasibility of high throughput studies using the fabricated device. The fabricated device is expected to aid biofilm studies and high throughput screening of potential antimicrobial molecules.

Table of Contents

Table of Tables

Table of Figures

Table of Figures

Table of Figures

Table of Figures

Research Thesis: Declaration of Authorship

Print name: Jelena Pisaruka

Title of thesis: Development of a miniaturised system for the high throughput investigations of biofilm responses to antimicrobial agents.

I declare that this thesis and the work presented in it are my own and has been generated by me as the result of my own original research.

I confirm that:

This work was done wholly or mainly while in candidature for a research degree at this University;
Where any part of this thesis has previously been submitted for a degree or any other qualification at this University or any other institution, this has been clearly stated;
Where I have consulted the published work of others, this is always clearly attributed;
Where I have quoted from the work of others, the source is always given. With the exception of such quotations, this thesis is entirely my own work;
I have acknowledged all main sources of help;
Where the thesis is based on work done by myself jointly with others, I have made clear exactly what was done by others and what I have contributed myself;
None of this work has been published before submission

Signature: ..... Date:.....

Acknowledgements

This PhD work would not have been possible without the continuous support and guidance of my supervisors:

- Prof. George Attard
- Prof. Sumeet Mahajan

Their help and valuable comments throughout the course were instrumental in producing the best work possible.

I am also immensely grateful to Dr Marcus Dymond from the University of Brighton for sharing his knowledge on 3D printing.

I am deeply grateful to Dr Stephanie Tweed and Andrew Brown from Aspire Pharma Ltd for their input and support throughout this project.

I want to thank my second supervisor Prof. Jeremy Webb and his group for assisting me with microbiology matters.

Finally, I want to acknowledge the appreciation of my family for their unyielding love and care throughout the project.

Definitions and Abbreviations

ABS ..... Acrylonitrile Butadiene Styrene

CHX ..... Chlorhexidine

CLSM ..... Confocal Laser Spanning Microscopy

CTC ..... 5-cyano-2,3-ditolyltetrazolium chloride

CRM ..... Confocal RAMAN Microscopy

CV ..... Crystal Violet

DAPI ..... 4',6-diamidino-2-phenylindole

FDS ..... Fluorescein-Diacetate

FIB SEM ..... Focused Ion Beam Scanning Electron Microscopy

FISH ..... Fluorescence *in situ* Hybridization

HTS ..... High Throughput Screening

Inner lumen ..... Inner part of the cylinder

LB ..... Luria-Bertani Medium

MGV ..... Mean Grey Value

PEEK ..... Polyether Ether Ketone

PI ..... Propidium Iodide

PLA ..... Polylactic Acid

TB ..... Trypan blue

Chapter 1 INTRODUCTION

Most bacteria form biofilms during their lifecycle. These biofilms can be single-species systems or, more commonly, multispecies communities of bacteria, archaea, and fungi. A biofilm is a sessile aggregation of microbial cells attached to the surface and each other, embedded in a self-produced extracellular polymeric substance (EPS). Bacterial cells within biofilm display an altered phenotype with respect to growth rate and gene transcription (1), (2). Most of the information about bacteria has been learned from planktonic experiments. Studying biofilms provides more representative results of the lifecycle of bacteria, while bacteria in planktonic form exist for a short amount of time and are part of a biofilm cycle. Studying biofilms is critical due to the changes in phenotype, metabolism, and gene expression when bacterial cells are within the biofilm compared to planktonic bacteria of the same strain. Several approaches exist to growing and studying biofilms in a laboratory environment, which are essential to understanding the mechanisms behind biofilms. EPS production and molecular signalling within biofilms introduce complexity when studying bacterial communities. These processes are involved in antibiotic resistance of biofilms, and EPS provides a protection and survival mechanism to persister cells within biofilms.

This thesis details the development of a high throughput device to study biofilms. The thesis focuses on developing a robust device that is cheap, quick to fabricate, and easy to use for different studies of biofilms. The device incorporates a fully transparent area for non-destructive observations of biofilms. Besides the transparency, that area consists of parallel running channels which enables multiple biological repeats. The device allows the setting up of multiple ways of growing and maintaining biofilms and is easy to operate and control due to its small size.

This chapter covers the basics behind biofilms and their formation and current assays for biofilm development and analysis in a laboratory environment.

1.1 STRUCTURE OF A BIOFILM

The biofilm formation cycle consists of three stages: attachment of cells to the surface, growth and development of biofilm, and detachment of cells to inhabit other surfaces (3). Attachment can be subdivided into two stages: initial reversible attachment and irreversible attachment. Free-floating planktonic cells deposit on the surface during the reversible attachment but can detach. Cells move with the help of a flagellum and pili (4). The deposition of bacterial cells to the substratum surface is mediated by sedimentation, Brownian motion, and hydrodynamic forces.

Cell-surface interactions are vital to the adhesion to the substratum (5). The adhesion between bacterial cells and substratum is governed by the physicochemical properties of bacterial cells, surface properties, e.g. roughness, and environmental conditions (6), (7). Irreversible attachment occurs when bacteria settle upon the surface and begins to multiply and form microcolonies. Cell-to-cell interactions via quorum sensing begin at this point to coordinate biofilm formation. Quorum sensing is a molecular signalling system that responds to population cell density (8). Bacterial cells begin to secrete a slimy extracellular matrix (EPS) of proteins, polysaccharides and nucleic acids that hold cells together and promote cell attachment to the surface at this stage (9).

Production of EPS increases during the development of the biofilm lifecycle. The composition of EPS varies between different bacterial cells and the same bacterial strain under different environmental conditions. However, in all biofilms, it is involved in the attachment of cells and development. Moreover, it provides protection from mechanical damage, shear caused by fluid flow, and antibiotics. On average, the EPS matrix contributes 85% by volume in biofilm, and the rest, 15% by volume, are bacterial cells (2). EPS matrix plays a significant role in biofilm development and survival by acting as a barrier for antimicrobial agents and reducing their diffusion into the biofilm. Moreover, EPS acts as a defensive barrier to protect bacteria cells from mechanical damage and stress and is a perfect environment for chemical reactions and nutrient entrapment (10). At the same time, it provides difficulties in studying biofilms due to their composition and ability to interact with antimicrobial reagents. Cells multiply and communicate via quorum sensing during biofilm growth as population density increases. Cells produce autoinducer molecules (e.g., N-acyl homoserine lactone (AHL)) and release them into their surroundings. As threshold concentrations are reached, these molecules bind to the signal receptor proteins on bacterial cells and activate gene expression involved in group behaviour (11). With the help of quorum sensing and EPS production, bacteria cells organise themselves into 3-dimensional biofilms of different shapes. During the development stage, small nutrient, waste, and water transport channels are formed within biofilm aggregates to support biofilm. Moreover, due to the 3D structure of a biofilm, oxygen and nutrient depletion occurs as biofilm depth increases (12). Cells at the top of the biofilm continue to utilise oxygen and nutrients, while cells deeper in the biofilm switch to anaerobic metabolism and reduce their metabolic rate to survive, and some enter the dormant form.

The final part of the biofilm lifecycle is the detachment of cells to invade other surfaces. Over time, nutrient and oxygen depletion initiates the detachment of biofilm parts. Cells from the upper layer of biofilm may detach and move in the system to attach to different areas and develop another biofilm. Under harsh conditions, clusters of cells held by EPS detach and get carried away. It is still a biofilm and possesses the same characteristics as the initial biofilm. It can

float in the system or may attach to the surface to continue into a development stage. The final mechanism of dispersal is surface dispersal, a representation of biofilm movement on the surface. The biofilm can move on the surface via shear-mediated transport (3).

1.2 EXAMPLES OF BIOFILMS IN THE ENVIRONMENT

Biofilms are both beneficial and harmful to the environment and humans. Bioremediation and wastewater treatment are examples where bacterial biofilms are helpful for the environment (13). From a medical point of view, biofilm formation creates many problems and is involved in chronic infections. Biofilms are found in chronic wounds of patients with diabetes, and they actively grow on metallic implants, valves, and urinary catheters. Biofilms form dental plaque, grow on contact lenses, cover the lungs of patients with cystic fibrosis and are responsible for skin infections, such as acne and atopic dermatitis (2) Table 1.1.

Table 1.1 Summary of advantages of biofilms to the environment and host and problems caused by biofilm formation.

Advantages	Problems
Bioremediation – treatment of contaminated media (13).	Colonization of medical devices: valves, implants, urinary catheters, contact lenses (2).
	Health: Cystic fibrosis (14), Otitis media (15), Chronic bacterial prostatitis (16), Periodontitis (17), and Skin infections (18).
Wastewater treatment to remove organic waste (19).	Diabetes – formation of biofilms on the wounds that leads to amputation (20).
	Biofouling, metal corrosion: ships, water pipes (21).

Biofilm acts as a protection for bacteria cells and supports their lifecycle, therefore is beneficial to cells within the biofilm. On the other hand, biofilm creates a system where some cells may benefit over other cells. Biofilm has advantages to the cells within the biofilm and some disadvantages summarized in Table 1.2.

Table 1.2 Summary of advantages to the cells within biofilm and limitations of biofilm.

Advantages	Limitations
Antibiotic resistance due to: Slower diffusion through the EPS, genetic modification; altered growth rate; different cells within the biofilm (2).	"Cheater cells" – cells that save energy and do not perform like other cells within the biofilm (22). If their amount is high – the biofilm becomes weaker, but it is beneficial for "cheater cells" to be within the biofilm because other cells take on their responsibilities (23).
Persister cells – are dormant cells that survive under harsh conditions (24).	
EPS in biofilm provides structure and stability (25).	Toxic effect due to insufficient waste removal in open systems/ no removal in closed systems (26).
The monoculture within the multicultural biofilm (27). The spatial arrangement of different species within the biofilm **(**28).	

It is essential to understand the structure and functioning of biofilms to treat medical conditions and infections and eliminate biofilms from surfaces. A better understanding of biofilms with the development of new approaches to target biofilms will help to treat these conditions or prevent their formation.

1.3 BIOFILM MODELS - TECHNIQUES TO GROW BIOFILMS

Growing biofilms in a laboratory outside their normal biological environment is a challenging process, not only because it requires careful monitoring of all growth parameters of biofilm and environmental changes but also due to the unique inefficiencies of all individual methods. Biofilm properties depend on how the system is formed. Therefore, being able to control seed density, time for the attachment of cells to the surface, nutrient composition of media, and ability to control flow rate with time and temperature is critical for biofilm formation to mimic naturally occurring biofilms. Several methods are available to monitor biofilm progression, but their applications are limited by low sensitivity, high labour intensity, intrusive sampling, and long-time lags from sampling to result. The reproducibility of biofilms is an issue, especially in a dynamic system, and current methods do not allow for the statistical analysis of data.

Biofilms can be studied either as a static aggregate – closed model or as a continuous developing system – open or dynamic system. Natural biofilms are dynamic in their nature; therefore, more representative results of naturally occurring biofilms are obtained when open systems are used for *in vitro* growth. Nevertheless, static techniques are very commonly used because their setup and analysis are less complex than open systems. Static systems also allow investigation of the

effect of different experimental conditions, such as temperature and nutrient content, in high throughput experiments.

The most frequently used static assay is a microtiter plate-based assay. Like most static methods, it is used to monitor the initial attachment of bacterial cells and biofilm growth in the early stages of biofilm development (29). It allows for high throughput studies that are important during initial biofilm investigation and antimicrobial screening. Different bacterial species and strains can be studied simultaneously under different conditions. In this method, there is no flow of fresh media and no waste removal in/out of the reactor; hence experimental conditions change over time. This method is cost-effective, requires a small volume of reagents, and allows high throughput studies.

Colony biofilm assay is another method to grow static biofilm. It is performed on the agar plate, and biofilm formation occurs on a semipermeable membrane. Formation on a membrane allows for nutrient replenishment by moving colonies into a new agar plate (30).

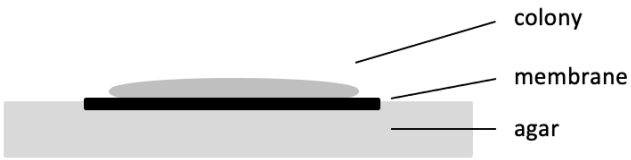

Figure 1.1 Side view of a colony biofilm assay. Colony biofilm is growing on a semipermeable membrane on top of an agar plate in a petri dish.

Kadouri biofilm assay is a static assay that allows for continuous nutrient supply without any manipulations to biofilm. Biofilm grows in the well covered with a lid, with two tubes going through the lid into the well. One tube is used to supply nutrients; the second tube is used to remove waste products from the well.

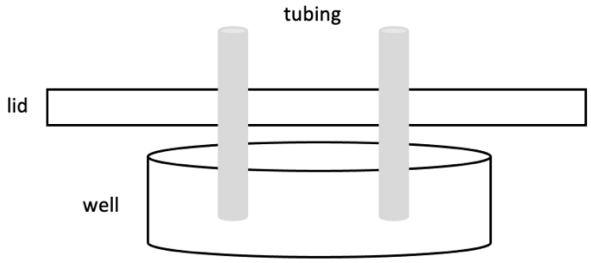

Figure 1.2 Kadouri biofilm assay. One tubing is used to supply fresh nutrients to the well, second one – to remove waste

Calgary biofilm device is commercially available as an MBEC Assay system, MBEC Bioproducts Inc., Edmonton, Alberta, Canada. It consists of two parts: the bottom part is a 96-well plate with

channels for nutrient flow, and the top part is a lid with pegs. The top and bottom parts are sealed during biofilm growth, and biofilm grows on pegs. When biofilm growth is complete, pegs are removed from the device for analysis.

Several dynamic models exist. The simplest model is a silicone tubing in which biofilm is formed, and then a tube is cut into pieces for analysis (3). The flow displacement biofilm model is widely used to grow and study biofilms. In all dynamic models, there is a constant supply of nutrients and the removal of waste byproducts from a system.

The flow cell is a prevalent method for biofilm studies. The cell can have a single channel or several channels running in parallel. Due to the constant flow of the medium through the cell, planktonic cells are washed off to the waste, and only sessile communities are studied. Nutrient flow and other environmental parameters, like temperature and nutrient concentration, can be regulated. Flow cells are usually made of transparent material, like glass or silicone, which allows for real-time observations under the microscope. Flow cells can be fabricated directly in a lab, but only some commercial flow cells are available. Flow cells are usually used to investigate the effect of antimicrobial compounds on single or multi-species biofilm on different surfaces, as well as biofilm structure and growth. In recent years, microfabrication has become very popular for device production for biofilm growth. Very few commercial microfluidic devices exist for biofilm growth, for example, BioFlux by Fluxion Systems (South San Francisco, CA).

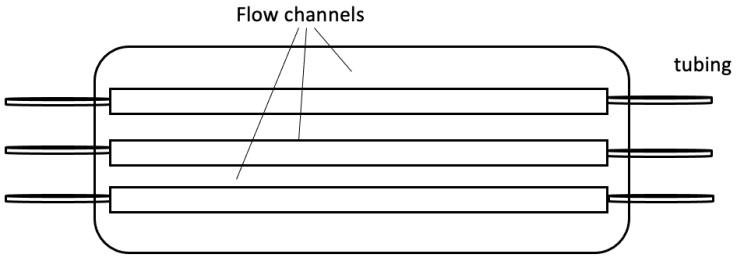

Figure 1.3 Schematic of a flow cell with three channels.

A drip-flow reactor is another apparatus for biofilm formation. It employs the same setup as a flow cell but is much larger. Biofilm is grown on coupons – microscope slides – and media is dripped from the top of a chamber down the slide under 30° angle. Coupons are removed from the reactor after biofilm is formed and are investigated under a microscope. Standard coupons are made of glass, but different materials can be used. Commercial reactors exist. For example, BioSurface Technologies Corporation, USA, produces 4- and 6-channel biofilm reactors. It is also possible to purchase microscope flow cells and coupons made of different materials to investigate adsorption to different surfaces.

Figure 1.4 Image of a drip-flow reactor with four channels on a stand.

1.4 LIMITATIONS OF TECHNIQUES TO GROW BIOFILMS

The microtiter-plate assay is widely used for biofilm studies, but the main problem of this system is the depletion of nutrients and the build-up of waste over time. This leads to accelerated cell death; therefore, this method can only be used for short-term studies, with biofilms up to 48h growth time. Another limitation of this method is the inability to observe biofilm directly. Most assays that use this growth method require the removal of biofilm to form a suspension of cells for analysis.

Colony biofilm assay allows nutrient replenishment by moving the biofilm into a new plate. Biofilm can get mechanically damaged during this movement. Another static approach incorporating nutrient supply and waste removal is the Kadouri biofilm assay. The main limitation of this approach is the requirement to calibrate the influx/efflux rate to support a biofilm. All static models require the movement of formed biofilm for analysis, which is the major disadvantage of static assays. They do not allow for non-destructive observations of biofilm in real time.

Dynamic systems for biofilm formation have a constant supply of nutrients that supports biofilm during growth and the removal of waste material to prevent toxic effects. Biofilm formation in silicone tubing is the simplest example of a dynamic system. However, cutting the tubing to get to the biofilm damages the biofilm and is the principal disadvantage of this method.

Flow cells are widely used for biofilm studies but have several severe limitations. The major problem with flow cells is their manufacture. Sealing a silicone flow cell component is challenging and often results in leakage. With an increased number of channels within the system, the fabrication process becomes more challenging; hence only a few examples of flow cells allow for statistical repeats. The method is not robust, and the formation of air bubbles within the system affects the results (31). Variation in the production of flow cells between labs is an issue and

results in a significant variety of data. Another problem arises when channels within the flow cells are microfabricated, and laminar flow predominates in a system. Laminar flow creates low shear. Turbulent flow and high shear are preferable and promote bacterial adhesion to the surface and biofilm formation (2). This only allows for good mixing within the system if unique mixing systems are incorporated.

The biofilm formation in a drip-flow rector is unpredictable and follows different paths in each experiment due to the media dripping from the top of the reactor channel. Hence biofilm formation by this method is not reproducible, resulting in heterogeneity of biofilm development. Another limitation of this system is a very complex, time-consuming setup and large reactor size; hence large volumes of media are used. The reactor consists of 4 to 6 channels only, which does not allow for high throughput studies using this method (32). Moreover, no real-time observations of biofilms are possible using this method.

Commercially available devices for dynamic biofilm formation are expensive; therefore, many devices to study biofilms are produced within individual labs, which creates great variance in results.

1.5 CURRENT METHODS FOR VISUALISING BIOFILMS

Natural biofilm is a complex, usually multispecies community that is extremely hard to study. When studying biofilms, researchers are usually interested in determining the total biomass of biofilm and cellular composition, the overall shape of a community, the distribution of bacterial species within the biofilm, and cell number density. After the treatment of the biofilm with antimicrobial compounds, it is essential to determine the proportion of live/dead cells within the biofilm. Other research involves studying quorum sensing, metabolic activity, and biofilm matrix composition. Usually, dye or fluorescent staining is used to study metabolic activity and biofilm biomass, microscopy is used for direct measurements, and cell viability is also studied using staining methods. Some techniques are presented in Table 1.3.

Table 1.3 Summary of assays and techniques to visualise biofilms and a brief description of each.

Assay / Techniques	Brief Description
Crystal Violet	Method for quantification of biofilm mass. Not very reproducible due to variation between biofilms even when grown under the same experimental conditions. Do not differentiate between live and dead cells or polysaccharides found in EPS of biofilm; hence do not provide any information apart from quantification of the total biofilm mass (33).
FDA Test	Fluorescein-diacetate (FDA) is taken up by living cells within biofilm metabolized to fluorescein and fluoresced yellow (34). Detection of live cells only. Not suitable for the thick biofilm because FDA cannot diffuse through EPS, and only cells closer to the outer biofilm layer will fluoresce.
LIVE/DEAD BacLight™ viability staining	SYTO9 – a green dye that crosses the membrane of all cells. Propidium Iodide (PI) – is a more prominent compound that can only go through the damaged cell membrane and stains them red by expelling SYTO9 (35). Compatible with a fluorescence microscope or flow cytometry. Live/Dead cells observation and quantification. Requires careful calibration.
DAPI (4',6-diamidino-2-phenylindole)	DAPI crosses the membrane of live and dead cells and stains them blue (36).
CTC (5-cyano-2,3-ditolyltetrazolium chloride)	CTC is used to count actively respiring cells by staining them red (37).
Resazurin assay (7-hydroxy-3H-phenoxazin-3-one-10-oxide)	Metabolic assay, nondestructive. Blue dye is metabolized by the cells into pink-fluorescent dye (38). Quantification of live cells, but different bacteria species have different metabolic rates, hard to standardize.

Assay / Techniques	Brief Description
BioTimer assay (BTA)	Reagent – phenol red, when metabolized by biofilm, switches to yellow. The time required for the switch is correlated to the number of bacteria cells present (39). Required calibration and complex evaluation of multispecies specimens. Counting of living cells.
Fluorescence *in situ* hybridization (FISH).	The most common method of studying multispecies biofilms. Observation of very small amounts of targeted bacteria in a complex biofilm. Uses artificially produced oligonucleotides with a fluorescent tag that hybridises with 16s rRNA and produces a visible signal (40). Very complex technique due to the production of specific oligonucleotides and specific targeting.
Focused ion beam scanning electron microscopy (FIB SEM)	Suitable for biological samples. Observation of biofilm in 3D via removal of a layer that has been already captured (41).
Cryo-SEM	Fast application of low temperature to the biofilm (-210°C) to preserve the natural structure (42).
Confocal Laser Scanning Microscopy (CLSM)	The most common microscopy technique used to study biofilms. Optical microscope fitted with a laser beam. Used in combination with fluorescent dye for staining. Only a few colour dyes can be used simultaneously, which is a drawback when studying polyculture biofilm. Nondestructive, 3D study of the biofilm in its natural form (43).
Confocal RAMAN Microscopy (CRM)	The advantage of CRM over CLSM is that the combination with RAMAN allows for chemical composition identification together with the structure of the biofilm (44).

1.6 REQUIREMENTS FOR HIGH THROUGHPUT SCREENING IN BIOFILM STUDIES

High throughput screening (HTS) is a method used in drug discovery that allows the testing of a large number of compounds simultaneously and usually in an automated manner. This approach mainly aims to identify compounds that affect the target in the desired way (45).

In biofilm studies, the requirement for HTS is high. It is required to grow reproducible biofilms to have the ability to investigate biofilm lifecycle and to identify the active ingredients that can interact with biofilm in a number of different ways. For example, to destroy biofilms or reduce biofilm formation, prevent quorum sensing or interact with EPS and kill bacteria cells within biofilms. The greater the diversity of compounds and the range of their concentrations that can be run, the more successful the screen will be. HTS would speed up dose-response studies of antimicrobial compounds. The device with an incorporated number of statistical repeats for biofilm studies has an excellent opportunity to be used as high throughput screening and is of interest to this work.

1.7 RATIONALE FOR THE NECESSITY FOR A DEVICE WHEN STUDYING BIOFILMS

In order to produce biofilms *in vitro* that mimics naturally occurring biofilms several parameters have to be considered. The major requirement is the ability to support identical conditions during biofilm formation. This includes temperature control of the system, initial count of bacteria cells during attachment, ability to control flow rates through the system and nutrient composition and concentration. It also requires removing waste by-products from the system to support the lifecycle of the biofilm. Biofilm shape and structure are unpredictable and differ from one experiment to another, but with control of these parameters, controlled structures and behaviours of biofilms can be formed. In addition, controlling all these factors allows for studying biofilms with different requirements during growth.

The effect of antimicrobial agents on biofilm is another focus of biofilm research. Different stages of the biofilm lifecycle need to be studied. This requires unobstructed visual access to biofilm in real time.

To make experiments efficient, data should be collected in as little time as possible. This requires a method which allows a large volume of data to be generated quickly. Statistical repeats that can be generated simultaneously also speed up data generation.

All these biofilm growth requirements and manipulations must be incorporated into the new device. The device must allow high throughput studies with statistical repeats to speed up data generation. It has to be easy to operate and allow changes in the system's flow rate and temperature control. This is more easily achieved if the size of the device is small. The small device also uses a low volume of reagents for biofilm studies. All commercially available devices are of a high price; therefore, another requirement for the new device is its low cost of production and cost efficiency during usage. To obtain non-destructive observations of the biofilm, which is not possible with some of the existing methods, it is required for the device to be transparent to observe biofilm under microscopy without any disruptions to the biofilm. Transparency of the device will also result in the ability to observe a real-time change to the biofilm. Finally, a device that is easy to operate in different models of biofilm growth will further improve biofilm studies.

1.8 OUTLINE OF THE THESIS

The aim of the work described in this thesis is to design, fabricate and validate a high throughput device for biofilm studies against existing methods for biofilm formation. The first part of the thesis focuses on the design and fabrication of the device, followed by optimisation and validation of device performance. The second part of the thesis compares the performance of the device to existing static and dynamic systems for biofilm studies with two disinfection compounds and subsequent studies of plant-derived compounds for dose-response studies.

Chapter 2: Design and fabrication of the device.

This chapter outlines device design and fabrication stages to fulfil the requirements for biofilm studies. It presents the fabrication procedure of the device using the 3D printing method and assembly of the working device.

Chapter 3: Optimisation of growth conditions of biofilm by three different methods.

This chapter covers the optimisation of nutrient media concentration for biofilm formation in microtiter plate assay and the optimisation of biofilm growth period by static microtiter plate assay in a drip-flow reactor and in a fabricated device to produce comparable biofilms.

Chapter 4: Validation of fabricated device performance.

This chapter presents validation of flow through the separate channels within the device, and biofilm formation within each channel is demonstrated. The operational parameters of the fabricated device are specified at the end of this chapter.

Chapter 5: Validation of fabricated device against existing methods by dose-response studies of sterilising agents.

This chapter includes dose-response studies of ethanol and chlorhexidine on formed biofilm and a comparison of results obtained by three different methods to validate fabricated device performance.

Chapter 6: Validation of fabricated device against existing methods by dose-response studies of plant-derived compounds for high throughout studies.

In this chapter, the effect of plant-derived compounds on biofilm is reported and compared between the three methods of biofilm formation.

Chapter 2 METHODS

2.1 Bacterial strain and media

Class 1 *E. coli* WA321 stain from dsmz.de was used and was cultured in LB Broth (Lennox) from Sigma Aldrich. LB Broth preparation procedure: suspend 20g of powder in 1L of distilled water and autoclave for 15 minutes at 121°C. Distilled 18.2 MΩ water was used throughout the media preparation.

2.2 Bacterial cell counting

Aliquots (20µl) of cell overnight inoculum were mixed with 20µl of 0.2% trypan blue (ThermoFisher Scientific) (diluted with PBS (ThermoFisher Scientific)). Automated counting was performed using a Cellometer^{R} Vision Duo (Nexcelom) machine. Samples of 20µl were pipetted into Cellometer^{R} vision slides SD100 (Nexcelom). The sample was left to settle for 10 minutes prior to cell counting in brightfield mode to get the total number of cells in the sample. After the cell counting, samples of overnight inoculum were diluted to 4 x 10^6 cells/ml prior to addition to assays.

2.3 Biofilm formation

2.3.1 Overnight inoculum.

Frozen bacteria cells stock (-80°C) was added to 10ml of LB Broth with an inoculation loop to a sterile plastic test tube. The cap was left loosened, and the test tube was left in a shaking incubator at 37° C for 18h. After 18 hours of growth, the number of cells was counted using Cellometer and diluted to 4 x10^6 cells/ml before biofilm formation.

2.3.2 Static biofilm in 24-microtitel plate.

Static biofilms of *E. coli* were grown in Costar 24-well plates with sterile glass coupons within each well. Each glass coupon was autoclaved and aseptically inserted into each well. The overnight inoculum was diluted to 4 x 10^6 cells/ml (Cellometer). 800µl of 0.8 LB + 100µl of diluted inoculum was added to each well and left in a shaking incubator at 37°C for 24h.

2.3.3 Drip-flow reactor

BioSurface drip flow reactor with four chambers from BioSurface Technologies Corporation was used. The reactor with glass coupons inside and all required tubing was sterilised before each experiment. 15ml of 0.8 LB Broth was added into each chamber, followed by the diluted to 4 x 10^6 cells/ml overnight inoculum. The device was left in a shaking incubator for 14h at 37°C for the initial attachment of cells. After the initial attachment phase, the reactor was connected to the HPLC pump with a flow rate of 0.2ml/min for biofilm growth. The nutrient media was heated to 42°C using a hot plate and by the time media reached the chambers of a drip-flow reactor, the temperature of it dropped to 37°C.

2.3.4 Fabricated Device

Device channels were sterilised in both orientations using 70% ethanol for 15 min at a flow rate of 1ml/min. After sterilisation, the device was washed with DI water, followed by a 0.8 LB Broth for 15 min at 1ml/min. Tubing was autoclaved prior to each experiment. The inoculum was diluted to 4 x 10^6 cells/mil with LB broth, and 0.3 ml was added to the device. The device was incubated in a shaking incubator for 14 hours at 37°C to allow bacterial attraction. Sterile tubing was connected to the syringe pump and device before the flow rate was 25μl/min. The device was placed on a hot plate, maintaining a temperature of 37°C during the experiment time.

2.4 Antimicrobial agents' solutions preparation

Absolute ethanol and 2% chlorhexidine solutions from Sigma-Aldrich were diluted with distilled water to achieve the required concentrations. Tannic acid, gallic acid, berberine chloride, esculetin and (+)-usnic acid purchased from Sigma-Aldrich were weighted and dissolved in distilled water for required concentrations. Ellagic acid (Sigma-Aldrich) was dissolved in DMSO (≥99) (Sigma-Aldrich).

2.5 Antimicrobial agents testing protocol

2.5.1 Static-24-microtiter method

Liquid from each well was removed after biofilm formation was completed. 1 ml of a solution containing different concentrations of antimicrobial agents was added to wells and left for 5 min to react with biofilm. After the exposure time, the liquid from each well was removed.

2.5.2 Drip-flow reactor

After biofilm formation, the reactor was placed flat. 10 ml of a solution containing different concentrations of antimicrobial agents was added to each channel and left for 10 min to react.

2.5.3 Fabricated device

The flow of nutrients was stopped after biofilm formation. The syringe containing solution with an antimicrobial agent (6 ml) was connected to the device and the flow resumed at the flow rate of 25µl/min. Solutions were pumped for 15 min to fill the tubing and all channel length of the device.

2.6 Staining procedures

2.6.1 Static 24-microtiter method

Each glass coupon with biofilm was removed from the well and placed in another empty well. The empty well was filled with 0.4% trypan blue (ThermoFisher Scientific) or 1% aqueous crystal violet solution (Sigma-Aldrich). 1ml of staining agent was used to fill each well to cover the biofilm on a coupon. Coupons were left for 3min. After this time, excess trypan blue or crystal violet was carefully washed off by pipetting with DI water. Samples were left to dry standing to prevent damage/biofilm removal from the glass coupon.

2.6.2 Drip-flow reactor

Each glass coupon was removed from the reactor and placed in a solution of 0.4% trypan blue or 1% aqueous crystal violet for 3 min. Samples were carefully washed with DI water by pipetting to remove the access of the staining agent. Samples were left to dry with biofilm facing up to prevent them from being damaged.

2.6.3 Fabricated device

The device was disconnected from the flow and was carefully filled with 0.4% trypan blue or 1% aqueous crystal violet solution until all channels were filled and no air bubbles were present. The device was left standing for 3 min. The device was carefully washed with DI water to remove the access of dye and left dry overnight to eliminate all the water drops inside the channels.

2.7 Biofilm observation under light microscopy

The AmScope MD500 Digital eyepiece microscope camera was used to capture the biofilms.

2.7.1 Static biofilm

Each glass coupon with stained biofilm was placed on a microscope slide and was observed using a light microscope. Six images of biofilm were captured for the analysis on each side of the coupon, 12 images in total per glass coupon. Each image was saved in TIFF format.

2.7.2 Drip-flow reactor

Each glass coupon (microscope slide) with stained biofilm was placed under a light microscope. Twenty images of biofilm on each coupon were taken. The areas on the slide were selected randomly but had to include biofilm.

2.7.3 Fabricated device

In total, 40 images per channel were taken because the camera captures a $1mm^2$ area. As the channel's length is 22mm and width is 2mm, 40 images were needed to cover the entire channel, omitting 1mm on each side. Only the bottom surface of the channels was captured.

2.8 ImageJ analysis

All images were analysed using ImageJ software. Each colour image in TIFF format was converted to an 8-bit type. Using the threshold function, each image's total area of biofilm was selected and measured as %Area. The %Area of five-pixel groups (0-51, 52-102, 103-153, 154-204, 205-255) within biofilms was measured. The data was exported into an excel.

Chapter 3 DESIGN AND FABRICATION OF A DEVICE FOR CONTINUOUS BIOFILM GROWTH

The aim of the work was to design, fabricate and validate a device suitable for high throughput studies of biofilms and capable of yielding reliable and reproducible data. The performance requirements for the device are non-destructive observations of biofilm, quantitative read-out of biofilm loading, and leakage-free construction for continuous liquid flow with uniform flow rates. In addition, requirements for the device are minimum sample volumes and the opportunity to vary set-up conditions for biofilm formation and subsequent treatment. Minimising volumes indicates the use of mini channels in which nutrients and other compounds can flow with different flow rates. It also provides more robust control of the physical microenvironment. In addition to the previous points, the goal was to create a device with several parallel running channels within the device - Figure 3.1. Several channels allow biofilm formation side by side for control-treatment experiments. Separate channels provide an independent sampling opportunity for each device. This enhances the speed of experiments. In addition, replications are required to verify consistency of results and to determine the experimental error. To achieve this, the initial concept of a device had three channels.

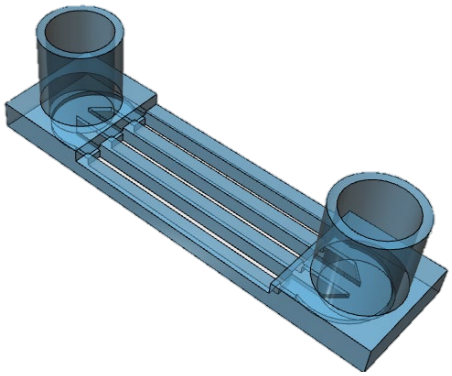

Figure 3.1 The initial concept of the device. Device length – 26mm and width – 7mm. Each channel length – is 14mm, width – is 1mm and depth – is 2mm.

To achieve results that can be compared across independent experiments, it is required to have a uniform flow through the channels within one device and between the devices that are produced. To accomplish this goal, it is required to develop a device design with one liquid inlet that subsequently separates into three channels and runs in an identical flow. In addition, it is essential to observe the entire length of channels under the microscope. Hence it is crucial to develop a device with a fully transparent channel area which is leakage free. The device should be as small as the production method allows in order to reduce the amount of growth media used during

biofilm formation, the quantity of active ingredients used for biofilm studies, and reduce the carbon footprint of the experiments.

Only a few commercially available flow cells are available. Some are produced by microfabrication, and some by placing a glass coupon between other material parts. Devices made by these two methods are more frequently produced within individual laboratories; therefore, there is no consistency in their design and performance between laboratories. All existing devices are flawed; all have disadvantages but help study biofilms. The problem with device fabrication is sealing device compartments; it is always challenging to produce devices for biofilm studies. Another method of fabrication widely used in many areas but not for biofilm studies is 3D printing. It is a rapid, inexpensive, low labour-demanding technique and was used in this project for device fabrication.

Biofilm growth outside its natural environment needs to be carefully controlled. Minor variations in guidelines affect biofilm development in a laboratory environment; therefore, it is essential to have a device that is easy to use. Continuous nutrient supply and waste removal must be incorporated into the device to support the life cycle of a biofilm when operating in dynamic experiments. In addition, the device must be robust, quick and easily fabricated.

It is vital to grow and study continuous biofilms because those studies represent real-world situations more than static biofilms studies. The device designed and produced during this project allows for the growth of continuous biofilm with subsequent opportunities for different studies of biofilm within the device.

This chapter describes the following:

- Design process of the device from the initial concept to the final version.
- 3D printing of designed device.
- Production of a method to assemble a working device which is leakage free and has a transparent channels area.

3.1 DESIGN OF A DEVICE

Autodesk 123D software was used throughout this project to visually conceptualise all steps in designing the device. The flow diagram of device development is presented in Figure 3.2.

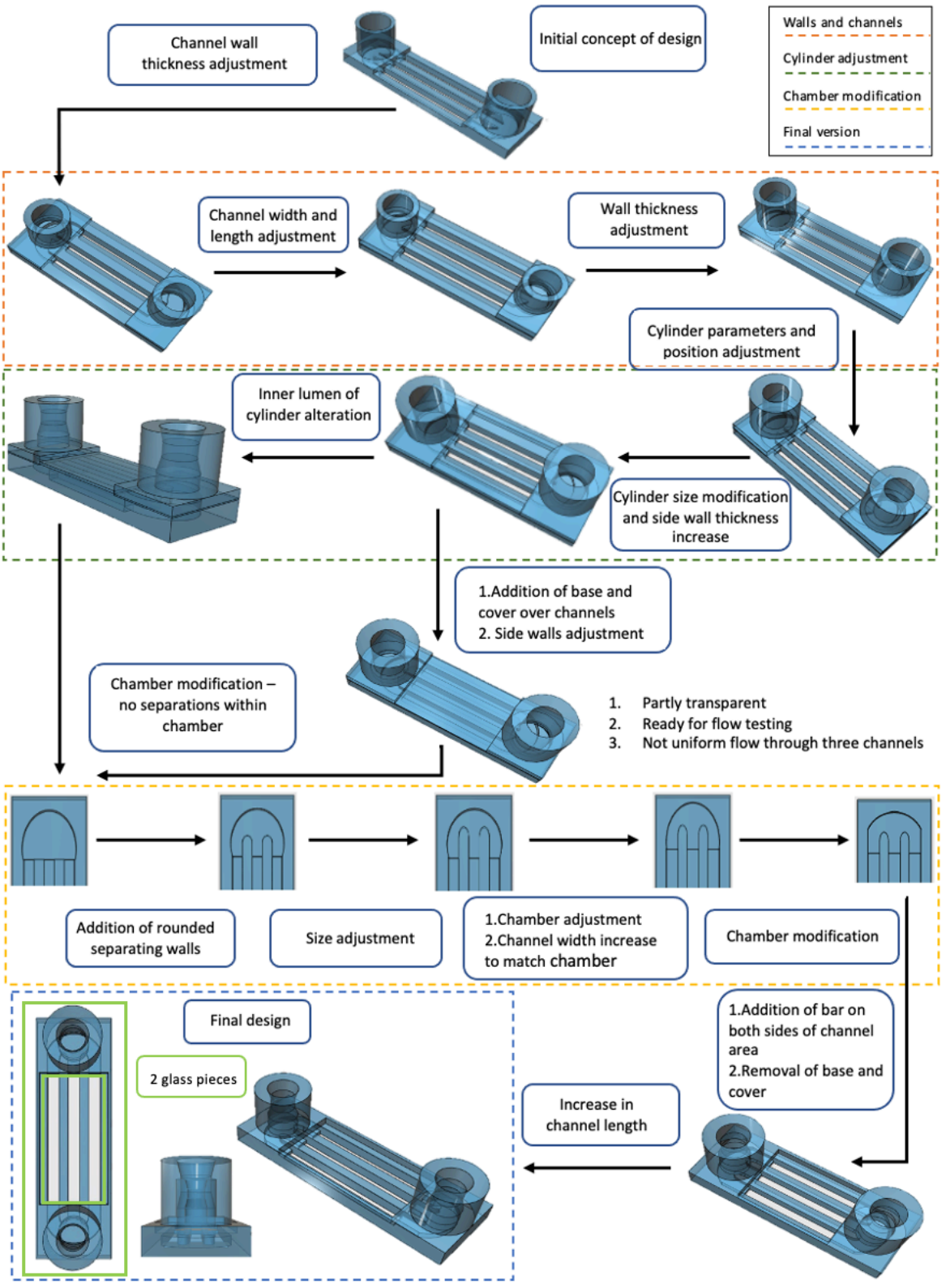

Figure 3.2 Flow diagram showing the key steps in developing a device 3D printed part.

The initial critical features of the design are:

- three channels parallel to each other;
- two identical chambers on both ends of the channels;

- cylinder on top of each chamber to connect the device to the tubing;
- opening holes from each chamber to three separate channels.

During the course of the project, key features got adapted to fit the requirements that were discovered. The parameters of each design step for the device framework are presented in Table 3.1. All the details of the channel dimensions are in Table 3.2. The design of the initial concept that shows the key parts of the device is presented in Figure 3.3.

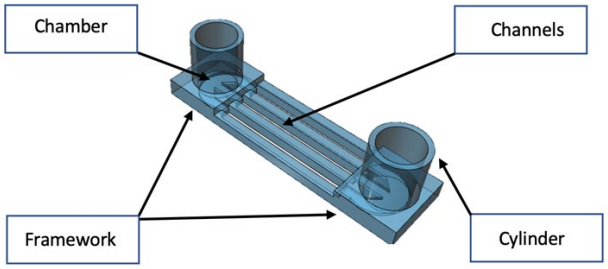

Figure 3.3 Diagram showing the essential parts of the initial design concept.

The initial parameters of the first design were too small for the 3D printer to produce a solid framework. When melted filament was extracted from the nozzle of a 3D printer and deposited on the surface of the printing platform, it did not merge. Instead, it formed two separate threads of filament next to each other. In addition, the walls were not strong enough and allowed the deformation of the channels. The height of the channel openings from the chamber was too small and was not observable in the printed version of the initial device concept.

The next step in design development was to increase the wall thickness, which also increased the overall width of the device, but this resolved problems with filament pasting together. The size of the chamber openings to the channels was still too small to be present on a printout after those manipulations; thus, the channel width of 1.5mm was designed to enlarge the openings from the chambers to the channels. Several manipulations to the design were made to fit the cylinders on top of the chambers, which led to the changing device width and can be observed in Table 3.1 and Table 3.2.

Steps 5 and 6, presented in Figure 3.2, involved operations with cylinder size and position to fit them above chambers and to print their wall without any splits of filament. It also involved device framework adjustments to do so. All alterations to the wall thickness of the device after those steps were made to keep the size of the device as minimal as possible while optimising the other vital needs of the device.

The next part of developing the working device was the requirement to connect the device to the tubing. The inner lumen of the cylinder was amended to make the elastic tubing fit inside the

cylinder to prevent any leakages during liquid flow. Instead of having the straight, one-size uniform inner lumen of the cylinder, the curved-shaped design was created and is presented in Figure 3.4. The radius of the outer circle is 4.5, and the height of each cylinder is equal to 8mm.

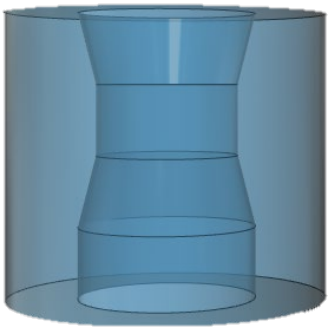

Figure 3.4 The design of the inner lumen of the cylinders of the device. The radius of each circle from top to bottom: r=2.5, r=2, r=2, r=2.5, r=2.5.

The next big step in developing the working device was introducing the base under the device and covering the area of the channels to print an enclosed device for liquid passage testing. The resulting device was ready for flow testing because channels were separated from the outside environment, but because the top and bottom of the channels were printed from the filament, the same as other parts of the device, the area of the channels was only partially transparent. This allowed to conduct the flow testing, but uniform flow through all three channels was not observed with this design parameter.

The following part of the design development focused on chamber alteration to obtain uniform flow. The depth of the chamber was kept constant – 1.2mm but its configuration and separators within the chamber varied. At first a chamber without any separators between openings to the channels was tested. This did not improve the performance of the device, and the liquid was predominantly going through the central channel. Separators with rounded edges of different sizes were introduced to split the flow from the chamber to the channels, which enhanced the liquid flow through the side channels.

Table 3.1 Summary of parameters for the framework part of the device. The numbers in bold represent the changes from the previous version of the device.

	LENGTH / MM	WIDTH / MM	DEPTH / MM	BASE / MM	COVER / MM	SIDES / MM
1	26	7	2	-	-	-
2	26	**11**	2	-	-	-
3	**34**	**13**	2	-	-	-
4	**32**	**11**	2	-	-	-
5	32	11	2	-	-	-
6	**34**	**14**	2	-	-	-
7	34	**11**	**2.4**	**0.4**	**16x11x0.4**	-
8	34	11	**3.4**	0.4	16x11x0.4	-
9	34	11	**2.4**	0.4	16x11x0.4	-
10	34	11	2.4	0.4	16x11x0.4	-
11	34	11	2.4	0.4	16x11x0.4	-
12	34	**12.5**	2.4	0.4	16x11x0.4	-
13	34	12.5	2.4	0.4	16x11x0.4	-
14	34	12.5	**2**	**-**	**-**	**16x0.5x1.5**
15	**40**	12.5	2	-	-	**22x0.5x1.5**

At this stage, the decision was made to increase the chamber size and width of the channels from 1.5mm to 2mm with a subsequent increase in chamber opening width to 2mm, further improving the flow. More manipulations of the chamber shape resulted in a uniform flow through all three printed channels in a device.

The final step of the working device development was the removal of the printed top and bottom covers. These printed parts did not provide the transparency needed for the observation of the biofilm within the device. The decision was made to replace them with glass parts as a post-fabrication of a device. To assist in the top cover attachment's post-fabrication and minimise chances of leakage, sides were introduced on both ends of the channel's area. Those additional parts were 16mm long, 1.2mm in height and 0.5mm wide.

For the final version of the device, the channel area length was increased from 16 to 22mm to allow better fitting of the device under the light microscope for observing biofilm in the channels.

It is presented at the end of the flow diagram in Figure 3.2. The total volume inside the final device – is 372.5 mm^3, 88mm^3 for each channel and 54.25mm^3 within each chamber.

Table 3.2 Summary of parameters for the channel area of the device. The numbers in bold represent the changes from the previous version of the device.

	LENGTH / MM	WIDTH / MM	DEPTH / MM	INNER WALLS WIDTH / MM	OUTER WALLS WIDTH / MM	OPENING HEIGHT / MM
1	14	1	2	1	1	0.9
2	14	1	2	**2**	**2**	**1**
3	**20**	**1.5**	2	2	**2.25**	**1**
4	**16**	1.5	2	**1.5**	**1.75**	1
5	16	1.5	2	1.5	1.75	1
6	16	1.5	2	1.5	**3.25**	1
7	16	1.5	2	1.5	**1.75**	1
8	16	1.5	**3**	1.5	1.75	**2**
9	16	1.5	**2**	1.5	1.75	**1**
10	16	1.5	2	1.5	1.75	1
11	16	1.5	2	1.5	1.75	1
12	16	**2**	2	1.5	1.75	1
13	16	2	2	1.5	1.75	**1.2**
14	16	2	2	1.5	1.75	1.2
15	**22**	2	2	1.5	1.75	1.2

3.2 MATERIALS FOR DEVICE 3D-PRINTING

3D printing is a widely accessible technique that allows rapid and easy changes to be quickly introduced to a design using respective computer software. 3D printing is a new manufacturing application technology that is growing exponentially. 3D printers vary in size, materials utilised for production, and application techniques employed in manufacturing (46). The fused deposition modelling technique was used throughout this project. It is the most accessible technique; the printers are small and easy to use. This method involves heating thermoplastic material and extruding it from the nozzle (47). It is a layer-additive process, meaning the object is produced by layers fusing together. The technique can accurately produce small and featured details on the object and provides good strength for those objects. After the object is designed in the software,

the program slices that object into layers and data is transferred to a 3D printer which produces an object layer by layer on top of the platform (Figure 3.5). The filament is drawn into the preheated extruder, where it melts and then slowly extrudes from the heated nozzle to build a designed object. The nozzle moves inside the printer horizontally while the building platform moves vertically to produce a 3D object. Different filaments are available for 3D printing. The choice of the material depends on the purpose of the study. ABS (acrylonitrile butadiene styrene) is the most widely used filament because it is very simple to handle, but multiple other filaments exist and have been used in this project.

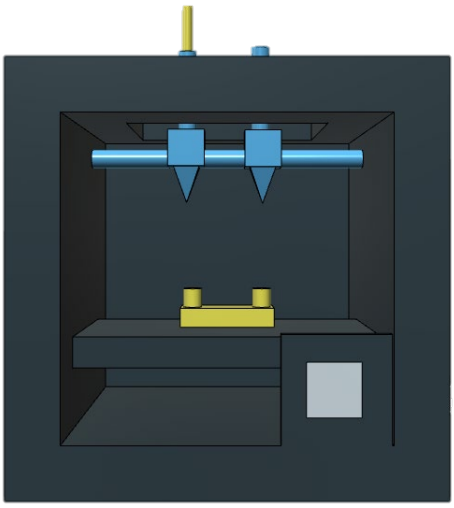

Figure 3.5 Autodesk 123D model of a fused deposition 3D printer, yellow thread - filament, blue - nozzle and extrusion tip. The device is located on the platform.

The advantages of 3D printing are the short amount of time required from the initial idea to the final printed object. The complexity of the design does not affect the price of production due to powerful design applications that can quickly construct any structure. What mainly affects the cost of production is the size of an object and the material used in production. Plastic filaments are inexpensive, approximately £15.00 for 750g, while other materials, like metals and printers that can operate them, are costly. The resolution of printing is a critical parameter contributing to the printer's price. The smaller and more complex an object has to be, the printer's resolution also has to increase, which leads to a price increase. The 3D printer used in this work was a MakerBot Replicator 2X.

Three filaments were used to print the device design 13 – (Figure 3.2): clear PLA, T-glaze and HDglass. Printed devices were used to test the transparency, especially in the area of the channels, and to assess device water tightness. Printer settings are listed in Appendix B. These filaments were chosen because they are capable of producing clear yet untransparent objects. None of the devices printed with those filaments produced a fully transparent channel area -

(Figure 3.6). Moreover, when tested with the liquid flow, T-glaze and HDglass printed devices leaked, and some of the PLA printouts leaked, but to a lower extent. This was impossible to solve by manipulating printer settings because small holes were present between layers of extruded filament. Some of the layers of filament did not fully merge during printing, even at its optimal temperature, leaving small holes invisible to the eye but accessible for the liquid under pressure. The increased temperature during printing would promote the merging of filament and eliminate some of those holes. However, it would dramatically affect the shape of the final product, especially parts printed without support. In the case of devices, these were openings from the chamber to the channels. Therefore, post-modification of printed devices was implemented to prevent leakage. PLA filament was chosen as a printing filament because it leaked to a lesser extent than the other two filaments. None of the other two was better at transparency in the area of channels in the device. Printed PLA devices were coated with XTC 3D™ coating – epoxy resin. It is an epoxy coating for 3D-printed devices. It covers the object uniformly and is transparent; therefore, it does not affect the device itself. After coating was applied to the PLA device, no leakage was observed.

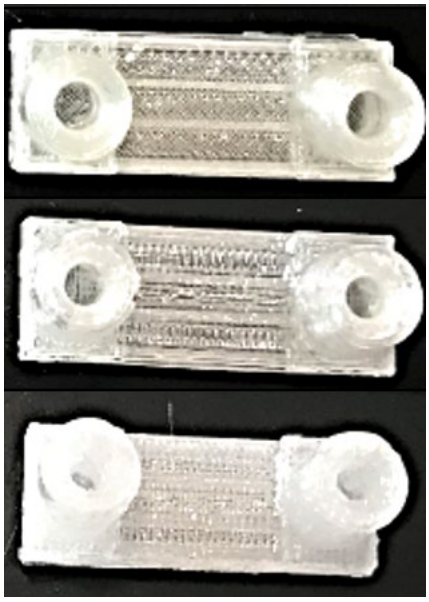

Figure 3.6 Photograph of printed devices using three filaments, from top to bottom: clear PLA, HDglass and T-glaze.

3.3 DEVICE FABRICATION

To achieve a fully transparent channel area of the device, the framework was 3D printed using PLA filament and glass pieces were used to seal the channel area. The glass used was cut from microscope slides of 1mm thickness. The length and width of the bottom glass are 25x45mm. The

top of the device is strictly restricted by the walls surrounding the channel area, and the specific glass pieces of 11x21mm were cut to fit the device.

The procedure of the device assembly follows the steps below:

1. Remove all left-over filaments remaining after printing. All trim pieces of filament threads must be removed to prevent any barriers to the liquid flow and not interfere with biofilm growing inside the channels.
2. Apply XTC 3D coating to the surface of the walls between channels - Figure 3.7 and insert a top cover glass piece into the channel area. The XTC coating acts as glue. Avoid any sliding of glass pieces over the surface; it will leave traces of XTC 3D coating on the surface of the glass and will ruin the transparency of the channel. Leave to dry for 1 hour.

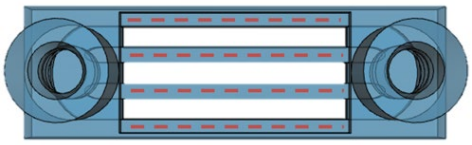

Figure 3.7 Schematic of XTC 3D coating applied to the surface of the channels.

3. Examine any holes between the channel framework and the cover glass slide. If gaps are present, carefully fill them with coating and leave them to dry. Repeat until all gaps are eliminated. If no gaps are present, move to the next step.
4. Fill the space between the top glass cover and sides of the device designed to minimise leakage risks and apply a thin layer of coating on both sides above the chamber openings to the channels - Figure 3.8.

Figure 3.8 Schematic of the second application of XTC 3D coating.

5. Cover the total area of the device's bottom with coating and place it on a clear glass piece. Be careful to avoid sliding the device when placed on the glass. This will leave traces of XTC 3D coating on the glass surface. Let it dry for 2 hours.
6. Surface of the device is not smooth and straight enough to attach to the surface of the glass evenly. There will always be holes left between the glass surface and the device. Carefully apply a coating to fill all gaps between the glass slide and the bottom of the device. Be careful to avoid applying any coating to the channel area because that will ruin the transparency of the device. Let dry. Repeat until no gaps are present.

7. Apply a thin layer of coating all over the PLA parts of the device that are not in the channel area. This will prevent leakage through the PLA filaments.
8. Connect the fabricated device to the pump and run liquid through it. If no leaks are present – the device is ready to use - Figure 3.9.
9. If leakage is detected during liquid flow, apply another coating layer.
10. Repeat until the device is fully sealed.

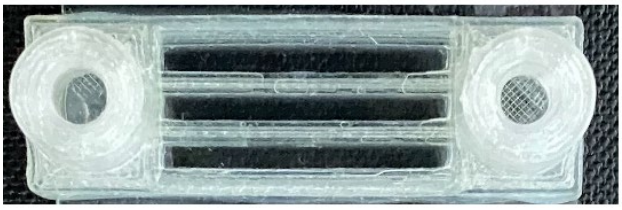

Figure 3.9 Photo of a fabricated device sealed with glass.

The final fabricated device meets all parameters stated at the beginning. It has a fully transparent channel area. It makes it ready for microscopy observations without any extra steps to study biofilm. The device is leakage free, which allows for the continuous supply of liquid through the system. The transparent area has three channels running in parallel, introducing three individual repeats to each experiment. Even though it was impossible to produce a working device with transparent channels using PLA filament only, the method was developed to overcome this issue. The total transparency of the device channel area was achieved by introducing glass to seal the channel area. The device is not reusable but quick and easy to fabricate. In addition, it is light and robust, which makes it easily transferable.

3.4 DEVICE OPERATION

Before biofilm growth, device channels are sterilised in both orientations using a flow rate of 1ml/min with 70% ethanol for 15 min. After sterilisation, the device is washed with DI water at 1ml/min for 15 min. The last step is conditioning the device with the LB Broth for 15 min at 1ml/min. Tubing for the inlet and outlet is autoclaved before connection for the continuous phase.

During the device performance testing, images of the device channels were taken after the sterilisation procedure followed by staining with crystal violet and trypan blue in order to confirm that there are no bacterial cells present within each channel (Figure 8.33).

Overnight bacterial inoculum is diluted to 4 x 10^6 cells/mil with LB broth, and 0.3 ml is added to the device. The device is incubated in a shaking incubator for 18 hours at 37°C to allow bacterial attachment to the surface of the channels.

Sterile tubing is connected to the syringe pump with a flow rate of 25µl/min. When the tubing is filled to the end, it is inserted into the incubated device. For the first 10 min, the device outlet side is raised to help eliminate air bubbles introduced during the tubing attachment. After all air bubbles are removed from the system, the device is placed flat for biofilm growth. The temperature of the device during the growth is maintained at 37°C by the hot plate on which devices are located.

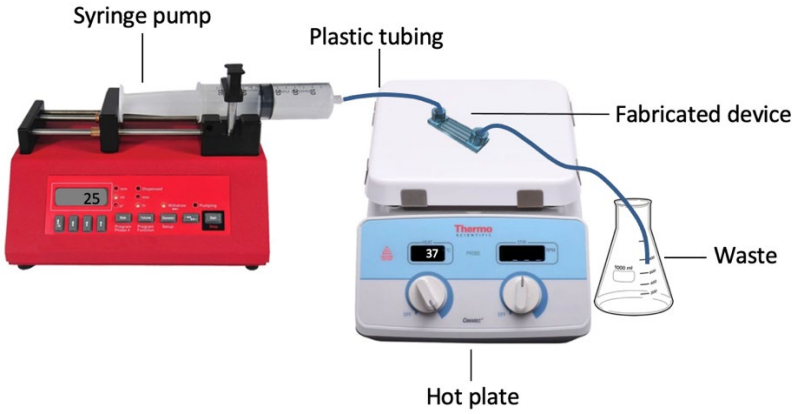

Figure 3.10 Fabricated device operation set-up. The device is connected to the syringe pump and the waste reservoir by plastic tubing, located on a hot plate for temperature control during continuous biofilm growth.

3.5 CONCLUSION

The device that can be used for biofilm studies was designed and fabricated using 3D-printing technologies. The device incorporates three channels running in parallel for biological repeats. Due to the implementation of 3D-printing technologies, the production of the device is cheap and quick. The fabricated device is robust due to the production method and can be easily modified and adapted for different experimental needs.

In addition to 3D-printed parts of the device, two glass slides were incorporated into the design to seal the device channel area. The method was developed to seal the 3D-printed parts of the device to two glass slides to produce a leakage-free assembly of the device. Implementation of two glass slides allowed for full transparency of the device channel area for non-destructive observations of biofilms.

The procedure for the device sterilisation and conditioning was developed and tested to confirm the absence of bacteria before the addition of the inoculum for the initial attachment of bacterial cells for biofilm formation.

Chapter 4 OPTIMISATION OF *E. COLI* BIOFILM GROWTH CONDITIONS

In this chapter, the optimisation of the methodology to study biofilm formation is detailed. Investigation of biofilm development by three different assays was performed: static biofilm formation in a 24-well-plate, continuous biofilm formation in a drip-flow reactor and continuous biofilm formation in a fabricated device. Each method must be optimised to produce robust and comparable data under identical conditions. In order to standardise the performance of the fabricated device and prove that it is suitable for biofilm studies, its performance was compared to the existing two methods – one static and one dynamic model.

E. coli WA321 biofilm-forming bacterium was chosen for these studies because not every *E. coli* strain forms biofilm, or is poor biofilm former (48). Risk Group 1 *E. coli* strain – a microorganism unlikely to cause disease, was purchased from DSMZ. Because this strain is non-pathogenic and forms biofilms, it serves as a good model system.

There are two *in vitro* approaches to growing biofilm in the laboratory: static and continuous. Static methods have no flow and no new nutrients added during growth, while dynamic systems have constant flow and nutrient supply. Examples of these two systems are used in this study to demonstrate that fabricated devices can produce both extremes and any combinations in between.

Examples of static biofilm assays include microtiter plate-based systems (49), colony biofilm assays (30) and Calgary biofilm devices (50). They are quick and easy to set up. Continuous assays are more complex in their setup and require more time to conduct. The primary examples of continuous biofilm devices are drip-flow reactor (51) and microfabricated devices – flow cells.

None of the assays is perfect and fully representative of the naturally occurring biofilm; hence, more devices need to be added to biofilm research. Each method has its advantages and drawbacks, as mentioned in the introductory chapter. A careful decision has to be made when choosing which type of assay to use, depending on the purpose and nature of the experiment.

Parameters that affect biofilm formation need to be carefully monitored to produce repeatable results of biofilm growth. The main parameters that can be controlled *in vitro* studies are temperature, nutrient supply composition and concentration, the flow of liquid through the system, and time for biofilm formation. In order to produce reproducible biofilms in the laboratory, these conditions have to be precisely controlled. The ability to use complex and time-

dependent combinations of parameters is essential to exploring biofilm behaviours and properties. In this study, the *E. coli* WA321 strain was used. Its cultured condition specified by the supplier – 37°C temperature and LB broth as a media. Hence, the temperature remained constant at 37°C, and an LB medium was used as a nutrient supply. Two studies were performed. The first was to determine the lowest LB medium fraction to be used in experiments, while the second was to optimise biofilm formation time by three methods.

4.1 OPTIMISING GROWTH MEDIUM CONCENTRATION FOR BIOFILM GROWTH

Growing biofilm under static conditions is challenging due to eventual nutrient limitations; therefore, it is crucial to investigate the growth medium concentration that will support biofilm during the growth phase. Getting the right conditions for this model to produce a biofilm that can be compared with biofilms grown in other systems is a starting point for compositions for the other systems. This project studied a static biofilm assay in a 24-well plate with glass coupons (slides) inserted into each well. It is essential to have enough nutrients to support biofilm development during the growth period before cells begin to die due to nutrient starvation or medium toxification from waste products in each well. The biofilm formation time for the 24-well-plate assay was 24h after the addition of inoculum (52). Matured biofilm formation takes 20 – 40 hours, depending on the strain and growth conditions. After 24h of static growth, biofilm formation was observed and was visual under the microscope.

Trypan blue (0.4%) is a dye used to determine cell viability by staining dead cells only. It enters and concentrates in membrane-compromised dead cells, staining them blue. The darker the biofilm appears after staining, the fewer viable cells, and vice versa. Live cells with intact membranes do not stain with trypan blue (53).

The mean grey value (MGV) is a measurement parameter in ImageJ software that measures the mean intensity of the selected region; in this study, the mean grey value of the selected biofilm. It ranges from 0 – 255 pixels in a grey-scale image, where 0 is black and 255 is white. The lower the pixel intensity of a biofilm, the higher the absorption of the dye. Non-TB absorbance regions, live cells, and EPS contribute to the MGV reading. Controls of unstained biofilms show MGVs between 150-204. This value is also affected by the thickness of a biofilm.

Biofilms in each well require an optimum amount of nutrients in LB media to support live biofilm, which will be comparable with biofilms grown in dynamic systems with a constant supply of nutrients. This is vital because biofilm formation in a static assay occurs without a fresh supply of

nutrients, which leads to nutrient depletion and accelerated cell death. LB solutions of different volume fractions were prepared to investigate their ability to sustain biofilm for 24 hours in a microtiter plate assay.

Different LB fractions were prepared using the equation below, where V_i is the volume of LB Broth, V_j – the volume of all constituents of the mixture. Mixing was performed with DI water:

$$\emptyset_i = \frac{V_i}{\sum_i V_j}$$

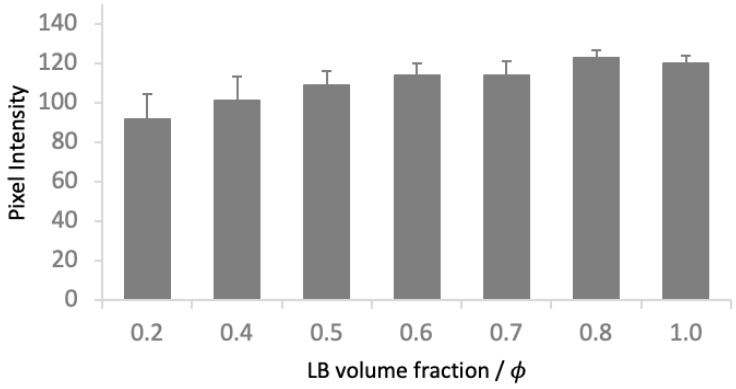

Figure 4.1 Graph showing the MGV of static biofilms grown in different LB Broth concentrations, trypan blue staining, N=6, error bars - standard deviation.

Figure 4.1 shows an increase in MGV of a 24h biofilm as the volume fraction of LB in a solution increases. 0.2 LB fraction in a solution is not enough to sustain live biofilm for 24h because nutrient depletion occurs, and cells within biofilm die during the 24h growth period; hence excessive staining with trypan blue was observed. As the volume fraction of LB in a solution increases, the MGV of biofilms gradually increases, meaning that more viable cells are present in the biofilm at the staining time. At 0.8 and 1 LB volume fraction in a solution, the mean grey value of biofilm is the highest and is equal to 120 MGV. The visual appearance of biofilms grown with different volume fractions of LB in solution and stained with trypan blue dye is illustrated in Figure 4.2.

At 0.8 and 1 volume fraction of LB in a solution, cloud-like white/grey biofilm with patches of blue is visible on the air-liquid interchange on the glass coupons within the well. As the LB fraction decreases, biofilm absorbs more trypan blue and appears blue at 0.7 LB in a solution, grey at 0.5 LB, and black at 0.2 LB under the light microscope.

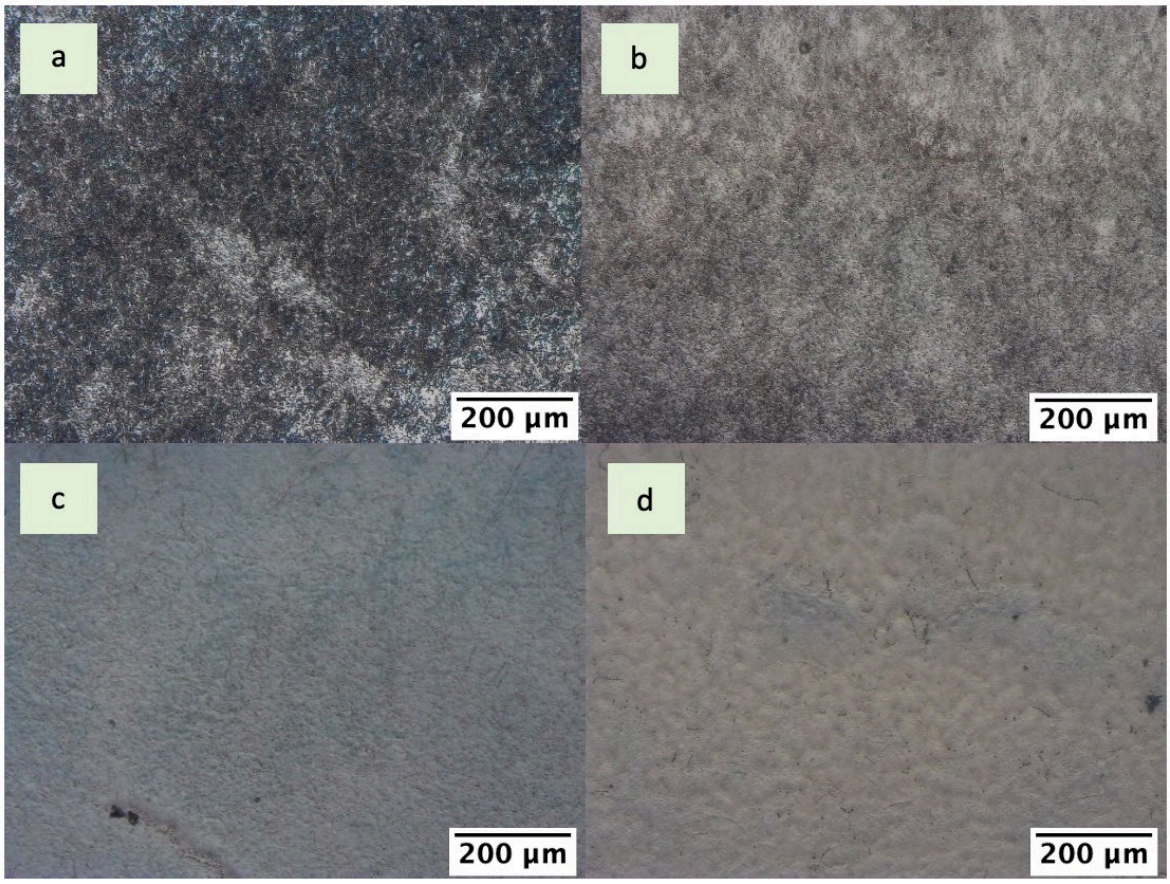

Figure 4.2 Photos of static biofilm grown at different LB broth volume fractions. a - 0.2 LB, b - 0.5 LB, c - 0.7 LB, d – 0.8 LB. Trypan blue staining, light microscopy, digital magnification 64x.

A convenient way of quantifying the optical absorbance data is to use pixel intensity distribution within biofilm using ImageJ software. Total pixel intensities range from 0 – 255. This range was split into five equal groups, Group 1 - 0 – 51, Group 2 - 52 – 102, Group 3- 103 – 153, Group 4 - 154 – 204 and Group 5 - 205 – 255. The number of pixels in each group within a biofilm can be measured and plotted as the %area they occupy in the biofilm, as shown in Figure 4.3. The first group of pixels (0 – 51) represent the darkest areas in biofilm. It occupies 7.06% of biofilms grown in 0.2 LB volume fraction media, N=6 - Figure 4.3. As the LB fraction in the solution increased to 0.4 LB, the first group of pixels diminished, and the second group of pixels (52 -102) dominated the biofilm area. As the LB fraction increases to 1, the second group of pixels gradually decreases. The third group of pixels increases and reaches 95% at 0.8 LB fraction in solution and pure LB. Pie charts in Figure 4.3 show the percentage of each pixel group present in the biofilm grown at 0.2, 0.5, 0.7 and 0.8 LB fraction in media and the total % area occupied by the biofilm in the biofilms analysed N=6.

Biofilm is an aggregate of cells grown layer upon layer. It is impossible to quantify the number of viable cells in biofilm using this method. However, it is possible to determine whether biofilm is

live or mainly consists of dead cells using pixel intensity allocation and MGV. MGV of biofilm increases as the concentration of LB in the solution increases. This means biofilm absorbs less trypan blue dye and appears lighter as the LB fraction in growth media increases. Almost no staining is observed with trypan blue at 0.8 LB and above. Below 0.8 LB in a solution, the biofilm appears darker due to the absorption of trypan blue by dead cells within the biofilm.

At 0.2 LB fraction, pixel intensity Groups 1 (0-51) and 2 (52-102) dominate in biofilm, as shown in Figure 3.3. When the concentration of LB in the growth solution increases, the pixel intensity of Groups 1 (0-51) and 2 (52-102) diminish and disappear, while Group 3 (103-153) increases drastically. From 21.39% of the total biofilm area at 0.2 LB in a solution to 95% at 0.8 LB. As the concentration of LB increased in a solution, biofilm formation was more uniform, without empty spaces in the structure.

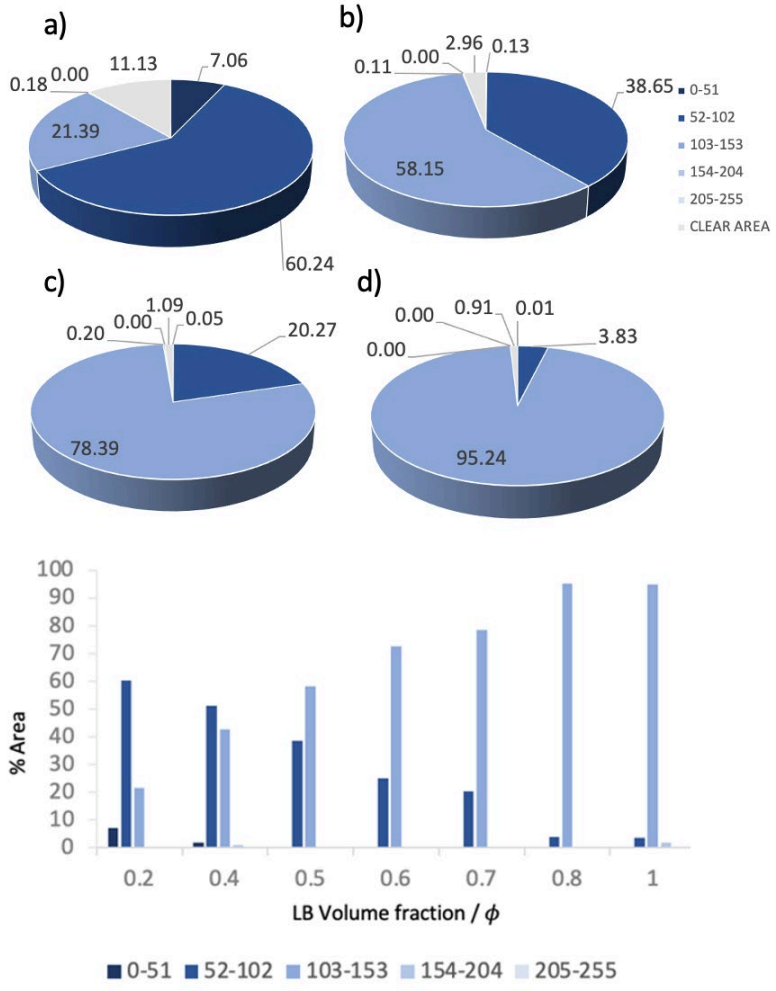

Figure 4.3 Graph showing the % area of each pixel intensity group within the static biofilm. Pie charts showing detailed pixel distribution and area clear from biofilm (grey), a) – 0.2 LB, b) – 0.5 LB, c) – 0.7 LB and d) – 0.8 LB. N=6.

A conclusion could be made that for 24h static biofilm minimum nutrient concentration of 0.8 LB is required to support living cells within a biofilm for the growth period. When analysed in ImageJ, viable biofilm is represented by pixels 102 – 255, and pixels below 102 correspond to an increased number of dead cells.

Based on these studies, an 0.8 volume fraction of LB was used in studies of biofilms grown under static and dynamic conditions.

4.2 OPTIMISATION OF THE GROWTH PERIOD FOR *E. COLI* BIOFILM FORMATION

In order to visualise biofilm under the microscope, enough time has to elapse to allow biofilm development to cover the surface of the device channels or glass coupons. The time of biofilm development in each assay has to be identified to be able to reproduce experiments and make direct comparisons between them. On the one hand, the biofilm development period has to be sufficient to visualise it under the microscope. On the other hand, the growing time must be minimal to reduce the experiments' time. This does not apply to the studies where, for example, investigating the maximum growth time was required. Considering the dose-response studies, biofilm should attain a steady state in the shortest possible period to speed up the experimental process. The optimisation of biofilm growth time was investigated in three assays – for static biofilm in a microtiter plate and two continuous assays, one in a drip-flow reactor and one in the fabricated devices.

In addition to trypan blue staining, crystal violet staining was used to visualise biofilms after their formation. Trypan blue and crystal violet are key to optical readout signals used to quantify the growth of biofilms in the fabricated devices and to compare biofilm formation to the other two methods. Trypan blue stains dead cells only, while crystal violet is commonly used to quantify the total biomass of a biofilm. Crystal violet dye does not differentiate between live and dead cells and binds to other components in the extracellular matrix (54). Since two dyes have different binding mechanisms, they were used to achieve a quantitative intercomparison of biofilm growth to validate the performance of the fabricated device.

4.2.1 Studying static biofilm formation time

Static biofilms were grown on sterile glass coupons inserted into each well of a microtiter plate. Standard 24-well microtiter plates were used, three wells per each condition repeated three times undependably. The overnight inoculum was prepared from frozen stock by mixing it with

10ml of LB in a sterile test tube. The tube was left in an incubator for 18h at 37° C. After the growth period, cells were counted using Cellometer^{R} and diluted to 4 x 10^{6} cells/ml. After adding diluted overnight inoculum to each well and adding LB broth, plates were incubated in a shaking incubator for 24h at 37°C (52).

Experiments to grow static biofilm followed identical procedures until the staining. Half of the samples were stained with 0.4% trypan blue, and another half were stained with 1% crystal violet.

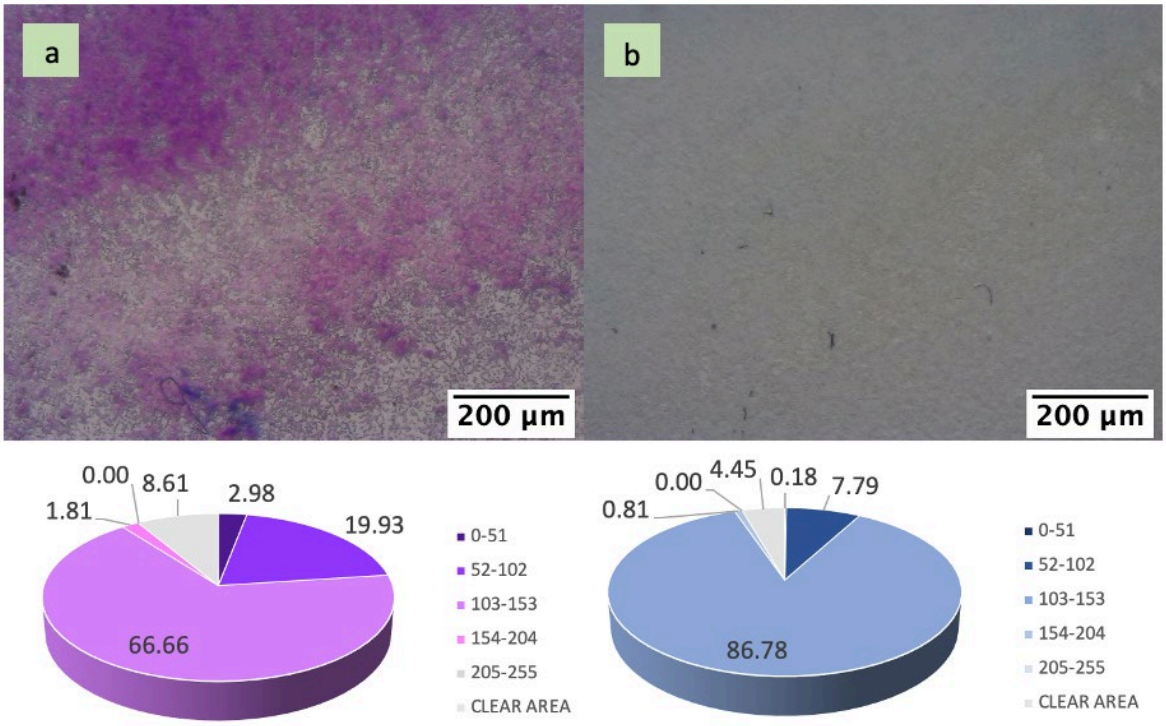

Figure 4.4 Images of 24h static biofilm stained with two dyes: a - crystal violet, b - trypan blue, pie charts with detailed pixel distribution of each biofilm, digital magnification 64x, N=12.

24h of static biofilm formation allows for visualising biofilms using two staining methods. Both staining methods show a similar pattern in pixel distribution within biofilms (Figure 4.4). Static biofilm stained with trypan blue appears cloudlike white/grey with small patches of blue. 87% of biofilm is represented by the third group of pixels (103 – 153), as in the previous chapter. Crystal violet staining is more intense due to the staining of entire biofilm biomass and has a more significant proportion of pixel groups 1 and 2 present in biofilms.

4.2.2 Investigating continuous biofilm formation in Drip-flow reactor for 24h, 48h, and 72h intervals.

The drip-flow reactor was used in this study as an example of a dynamic system to benchmark the performance of the fabricated device.

Drip-flow reactor with four chambers was purchased from BioSurface technologies and was used as per the operator's manual (55) with some modifications outlined in the next paragraph. Briefly, a glass slide was inserted into each chamber, and effluent tubing was attached to each port prior to sterilisation. The ends of effluent tubing were covered with foil to maintain sterility when out of the autoclave. Effluent tubing was clipped to prevent liquid from draining out of the reactor during a batch phase. 15ml of 0.8 LB Broth was added into each chamber with 1ml diluted overnight inoculum (4 x 10^6 cell/ml). The device was incubated flat in a shaking incubator for 14h at 37°C. After the initial attachment phase, the device was placed on a 30° stand and connected to a pump.

The main difference between the method used compared to the operation manual was the use of an HPLC pump instead of a peristaltic pump and a different flow rate. In order to connect the HPLC pump to four chambers with equal flow through each of them, a tubing system was introduced, as displayed in Figure 4.5. The initial 1ml/min flow from the HPLC pump split to 0.25ml/min via tubing assembly to get the flow into four chambers simultaneously. In addition to the split tubing assembly, the insertion of PEEK tubing into the silicon rubber tubing and the needle assisted the production of constant and uniform flow into each chamber.

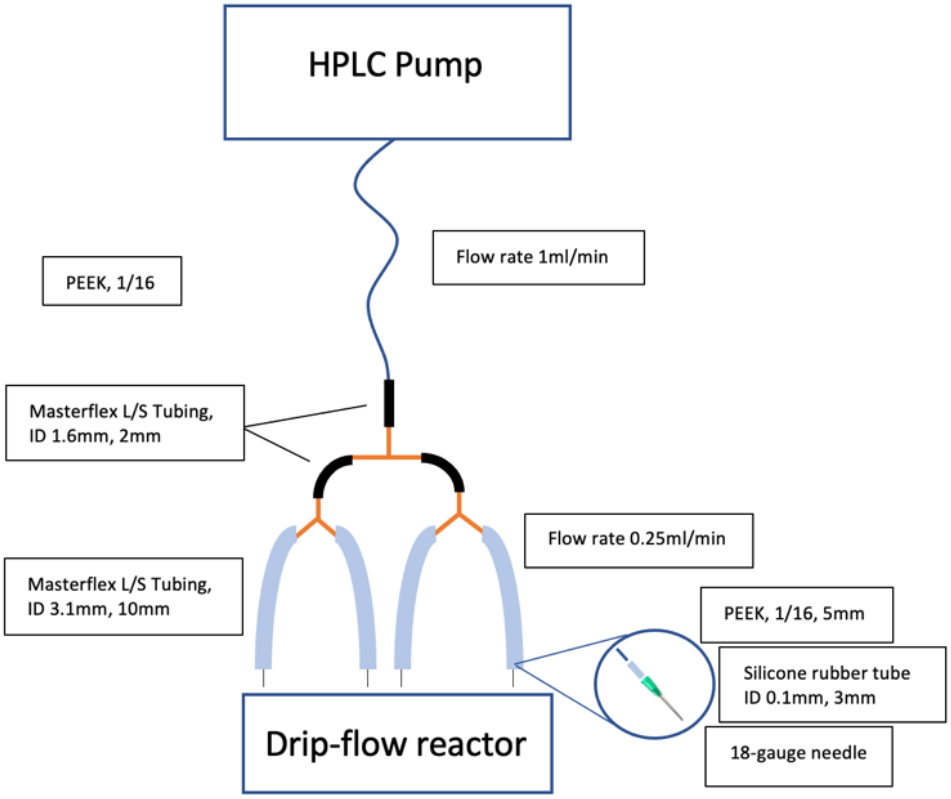

Figure 4.5 Tubing assembly from HPLC pump to drip-flow reactor chambers.

For this study, biofilm was grown in a drip-flow reactor for 24h, 48h, and 72h periods. After 24h of a continuous flow of nutrients, no biofilm formation was observed. Some cells or small clusters of cells were evident and occupied less than 5% of the surface analysed, as shown in Figure 4.6. After 48 hours of growth, a fully developed biofilm was formed in a drip-flow reactor. Biofilm was stained with crystal violet and trypan blue dye, and both stains revealed the same amount of biofilm present in the analysed samples. Due to the nature of a drip-flow reactor assay, biofilm formation happens following the path of liquid flowing down the coupon. In other words, biofilm is not forming uniformly over the glass slide but follows the media traces. In the middle of media paths, the biofilm is thick, rugged, and has a highly uneven distribution. On the edges of the flow, it is thinner and flatter because fewer nutrients are available. The sampling was performed in the areas of well-developed rugged biofilm.

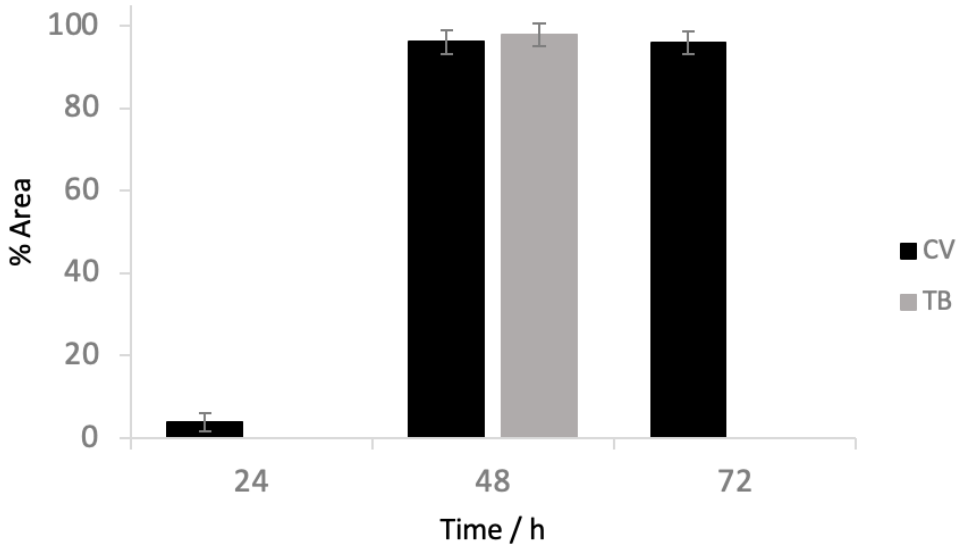

Figure 4.6 Graph showing the % area occupied by biofilm at three different time points in a drip-flow reactor, with trypan blue and crystal violet staining, N=9, error bars – SD.

At 72h growth, fully developed biofilm was present but showed no difference to 48h biofilm. Therefore, there is no need to grow biofilm for an extra day; hence 48h formation was chosen as a standard biofilm growth time for this project. The photos of biofilm and corresponding pie charts of pixel composite are presented in Figure 4.7.

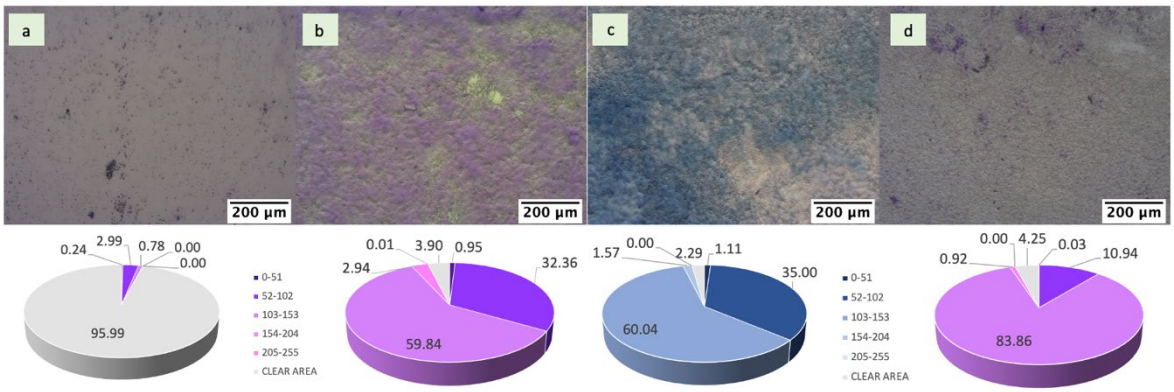

Figure 4.7 **Figure showing the biofilm appearance at a – 24h crystal violet stain, b – 48h crystal violet, c – 48h trypan blue staining, d – 72h crystal violet and pie charts of pixel distribution of these biofilms in a drip-flow reactor, digital magnification 64x, N=9.**

Due to the nature of biofilm, its uneven formation, and its rugged structure, the pixels of biofilm formed in a drip-flow reactor are distributed between pixel intensity Groups 2 and 3 than static film, which is flatter, and most of the biofilm consists of pixels in Group 3. The predominance of pixel Group 3 (103 – 153) is the largest and is equal to 60% of the total biofilm mass, but group 2 (52 - 102) makes up around 35% of the biofilm. The pixel intensity distribution of 48h biofilm with crystal violet and trypan blue staining shows the same pattern.

4.2.3 Comparison between 24h, 48h, and 72h growth periods of continuous biofilm formation in the fabricated device

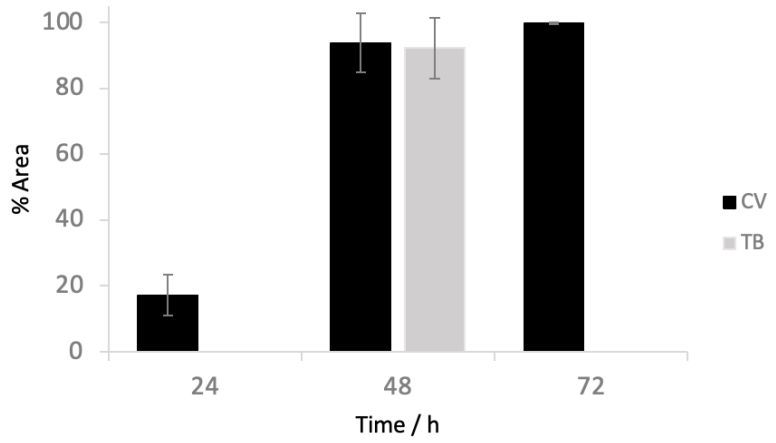

Figure 4.8 **Graph showing the % area occupied by biofilm at three different time points in fabricated device, N=6, error bars – SD.**

More than 24h growth time is needed to produce a biofilm in the fabricated device, as illustrated in Figure 4.8. Some individual bacterium cells and clusters were observed, and 85% of the channel area was clear from the biofilm. 48h is sufficient to form a biofilm that covers the whole channel.

6.28% and 7.8% of the area of the channels were empty from biofilm, crystal violet and trypan blue staining, respectively. Both staining methods show the same area coverage by biofilms, and the same pixel intensity distribution pattern was observed. Area coverage by 72 hours biofilm is denser compared to 48h, and no empty area from biofilm is present but does not differ significantly compared to 48h. Therefore, 48h is adequate to form a biofilm in the fabricated device and is used throughout this project for the rest of the studies.

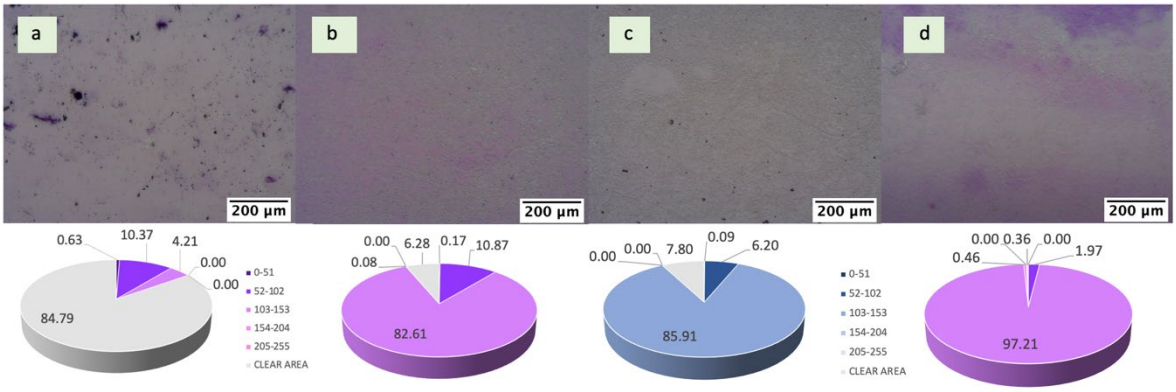

Figure 4.9 Figure showing the biofilm appearance at a – 24h crystal violet stain, b – 48h crystal violet, c – 48h trypan blue staining, d – 72h crystal violet and pie charts of pixel composite of these biofilms in the fabricated device, digital magnification x 64.

The biofilm formation in the fabricated device differs from the static biofilm and biofilm in a drip-flow reactor. Two different surfaces are present in the channel area: rough PLA sides of the channels and smooth top and bottom of the channels made of glass. Initial biofilm formation is observed at the sides of the channels, and it is proposed that the biofilm growth arises from the sides towards the middle of the channel. Due to gravity, it is more likely for the initial attachment of bacteria to take place on the rough sides of the channels and the bottom side of the channel. 48h is sufficient for the biofilm to aggregate the entire surface of the channel on the sides and in the middle, and there is no difference between those regions. The same is true for the 72h biofilm, but the amount of film in the centre of the channels is evener. This conclusion is made by observations of the biofilm under the microscope. This was expected as the biofilm constantly develops; it will occupy as much space as possible and eventually block channels.

Biofilm in a fabricated device covers the whole area of channels. This is confirmed with crystal violet staining. This is due to the constant flow of media through the channels, which brings nutrients for biofilm development. The flow of liquid follows the same path; as a result, biofilm formation is unform across all areas of the channels.

Based on these observations, it was decided to use 48 hours as a standard growth time for biofilm formation in a fabricated device. It allows complete coverage of channels in minimal timing. The appearance of biofilm after 72h is insignificant compared to 48h growth.

4.3 CONCLUSION

Developing a systematic approach for biofilm formation is essential for experimental reproducibility and hence validation of the performance of the device. Optimisation of the biofilm growth time is critical for the experiments. For the static assay, 24h is a standardised time for biofilm formation. For continuous biofilms, more time is required to form a developed biofilm. 48h growing period was selected for both continuous assays. It also allowed minimising experimental timing by comparing biofilm formation between 48h and 72h. The experiments in this chapter established that the optimal LB broth media volume fraction is 0.8 LB to support biofilm in a static assay.

The source of variation between biofilms can be neglected because every biofilm grown differs from previous *in vitro* and *in vivo* conditions. What is more important and was shown in this chapter is that the staining methods show the same pattern of the pixel intensity distribution of developed biofilm with the same dye on different repeats and between different dyes - Figure 4.10.

Pixel intensity distribution within biofilm growing in a drip-flow reactor shows two prominent peaks of Groups 2 (52 – 102) and 3 (103 – 153) after the analysis. It absorbs more staining agents due to the rugged structure of the biofilm. The produced pixel intensity distribution is due to the uneven structure of the biofilm. Denser parts of the film are stained more compared to the flatter ones. Static and biofilm in their fabricated device are more even in their structures and show the same staining patterns and pixel intensity distribution of biofilms, with the predominance of pixel intensity Group 3 – more than 80% of biofilm when developed biofilm is stained.

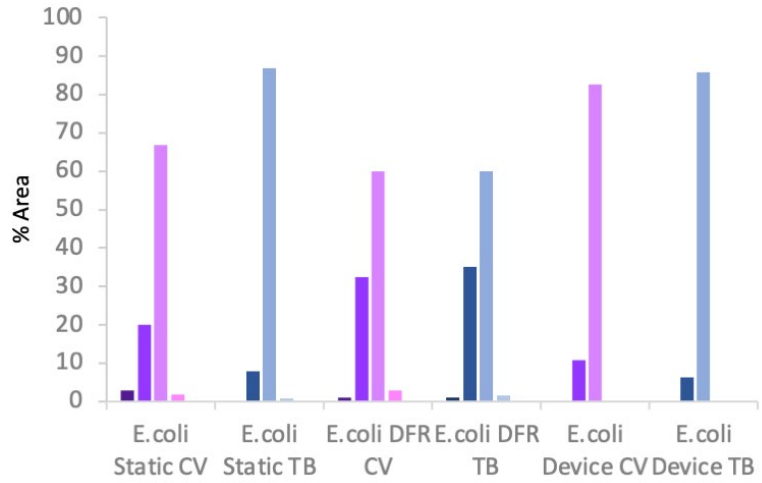

Figure 4.10 Graph showing the average pixel intensities of *E. coli* biofilm formed by three assays with crystal violet (pink) and trypan blue (blue) staining, N=9.

Chapter 5 PHYSICAL VALIDATION OF DEVICE PERFORMANCE

This chapter describes the quantification of the physical performance of the biofilm growth in a fabricated device. When developing a new device with several channels running in parallel, it is projected that the performance of each channel is identical. It is vital to have an even flow through each channel to produce comparable results. The flow in the device contributes to biofilm formation in each channel of a device; therefore, flow uniformity and inter-device reproducibility of flow are critical for growing comparable biofilms.

5.1 EVALUATION OF FLOW THROUGH THE DEVICE CHANNELS

The flow rate range within a device must be controllable and easily adjustable for biofilm formation. Hydrodynamics has an influence on biofilm development. Meagre flow rates result in laminar flow, which is not preferable for biofilm attachment and development. Too high flow rates would result in the mechanical detachment of biofilms from the surface or even result in device leakage.

The flow rate used in microfluidic devices could be as low as 10μl/h (56) in order to reduce the shear stress. A higher flow rate can be used in a fabricated device due to the size of the channels. The device was used with the syringe pump. The syringe pump is restricted by its maximum volume capacity of 60ml, which can be used without re-charging a syringe. Considering previous facts, a decision was made for the flow rate to be kept relatively low. It was decided that the flow rate between 20 and 50 μl/min could be used to grow biofilm for 48h with a need to change the syringe just once per cycle.

Several flow rates were tested to assess the flow through the channels within one device, as can be observed in Figure 5.1. Three ml/min flow rate fills the device in 1.76 seconds. The flow is uniform but extremely fast and cannot support biofilm growth. It is likely to detach biofilm from channel surfaces and requires several amendments of a syringe pump. One ml/min flow rate fills the device in 5.28 seconds. It is also uniform, yet it is still too fast. Experimentally it was established that uniform flow in the devices could be achieved with speeds as low as 25 μl/min, and this flow rate was used throughout the experiments. At this flow rate, three device channels were filled in 3.5 minutes (210 seconds). The flow was uniform at all three channels. All channels have the same speed of filling the channel, as seen in Figure 5.1., and the same pattern.

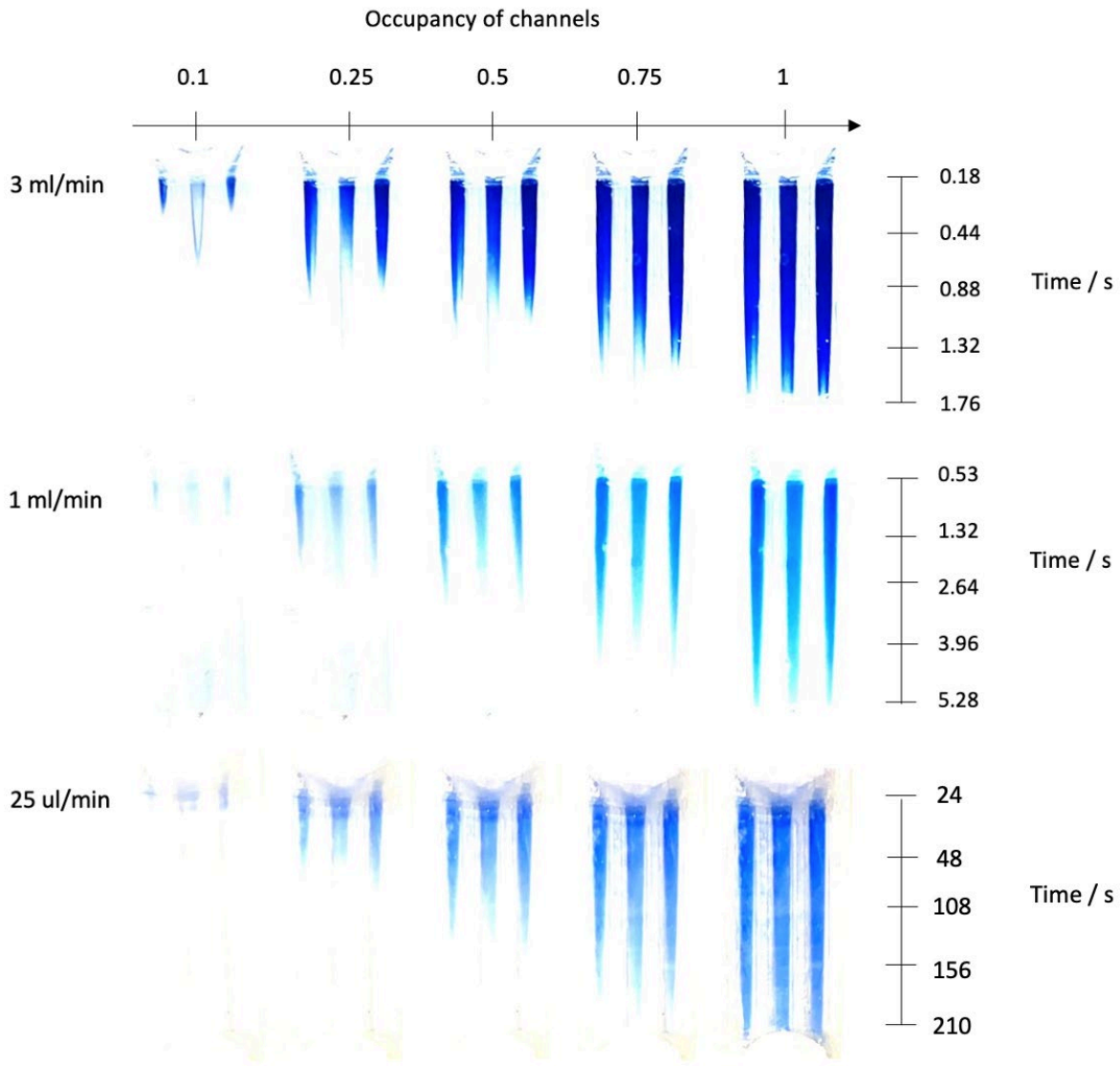

Figure 5.1 Graph showing the pattern in channels occupancy under 3 ml/min flow rate, 1 ml/min and 25 μl/min with a syringe pump, N=15.

The uniform flow through each channel in 15 identical devices was achieved. The flow rate can go down up to 25μl/min without any difference in the channel occupancy rate. This allows conducting experiments with minimal additional manipulations to the device due to nutrient re-stock.

5.2 QUANTIFYING THE INTER-CHANNEL CONSISTENCY OF BIOFILM COVERAGE

A parameter that must be validated prior to using a device during dose-response studies is the uniformity of biofilm formation in each channel within one device and between the devices. It is essential to have the same percentage of channel area covered by biofilm to produce comparable results.

After biofilm formation, the images of each channel were taken for analysis. When analysing the images in ImageJ, the total biofilm in each image was selected, and its percentage area was measured. In total, 40 images of each channel were taken, covering the whole area of the bottom part of each channel (2x2x20).

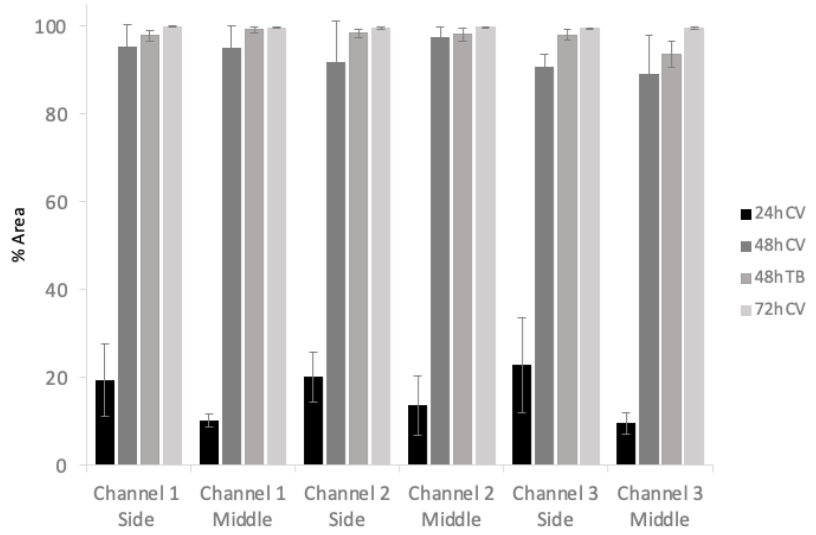

Figure 5.2 Graph showing the % area of each channel – side and middle- occupied by biofilm at three-time points, N=12, error bars – SD.

The biofilm formation after 48h growth time is homogeneously distributed in each channel within each device. This was confirmed with crystal violet and trypan blue staining. The comparison between the sides of the channels and the middle part of the channels are presented and illustrated in Figure 5.2. After 48 hours of growth, there was no difference between the side and internal part of the channel's biofilm coverage, meaning that biofilm had enough time to develop and occupy the surface of the channels fully. The percentage area covered is less than for 72h biofilm formation, which was expected, as described in previous chapters. The biofilm developing for a more extended period in a fabricated device covers the surface without any empty areas. It was also interesting to contrast the side and middle parts of channels after 24h biofilm growth in a fabricated device. Figure 5.2 demonstrates that 24 hours of growth time was insufficient to develop biofilm to fully cover each channel within the device. This also supports the idea of the configuration in biofilm development in the device. Growth was more rapid on the rough sides of channels compared to the bottom and was developing into the middle of the channel.

The biofilm development is uniform within three channels on the device and is suitable for conducting dose-response studies. The uniform biofilm formation after 48h of the growth period was proved. There was no difference in the %area occupied by biofilm on the sides of channels and in their inner parts.

5.3 FABRICATED DEVICE AND ITS SPECIFICATIONS

A fabricated device is a non-reusable device designed to monitor and evaluate biofilm formation processes using microscopy and image analysis. The capabilities of the device are to aid studies of biofilm development with non-destructive observations with multi-channels. It allows for real-time evaluation of biofilm processes like attachment, growth, detachment, and interactions with active ingredients. The device is designed to be used over various flow conditions.

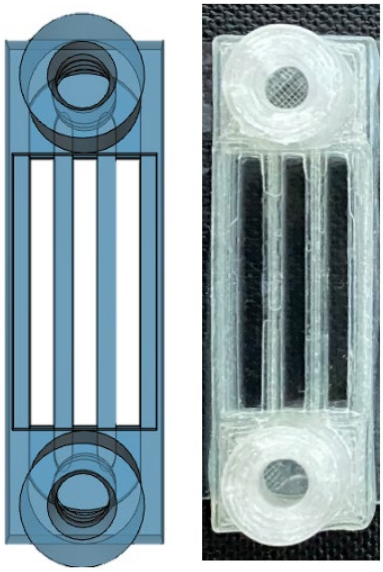

Figure 5.3 Design of a PLA part of the device (left) and final printed device sealed with glass (right).

The fabricated device is a triple-channel flow cell that uses glass as viewing windows. The flow channels are made using PLA plastic. PLA is not autoclavable, and the device needs to be sterilised with 70% ethanol prior to use. The dimensions of the device are listed in Table 5.1.

Table 5.1 Dimensions of the fabricated device.

Device Parameter	Value
Channel length	22 mm
Channel width	2 mm
Channel height	2 mm
Each channel volume	88 mm^3
Chamber volume	54.25 mm^3
Device length	40 mm
Device width	12.5 mm

Each device is constructed by sealing the printed PLA part to glass slides using XTC 3D coating, one on the bottom of the device (25x40mm) and the second over the three channels area (11x21mm), as shown in Figure 5.4. The device is integrated with two cylinders that accommodate 1mm ID tubing.

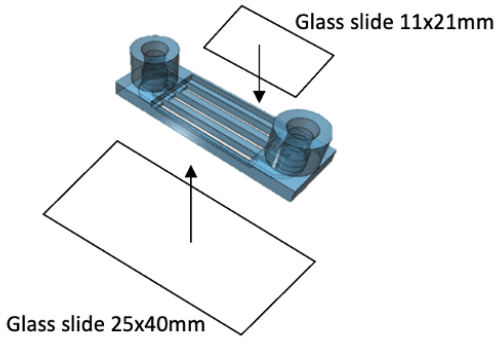

Figure 5.4 Schematic of 3D-printed PLA part of the device and two glass slides.

The device can be easily placed under the microscope for total channel length observations (Figure 5.5).

The device can withstand a flow rate of up to 3ml/min and can go down to 25μl/min without any changes to the uniformity of the flow pattern between the three channels. The operational temperature of the device is up to 60°C. Above this temperature PLA part will deform. During the experiments, devices were placed on a hot plate to maintain the temperature of 37 ± 2°C.

The production cost of one device is about 50 pence, including PLA material, glass pieces and coating.

Figure 5.5 Image illustrating the position of the fabricated device under the light microscope.

5.4 CONCLUSION

Physical validation of device performance was completed to demonstrate the identical behaviour of each individual device and intra-device performance. This was achieved by flow-rate studies that confirmed the matching flow of liquid through each channel within one device and between devices. The flow rate can be reduced to 20μl/min without loss of uniform flow. Quantification of the total biofilm mass was another parameter that was used for validation of the device performance for biofilm formation. Uniform development of biofilm within each channel of the device and inter-device was observed after 48 hours of continuous biofilm growth.

Finally, fabricated device specifications were stated in this chapter including device overall size specifications, channel size specifications and the total volume of liquid inside the device and within each chamber and each individual channel. The operational flow rate range and working temperature of the device were stated and finally, the cost of production of each device was quantified which is around 50 pence.

Chapter 6 PROOF OF CONCEPT 1: DOSE-RESPONSE STUDIES FOR STERILISING AGENTS

The performance of the devices in generating dose-response data was evaluated for two test compounds and benchmarked against analogous studies using static biofilms and biofilms grown in a drip-flow reactor. Two antimicrobial agents, ethanol and chlorhexidine, were used because their action on bacterial cells and biofilms has been extensively studied and reported (57), (58), (59), (60).

6.1 EFFICACY OF ETHANOL AGAINST *E. COLI* BIOFILM

Ethanol is an active component used in disinfectants. It is active against viruses, fungi, and bacteria. Ethanol concentration between 60 and 85% is considered effective against those organisms (61). Ethanol kills bacteria cells through the process of denaturation. Ethanol also dissolves lipids in the cell membrane, which disrupts the membrane and causes the death of cells.

The efficacy of ethanol against biofilms in a fabricated device was studied. The static biofilm assay and continuous method with a drip-flow reactor were compared to the fabricated device to validate its performance.

6.1.1 Action of ethanol on continuous 48h *E. coli* biofilm in the fabricated device

The effect of ethanol concentrations on a continuous biofilm grown in a fabricated device was studied to assess the device's performance. Fluctuation in MGV of biofilm with both staining methods was observed after exposure to different percentages of ethanol - Figure 6.1. Two parameters contribute to the fluctuation of MGV of biofilm in a device. The first factor is the removal of biofilm mass from the surface of channels. The second one is cell death within biofilm when in contact with ethanol. Therefore, these two paraments were studied independently to validate the performance of the fabricated device.

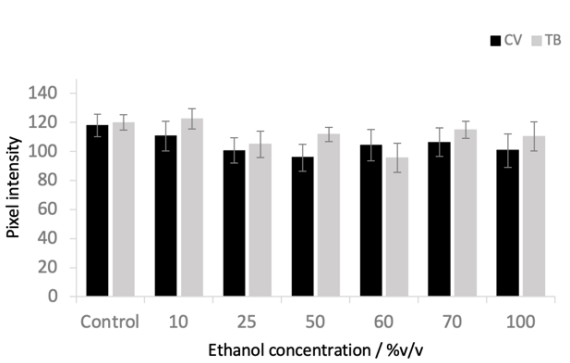

Figure 6.1 Graph showing the MGV of a continuous biofilm formed in a fabricated device after treatment with different ethanol concentrations, N=9, error bars – SD.

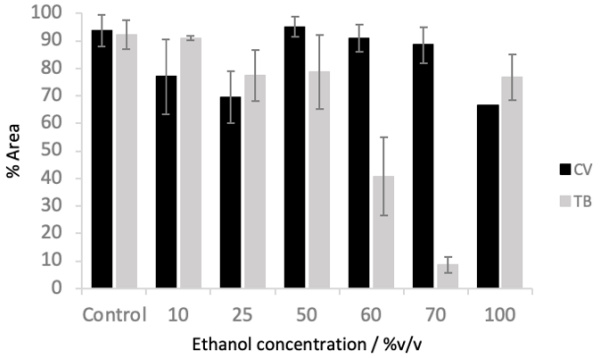

Figure 6.2 Graph of % area occupied by biofilm in a fabricated device after treatment with different ethanol concentrations with trypan blue and crystal violet staining, N=9, error bars – SD.

The gradual decrease of biofilm mass from the surface of the channels was observed with trypan blue staining up to 70% ethanol. At 10% ethanol, no difference in % area occupied by biofilm and a slight difference in pixel intensity distribution was observed compared to untreated biofilm - Figure 6.2, with trypan blue staining. As the ethanol concentration increased, more biofilm mass was removed from the channels when stained with trypan blue. At 25% ethanol, a minor portion of biofilm was removed from the channel. Biofilm appearance changes compared to 10% ethanol-treated biofilm - Figure 6.4. From cloudlike grey colour biofilm with patches of blue staining covering the entire surface of the channel, it changes to dark blue colour with visible empty spaces. At this ethanol concentration, cells within the biofilm begin to die and adsorb more trypan blue but are still attached to the channels' surface.

As the ethanol concentration increases to 70%, only small clusters of cells are present inside channels. Therefore, 10% to 70% ethanol causes the gradual removal of cells from the surface and accelerates cell death within a biofilm. This is supported by the pixel intensity distribution graph - Figure 6.3. As the concentration of ethanol increases from 10% to 70%, the decrease in pixel intensity Group 3 (103-153) is observed, from 90% within the biofilm area to 0%, respectively. This is due to the synergistic effect of biofilm removal from the surface and cell death. More significant biofilm removal was observed at 60% and 70% ethanol. The reduction from 92% area of untreated biofilm to 9% after treatment with 70% ethanol was observed. The addition of absolute ethanol to the biofilm system caused a lesser effect on biofilm. Pure ethanol is less effective as a disinfectant agent due to the coagulation of proteins in the outer cell membrane that protects

cells from death. It also evaporates very quickly and does not have enough time to penetrate the biofilm.

The combined effect of biofilm removal from the surface of channels and cell death within biofilm was observed when exposed to ethanol and stained with trypan blue.

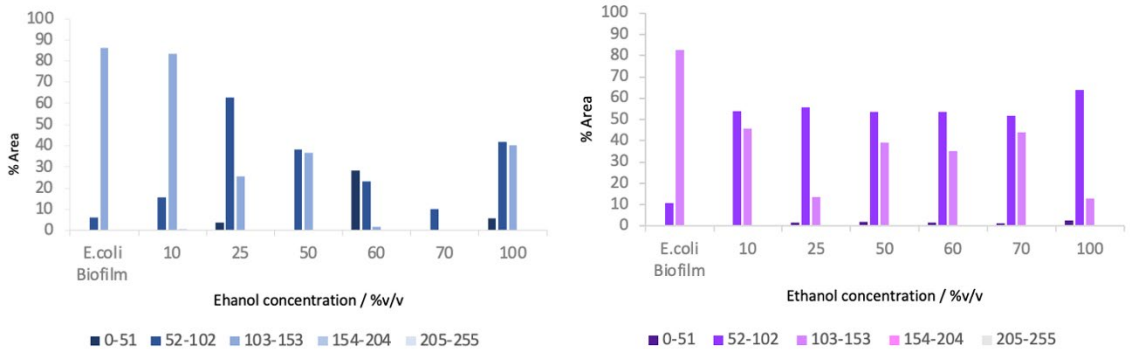

Figure 6.3 Graphs for pixel intensity distribution in a biofilm within a fabricated device. Left – trypan blue staining, right – crystal violet staining.

Fluctuation in %area of biofilm biomass was observed across all percentages of ethanol with crystal violet staining (Figure 6.2). Pixel intensity distribution within biofilm has similar allocations across all concentrations of ethanol - Figure 6.3, but differs from the untreated biofilm. There are two possible explanations for this observation. The first one – ethanol does not affect biofilms at any concentrations. This cannot be true because the effect of ethanol is extensively studied and was chosen for this study for its known action as a sterilising agent.

Furthermore, the pixel intensity distribution of untreated biofilm differs significantly from ethanol-treated biofilms. The second proposed explanation to this observation is bacteria cells release their intracellular proteins/DNA/lipids into the EPS during lysis, and crystal violet binds to them during staining. The visual appearance of biofilm after 70% ethanol exposure differs from lower concentrations of ethanol (Figure 6.4). It appears lighter, with grey/light purple areas, which differs from pink untreated biofilm in a device and biofilms treated with lower ethanol concentrations.

Two staining methods present different results when a biofilm is treated with the same ethanol concentration. Trypan blue and crystal violet have different action mechanisms when binding to biofilms. This might contribute to the difference in results observed.

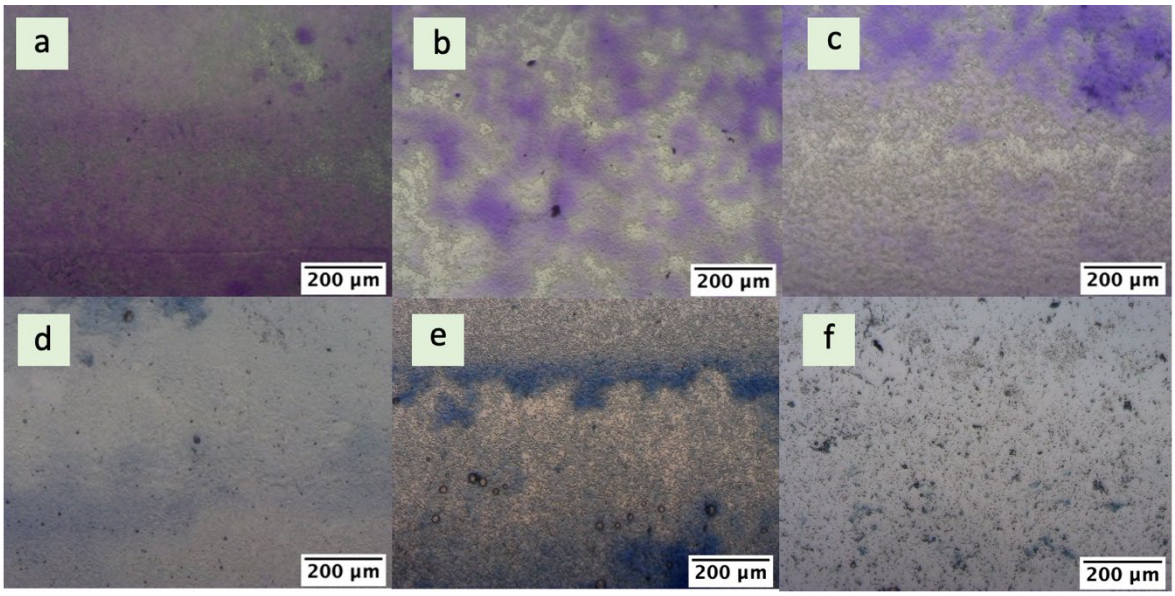

Figure 6.4 Images of biofilm in a fabricated device after exposure to different ethanol concentrations: a – 10% ethanol, crystal violet, b – 25% ethanol, crystal violet, c – 70% ethanol, crystal violet, d – 10% ethanol, trypan blue, e – 25% ethanol, trypan blue, f – 70% ethanol, trypan blue, digital magnification 64x.

If a sterilising compound kills and enhances the biofilm's detachment from the surface, it will be visible in the fabricated device. Two surfaces are present in a device – rough PLA on the sides of the channels and smooth glass in the middle of each channel. Hence two areas of biofilm within each channel were investigated – the sides and middle part of the channel.

After treatment with different ethanol concentrations, the distribution of biofilm within channels – side and middle, was plotted - Figure 6.5 and Figure 6.6. No difference in %area occupied by biofilm was observed when comparing individual channels of one device and inter-devices after exposure to 10% ethanol with trypan blue staining, N=9. No difference was observed when comparing the channels' side and middle space. Also, no difference was observed in the distribution of the biofilm in a device when staining with crystal violet; however, less area of channels was occupied by biofilm after exposure to 10% ethanol. When 70% ethanol was used, no difference in biofilm removal was observed between the channels when comparing different devices. %Area of the remaining biofilm on the sides was 1.53 times higher than in the middle of the channel. This is undoubtedly due to the different surface roughness of the side and middle of the device. With crystal violet staining, no reduction in the %area occupied by biofilm was detected, but the same biofilm distribution between the sides of the channels and the inner parts and between individual channels in devices was observed. This supports the idea that more biofilm biomass staining occurs as the ethanol concentration increases with crystal violet.

These observations further prove the uniformity of the flow within the device and uniformity of biofilm growth within the fabricated device, and evenness of active ingredient delivery to the biofilm in each channel.

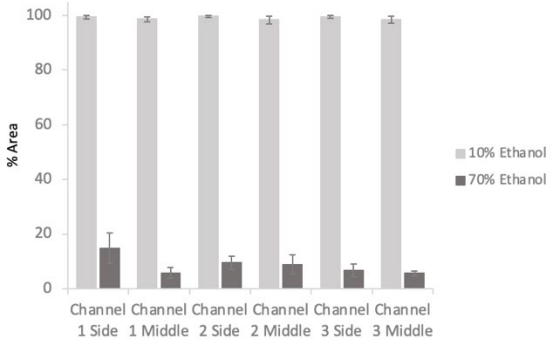

Figure 6.5 Graph showing biofilm distribution across each channel in a device after exposure to 10% and 70% ethanol, trypan blue, N=9, error bars – SD.

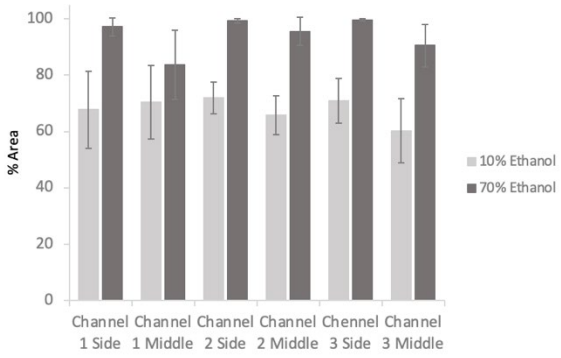

Figure 6.6 Graph showing the distribution of biofilm across each channel in a device after exposure to 10% and 70% ethanol, crystal violet, N=9, error bars – SD.

6.1.2 Effect of ethanol on static 24h E. coli biofilm

24h biofilms were treated with different ethanol concentrations to determine their effect on biofilm viability. No change in biofilm MGV was observed up to 50% ethanol with both staining dyes Figure 6.7. Above 60% ethanol, the decrease in MGV of biofilm stained with crystal violet dye was observed. Trypan blue staining had a lesser decrease in MGV as a concentration of ethanol increased from 60% to 100%.

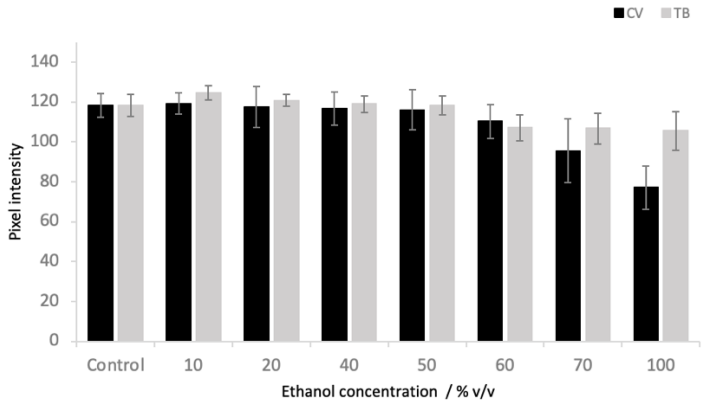

Figure 6.7 Graph showing the MGV of static biofilm across ethanol concentrations by two staining methods, N=12.

The pixel intensity distribution of biofilms treated with different concentrations of ethanol was plotted against the %area they occupy within the biofilm (Figure 6.8). Both staining methods have the same trend in pixel intensity distribution—no change to untreated static *E. coli* biofilm up to 50% ethanol. At 60% ethanol and above, the change was observed in pixel distribution with both dyes. Trypan blue staining also presents no difference in pixel intensity distribution between 60% and 100% ethanol. Biofilms after exposure to 60%, 70% and 100% ethanol had an increase in %area occupied by pixel Group 2 (52 – 102) from 0% to 30% and a decrease in pixel Group 3 (103 – 153) from 95% to 65%. This demonstrates that above 60% ethanol number of dead cells within biofilm increases, as demonstrated in previous studies (61) and has the same effect on biofilm viability at all concentrations above 60%.

Results obtained with crystal violet staining have the same trend up to 50% ethanol - no change in pixel intensities distributions compared to untreated biofilm. At 60% ethanol pixel intensity, Group 2 (52 – 102) doubles in the %area it occupies within a biofilm. As the ethanol concentration increases from 60% to 100%, there is a further increase in pixel intensity in group 2 and a subsequent decrease in the percentage of pixels in Group 3 (103 – 153). At 70% and 100% ethanol, pixel intensity Group 1 (0 – 51) shows an increase in Figure 6.8. As the ethanol concentration increases above 60%, more crystal violet dye is absorbed by the biofilm, which differs from the trend obtained when staining with trypan blue. This might be due to the release of intracellular components into the biofilm that binds crystal violet. This contributes to the increased dye absorption by biofilm as the concentration of ethanol increases from 60% to 100%.

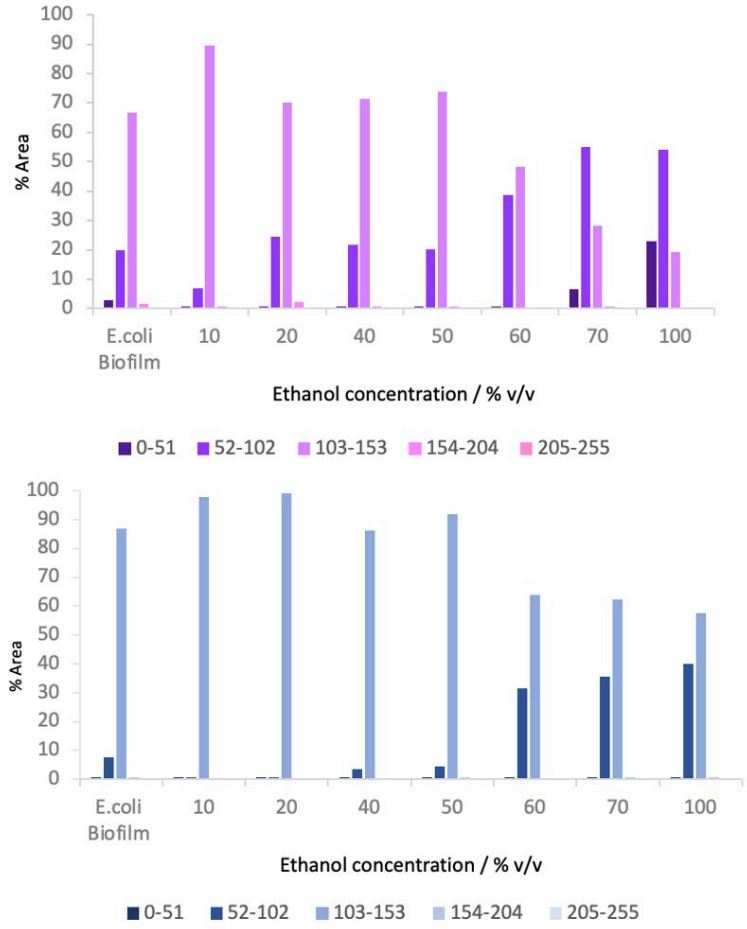

Figure 6.8 Graphs showing pixel intensity distribution against % area they occupy in a biofilm at different ethanol concentrations with crystal violet (top) and trypan blue (bottom) staining.

Another parameter that was measured after biofilm exposure to different concentrations of ethanol was the %area occupied by biofilm to investigate the effect of bacterial cell detachment. Figure 6.9 shows no biofilm detachment from the surface at any ethanol concentration. Therefore, ethanol above 60% kills bacteria cells within the biofilm but does not cause biofilm detachment from the surface if no mechanical force is applied.

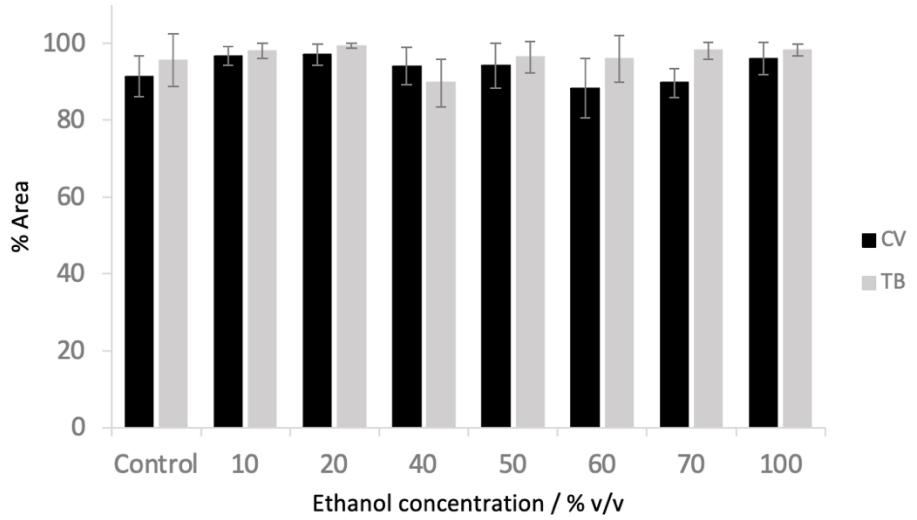

Figure 6.9 Graph showing the % area occupied by static *E. coli* biofilm after exposure to different ethanol concentrations, staining with crystal violet and trypan blue, error bars – SD.

6.1.3 Reaction of ethanol with continuous 48h E. coli biofilm in Drip-flow reactor

The structure of a biofilm grown in a drip-flow reactor is uneven in configuration. Parts of biofilm that are rougher compared to flatter parts will appear darker when stained due to the thickness of the layers. This is an uncontrollable process of biofilm formation within a drip-flow reactor.

No difference in biofilm pixel intensity composition and MGV was observed at any ethanol concentrations with crystal violet staining agent - Figure 6.10. It was suggested that due to the uneven structure of biofilm and binding of crystal violet to the living and dead cells, and EPS of biofilm, it is impossible to observe the effect of ethanol on *E. coli* biofilm with this method of staining. The pixel composition of untreated biofilm does not differ from biofilm exposed to any ethanol concentrations but differs visually - Figure 4.7. Therefore, this method is unsuitable for determining the effect of ethanol on continuous biofilm formed in a drip-flow reactor.

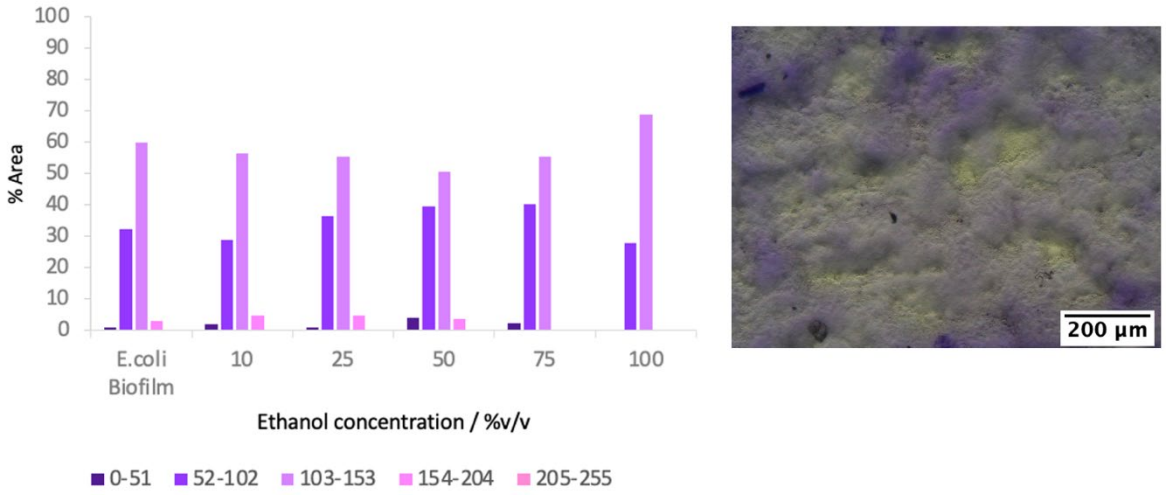

Figure 6.10 Graph showing % area of pixel intensity distribution within biofilms at different ethanol concentrations with crystal violet staining and image of biofilm after treatment with 70% ethanol, digital magnification 64x.

Trypan blue was used to stain biofilm after exposure to different ethanol concentrations. As the concentration of ethanol increases, the MGV of biofilm gradually decreases from 120 to 80 MGV until 40% ethanol is reached and fluctuates between 40% and 80% - Figure 6.11. At 100% ethanol concentration, the MGV of biofilm increases up to the level of 10% ethanol concentration, as with the fabricated device.

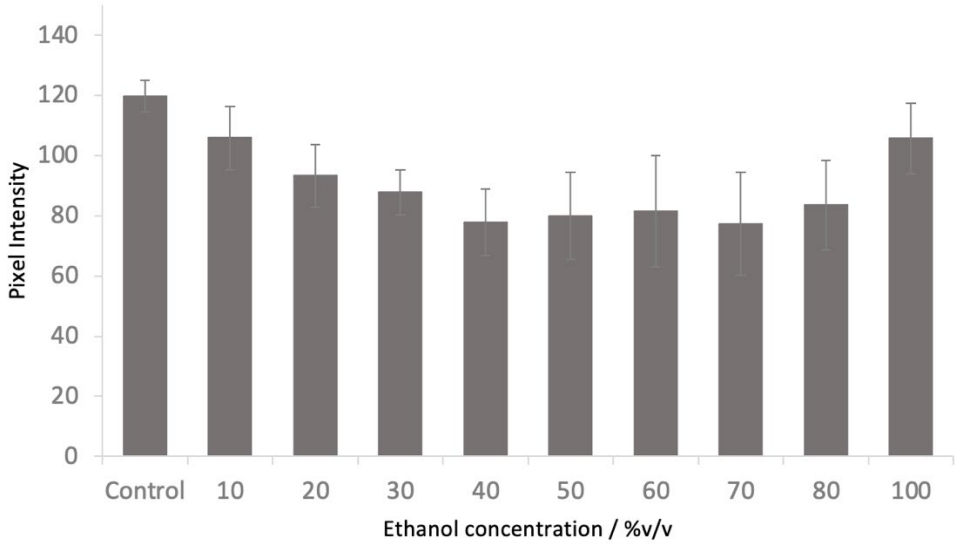

Figure 6.11 Graph showing the MGV of biofilm in a drip-flow reactor after treatment with different concentrations of ethanol, N9, error bars – SD.

With trypan blue staining, a clear trend in pixel intensity distribution was observed after exposure of biofilms to different concentrations of ethanol. Three regions can be identified on the pixel intensity distribution graph - Figure 6.12. The first region is from 10% to 30% ethanol. A gradual decrease in pixel Group 3 (103 – 153) and an increase in pixel Group 2 (52 – 102) are observed.

This shift in pixel intensities contributes to the decrease in MGV as a greater biofilm area appears darker after staining compared to untreated biofilm. The second distinct region is from 40% to 70% ethanol, where pixel intensity composition remains the same with the domination of pixel Group 2 (51-102) with about 60% of biofilm and fluctuation in pixel Group 1 (0-51) and 3 (103-153). This suggests no difference between 40% and 70% ethanol of biofilm viability. The third region is between 80% and 100% ethanol. A decrease in a pixel in Groups 1 (0-51) and 2 (52-102), together with an increase in pixels of Group 3 (103-153), indicate a lesser effect of ethanol concentrations above 70% on biofilm viability. These trends were possible to observe due to the trypan blue capacity to selectively bind dead cells only in a biofilm in contrast to the crystal violet staining agent.

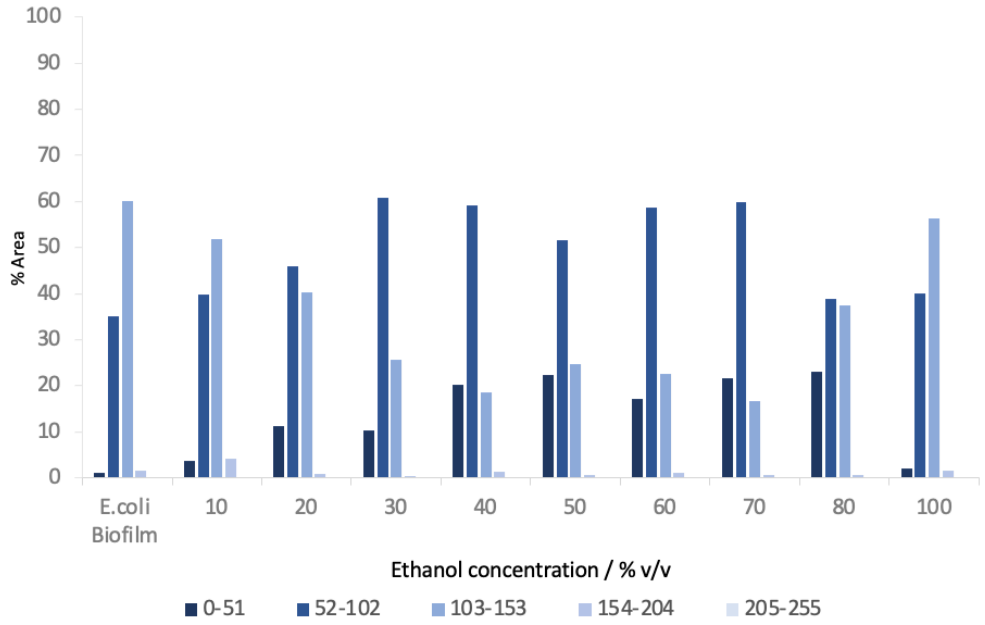

Figure 6.12 Graph showing the composition of pixel intensities in a biofilm subjected to different concentrations of ethanol with trypan blue dye staining.

No removal of biofilm mass grown in a drip-flow reactor from the surface was observed after treatment with ethanol - Figure 6.13.

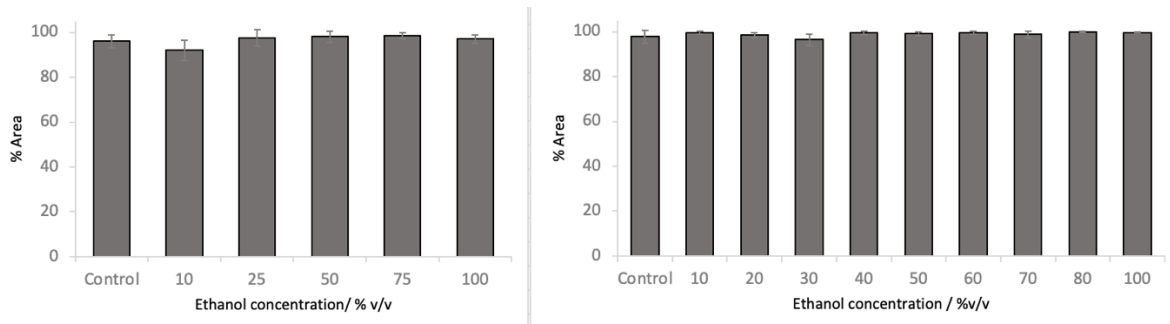

Figure 6.13 Graphs of % Area occupied by biofilm after treatment with different concentrations of ethanol. Crystal violet staining – left, trypan blue – right, N=9, error bars – SD.

6.2 EFFICACY OF CHLORHEXIDINE AGAINST E. COLI BIOFILM

Chlorhexidine (CHX) is another widely used antimicrobial agent. Chlorhexidine is active against gram-positive and gram-negative bacteria, fungi and viruses (62). It inhibits bacterial growth and kills bacterial cells. Chlorhexidine attaches to the phospholipid bilayer of cell walls and causes the rapture of the cell (63). This bursts cells open, leading to lysis and cell death. The uptake of chlorhexidine by cells is very rapid. At low concentrations, chlorhexidine binds to the cell membranes, breaks the membranes, enters the cell, and causes cell lysis. At high concentrations chlorhexidine solidifies the cytoplasm (64). Studies demonstrate that chlorhexidine can inhibit the adherence of microorganisms to the surfaces during biofilm formation (65). The most frequently used concentrations of chlorhexidine are in the range of 0.1% to 0.2%. The concentration that is used depends on the degree of sensitisation that is required and the sensitivity of the surface (66), (67).

6.2.1 Investigation of action of chlorhexidine on a continuous 48h biofilm in fabricated devices

When analysing the effect of CHX concentrations on biofilm within a fabricated device, two parts of the channel were considered – the sides of the channels and the middle part. With trypan blue staining, no biofilm removal from the channels' sides was observed at all concentrations of CHX - Figure 6.14. There was a reduced %area coverage of biofilm in the middle of channels compared to the sides and untreated biofilm due to the combined effect of flow through channels and CHX - Figure 6.15.

As the concentration of CHX increased to 0.16%, the reduction in %area covered by biofilm on the side of the channels decreased, with crystal violet staining (Figure 6.14). The gradual biofilm reduction was observed in the middle of the channels – (Figure 6.15).

Treatment of biofilm with different concentrations of CHX affected biofilm mass removal from the sides of the channels to a minor extent compared to ethanol but removed biofilm from the middle of the channels. This is more evident with crystal violet staining.

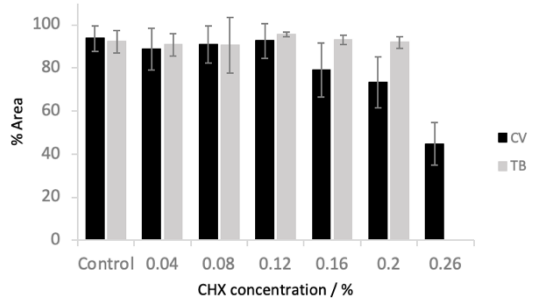

Figure 6.14 Graph showing the % area on the sides of channels occupied by biofilm in a fabricated device after CHX treatment N=9, error bars – SD.

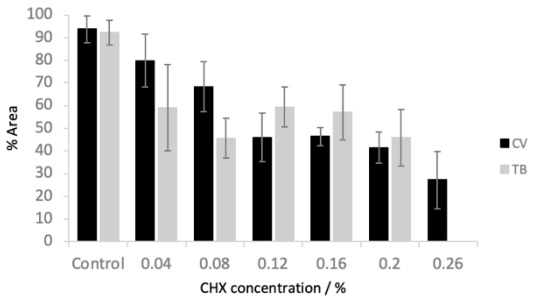

Figure 6.15 Graph showing the % area in the middle of channels occupied by biofilm in a fabricated device after CHX treatment, N=9, error bars – SD.

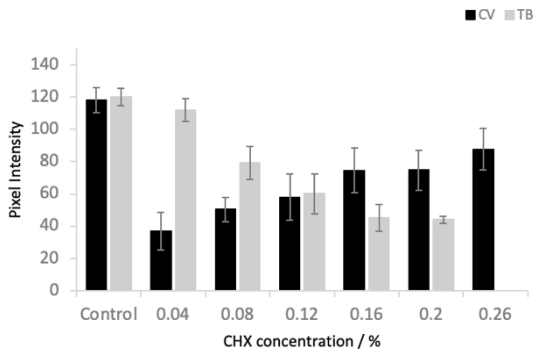

Figure 6.16 Graph of MGV of biofilm in a fabricated device side area after CHX treatment, N=9, error bars – SD.

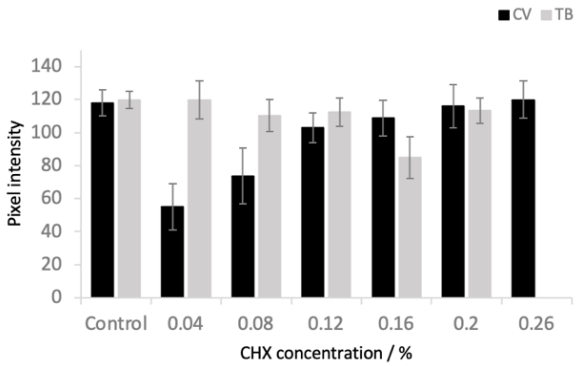

Figure 6.17 Graph of MGV of biofilm in a fabricated device middle area after CHX treatment, N=9, error bars – SD.

Two opposite trends were observed in MGV distribution within biofilm with two staining methods. With trypan blue staining, as the concentration of CHX increased from 0.04% to 0.2%, the MGV of biofilm decreased from 112 pixels to 44 pixels, respectively, in the side area of the channels – (Figure 6.16). In the middle part of the channel, MGV fluctuated at a 110-pixel level (Figure 6.17). MGV of biofilm stained with crystal violet after treatment with CHX increased as the concentration of CHX increased from 0.04% to 0.26%. Before that, there was a significant drop in MGV of untreated biofilm compared to biofilm after 0.04% of CHX. This is due to the combined effect of biofilm removal from the surface as the concentration of CHX increases from 0.04% to

0.26% and due to the inability of crystal violet to distinguish between live/dead cells and EPS of biofilm. Staining of crystal violet depends on the depth of the biofilm; hence as biofilm mass reduces, there is less staining and lighter MGV of a sample.

The pixel intensity distribution of biofilm stained with trypan blue shifts from 68.91% of Group 3 (103 – 153) at 0.04% CHX to 2.69% at 0.2% CHX - Figure 6.18. Pixel Group 1 (0 – 51) increases from 0% at 0.04% CHX to 64.58% at 0.2% CHX. As the concentration of CHX in the sample increases, MGV of biofilm decreases and pixel intensities shift to darker regions of the spectra. Hence more dead cells are present in the biofilm and are not being removed from the surface of the channels. With trypan blue staining, increased cell death was observed as the concentration of CHX increased, but no biofilm removal from the channels' sides was observed.

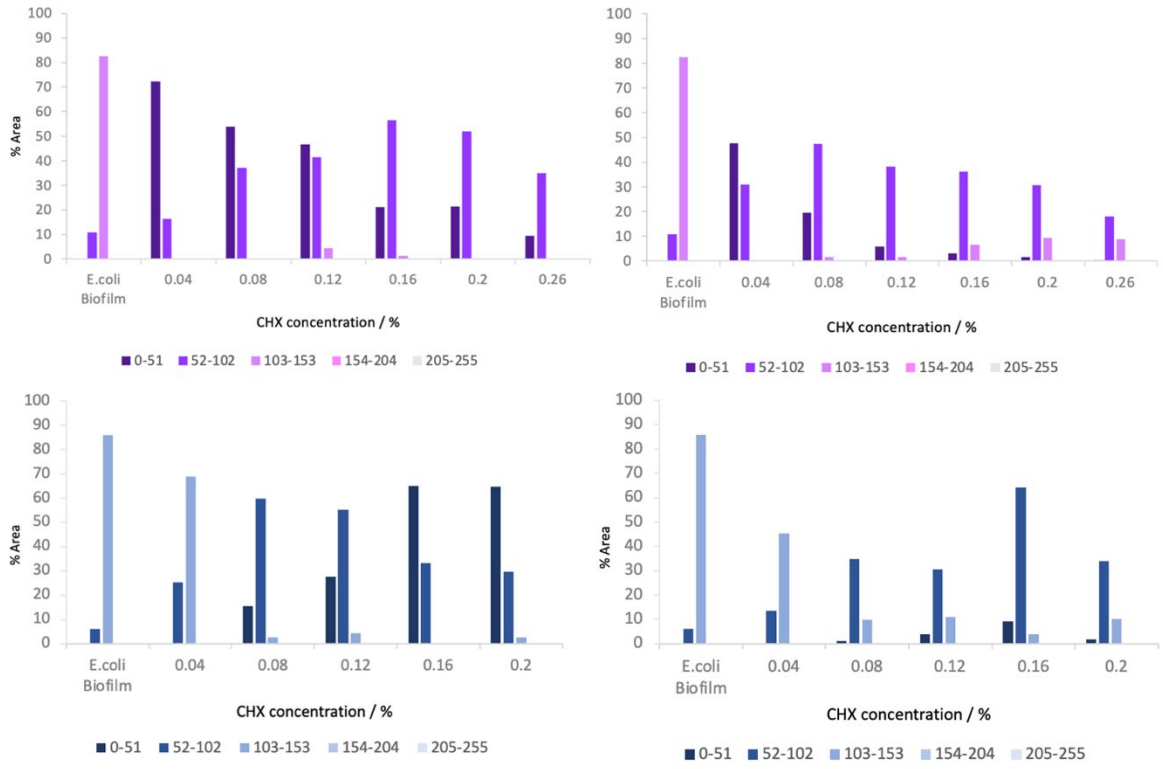

Figure 6.18 Graphs of pixel intensity distribution within biofilm after exposure to CHX concentrations. Top left – biofilms in the side of channels with crystal violet staining, top right – biofilms in the middle of the channels with crystal violet, bottom left – biofilms in the sides of the channels with trypan blue and bottom right – biofilm in the middle of the channels with trypan blue staining.

Both staining methods demonstrate biofilm removal from the middle of the channels when exposed to different concentrations of chlorhexidine. Both methods show higher MGV of biofilm in the middle of the channels compared to the values on the side of the channels. This is due to

the removal of biofilm from the middle of the channels. Hence, CHX not only kills bacteria cells within biofilm but also promotes attachment of biofilm.

Two methods show opposite effects when measuring MGV of biofilm exposed to different concentrations of chlorhexidine. As the concentration of CHX increases, there is a gradual decrease in MGV of biofilm stained with trypan blue. The gradual decrease begins from untreated (control) biofilm that fits this trend. Hence, as chlorhexidine concentration increases, biofilm absorption of dye increases, lowering the MGV of biofilm. Crystal violet staining shows a big difference between untreated biofilms MGV and 0.04% chlorhexidine, after which a gradual increase of MGV is observed.

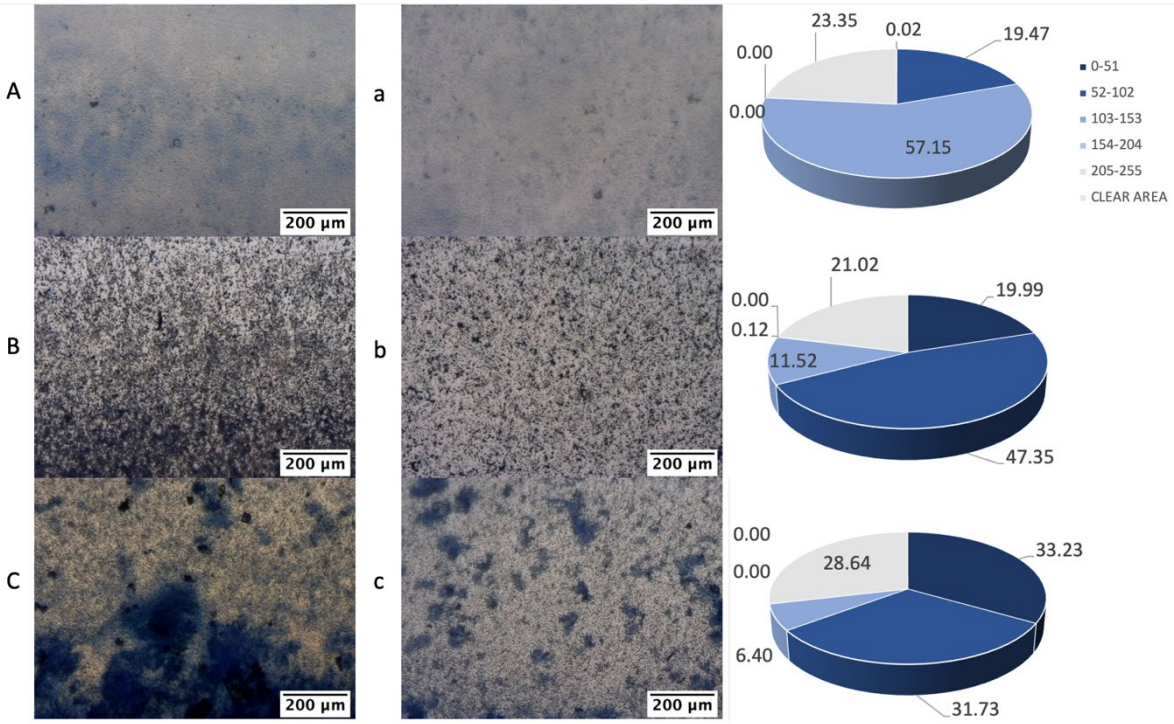

Figure 6.19 Images of biofilm in a fabricated device after CHX treatment and pie charts of their pixel intensity distribution, trypan blue staining. A – 0.04% CHX side of the channel, a – 0.04% CHX middle of the channel, B – 0.12% CHX side, b – 0.12% CHX middle, C – 0.2% CHX middle, c – 0.2% CHX side, digital magnification 64x.

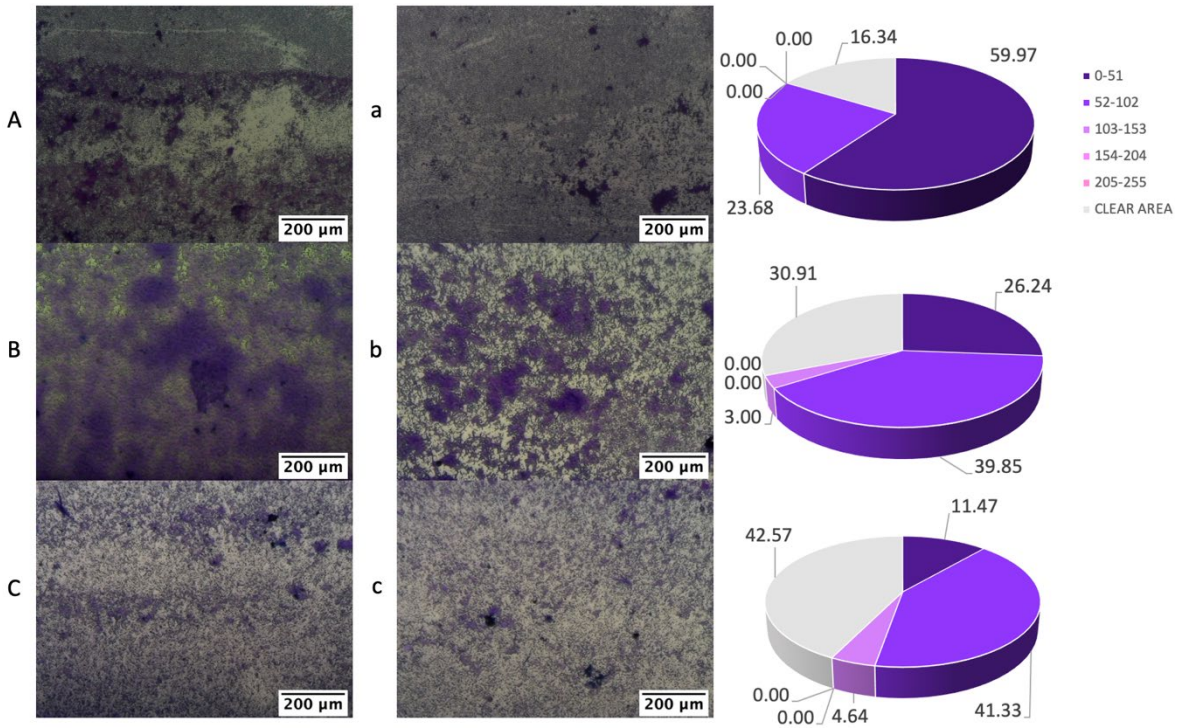

Figure 6.20 Images of biofilm in a fabricated device after CHX treatment and pie charts of their pixel intensity distribution, crystal violet staining. A – 0.04% CHX side of the channel, a – 0.04% CHX middle of the channel, B – 0.12% CHX side, b – 0.12% CHX middle, C – 0.2% CHX middle, c – 0.2% CHX side, digital magnification 64x.

Pixel distribution within biofilm with crystal violet staining presents a decrease in pixel intensity Group 1 (0 – 51) from 72.33% of the area within biofilm at 0.04% CHX to 9.55% of the biofilm area at 0.26% CHX. Pixel Group 2 (52 – 102) increases from 16.47% area at 0.04% CHX to 56.47% at 0.16% CHX - Figure 6.18. The total number of pixels decreases as the concentration of CHX increases as the biofilm area decreases within channels.

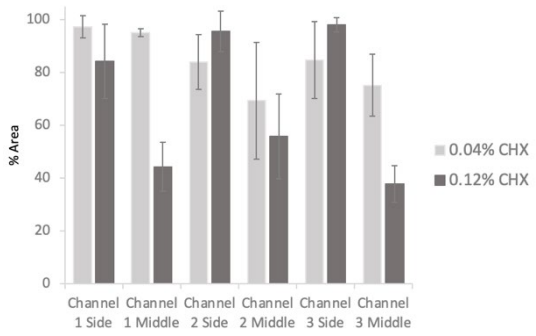

Figure 6.21 Graph showing the distribution of biofilm across each channel in a device after exposure to 0.04% and 0.12% CHX, trypan blue, N=9, error bars – SD.

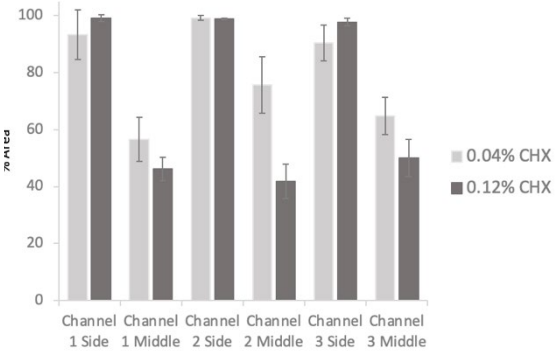

Figure 6.22 Graph showing the distribution of biofilm across each channel in a device after exposure to 0.04% and 0.12% CHX, crystal violet, N=9, error bars – SD.

The biofilm distribution between channels with trypan blue staining after treatment with CHX shows the same pattern between channels – (Figure 6.21). The abundance of biofilm on the sides of the channels at both concentrations and reduction of % area occupied by biofilm in the middle. 0.12% CHX causes more excellent biofilm removal from the middle of the channels compared to 0.04%. With crystal violet staining, there is a lesser reduction of biofilm from the middle of the channels at 0.04% CHX, but the distribution between channels is similar.

6.2.2 Effect of chlorhexidine on static 24h E. coli biofilm.

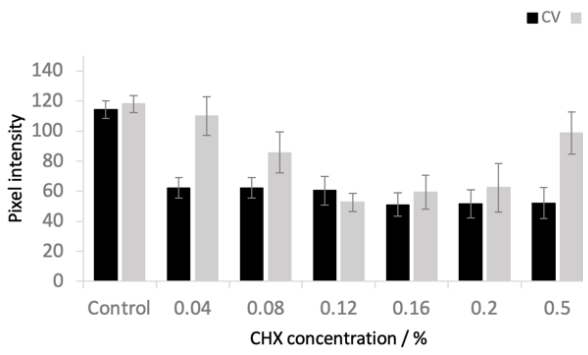

Figure 6.23 Graph showing the MGV of static biofilm after CHX treatment with crystal violet and trypan blue staining, N=12, error bars – SD.

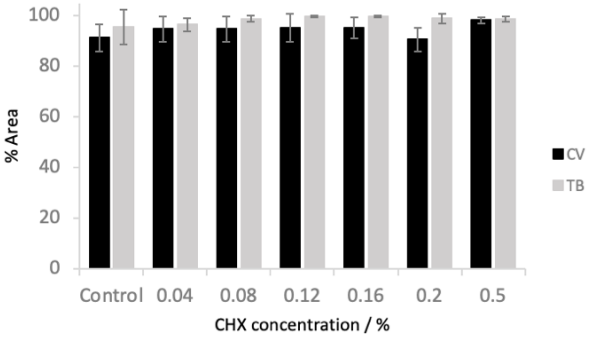

Figure 6.24 Graph showing the % area of static biofilm after CHX treatments with crystal violet and trypan blue staining, N=12, error bars – SD.

CHX does not cause the removal of developed biofilm from the surface (Figure 6.24). MGV of biofilm treated with CHX is 60 MGV at 0.04%, 0.08% and 0.12% CHX with crystal violet staining and decreases to 50 MGV with 0.16%, 0.2% and 0.5% CHX – (Figure 6.23). With trypan blue staining, there is a decrease in MGV from 110 at 0.04% CHX to 52 at 0.12% CHD. As the concentration of CHX increases further, the MGV increases up to 98 at 0.5% CHD.

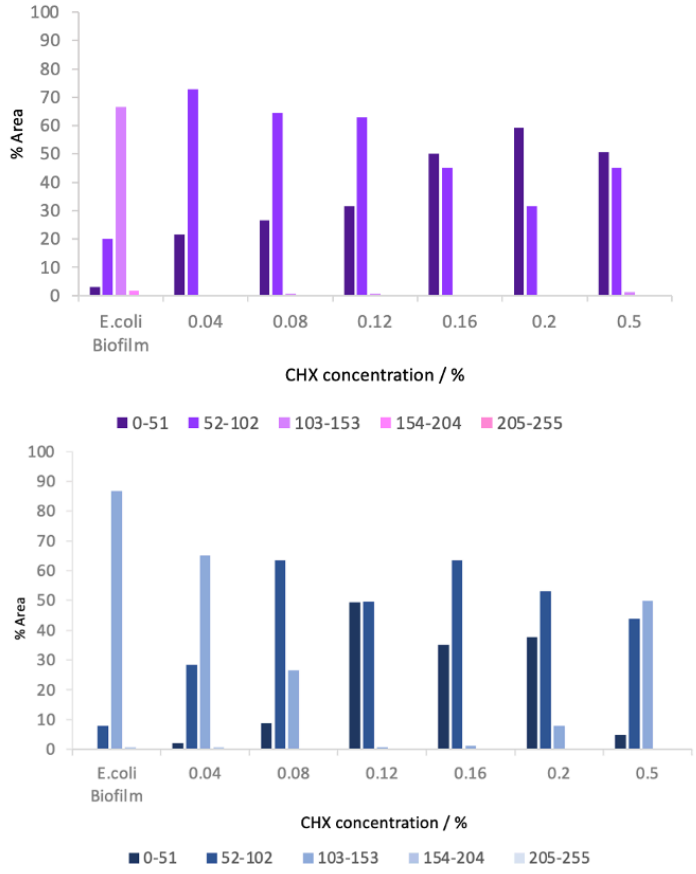

Figure 6.25 Graphs of pixel intensity distribution within biofilm after treatment with CHX, top – crystal violet, bottom – trypan blue staining.

At a low concentration of CHX, such as 0.04%, pixel intensity distribution differs from untreated static biofilm with crystal violet staining – (Figure 6.25). No pixels from Group 3 (103-153) are present in biofilms after CHX treatment. As the concentration of CHX increases from 0.04% to 0.5%, pixel Group 2 (52 – 102) decreases from 73% within biofilm at 0.04% to 31% at 0.2% CHX. Group 1 (0 – 51) increases within the biofilm as the concentration of CHX increases from 22% at 0.04% CHX to 59% at 0.2% CHX within a biofilm. 0.5% CHX causes modifications to the biofilm and crust formation on the surface of the biofilm that might be due to cytoplasm solidification.

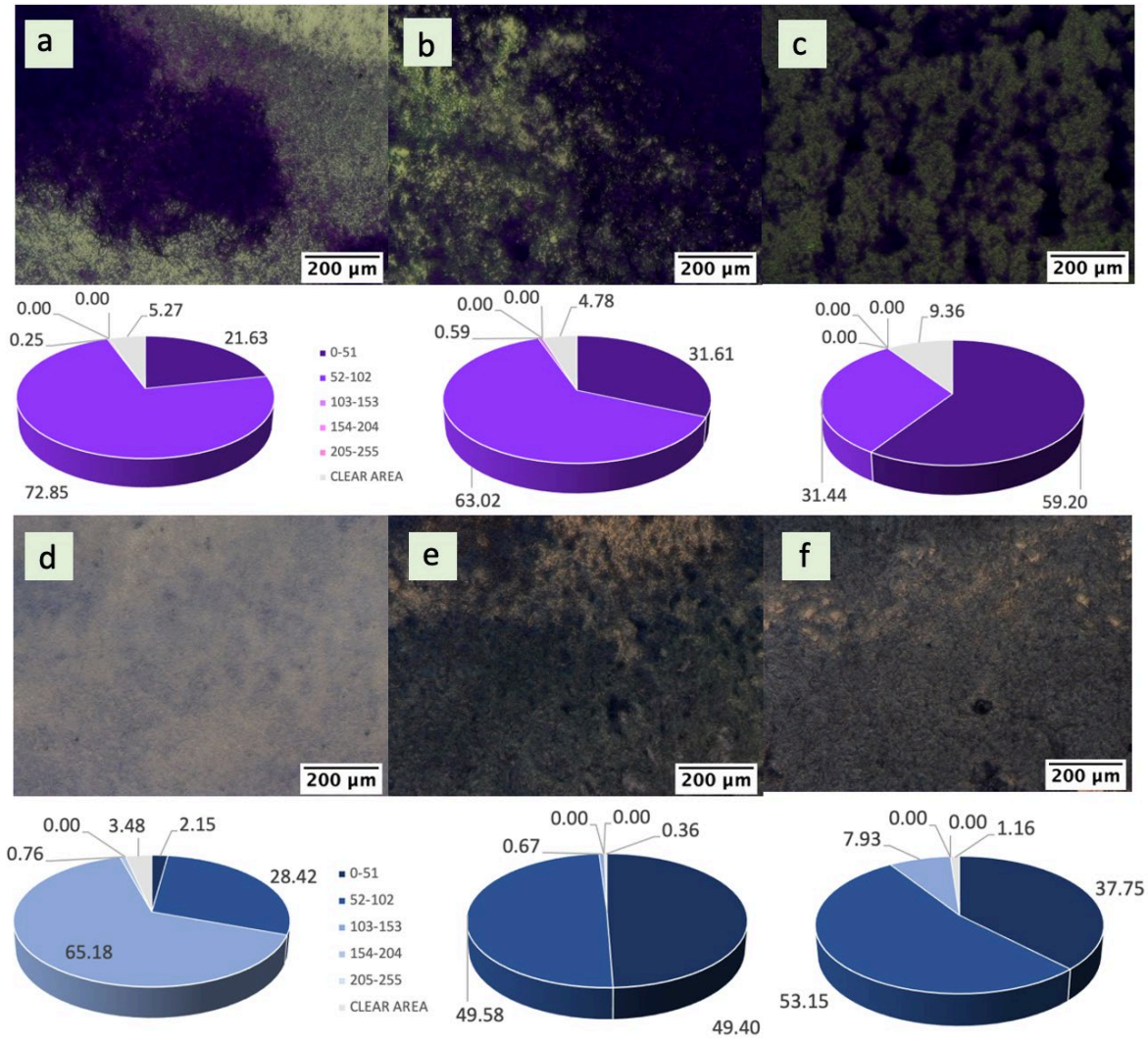

Figure 6.26 Images of biofilms after CHX treatment and their pie charts of pixel intensity distribution, a – c – crystal violet, d – f – trypan blue. a - 0.04% CHX, b – 0.12% CHX, c – 0.2% CHX, d – 0.04% CHX, e – 0.12% CHX, f – 0.2% CHX, digital magnification 64x.

With trypan blue staining, MGV of biofilm decreases as the concentration of CHX increases to 0.12% - (Figure 6.23). More dye is absorbed by biofilm; hence 0.12% CHX is the most effective against *E. coli* biofilm. At this concentration, pixel intensity distribution within biofilm consists of Group 1 (0 – 51) and Group 2 (52 – 102) in equal parts – (Figure 6.25). As concentration increases further, MGV increases; hence higher concentrations are less effective. At 0.5%, a CHX crust is observed on the surface of the biofilm. Biofilm changes from cloudlike white when untreated to blue at 0.04% CHX. As the concentration of CHX increases, biofilm becomes darker due to increased cell death and dye absorption (Figure 6.26).

6.2.3 Study of the effect of chlorhexidine on continuous 48h biofilm in Drip-flow reactor

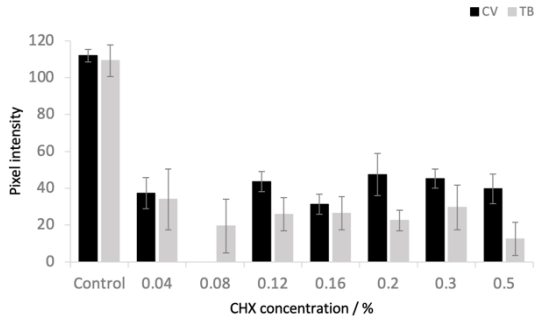

Figure 6.27 Graph of MGV of biofilm in a drip-flow reactor after treatment with CHX, N=9, error bars – SD.

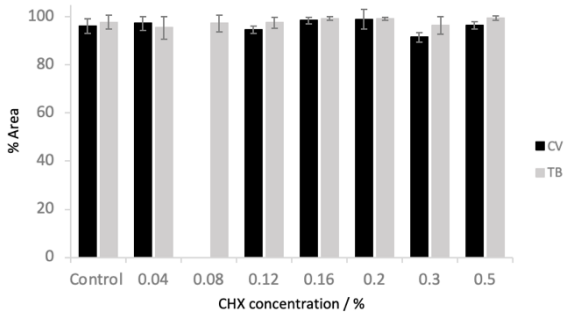

Figure 6.28 Graph of % area of biofilm in a drip-flow reactor after treatment with CHX, N=9, error bars – SD.

No biofilm removal was observed after CHX treatment – (Figure 6.28), and low MGV of biofilm indicate a high proportion of both dye's absorption into biofilm – (Figure 6.27). Two identical trends in pixel intensities distribution were observed with both dyes – the high peak of pixel intensities of Group 1 (0 – 51) and a small fraction of Group 2 (52 – 102). No gradual change in pixel intensity composition was observed across all concentrations of CHX. 0.04% CHX solution has the same effect on biofilm as 0.2% CHD.

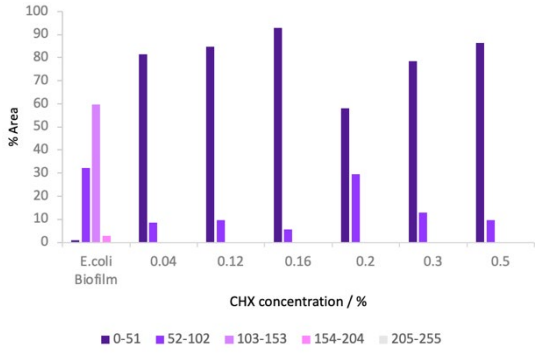

Figure 6.29 Graphs showing pixel intensity composite of biofilm after CHX treatment, crystal violet.

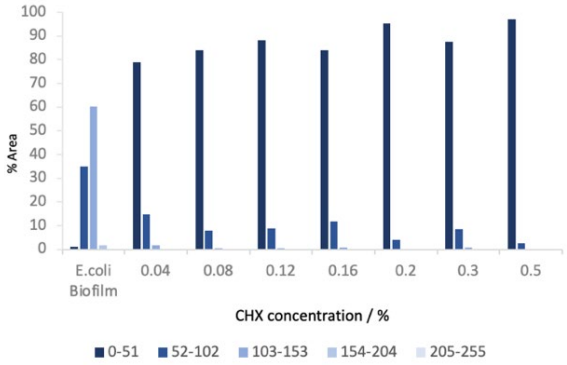

Figure 6.30 Graphs showing pixel intensity composite of biofilm after CHX treatment, trypan blue.

6.2.4 Testing the exposure of 72h E. coli biofilm to the chlorhexidine concentrations

To further confirm the 48h growth time for continuous biofilm, 72h biofilm was treated with CHX to compare the results. No biofilm mass was removed after treatment with CHX concentrations. The pixel intensity distribution pattern is the same as with 48h biofilm – all concentrations of CHX

have the same effect on continuous biofilm. 72h biofilm is thicker than 48h biofilm; hence an increase in pixel intensity Group 2 (52 – 102) compared to 48h biofilm was observed – (Figure 6.31). Therefore, 48h biofilm growth time is enough for the dose-response studies, and no need for extended experiment time is justified.

Figure 6.31 Graph showing the pixel intensity distribution of 72h continuous growth biofilm, crystal violet staining.

6.3 ETHANOL AND CHLORHEXIDINE EFFECT ON *E. COLI* BIOFILM: INTER-METHOD COMPARISON.

A fabricated device can be used to investigate the effect of sterilising agents on cell viability and detachment of developed biofilm from the surface. Both ethanol and chlorhexidine studies demonstrate biofilm removal from the middle of channels. A lesser amount of biofilm was removed from the sides of the channels due to the difference in surface roughness. More substantial biofilm was formed on the sides of the channels. It is suggested that biofilm formation begins from the sides of the channels and spreads towards the centre. This was supported by (Figure 5.2), where biofilm mass is greater on the sides of each channel compared to the middle part after 24 hours growth. After 48 hours, the whole channel is occupied by biofilm equally. This is due to the surface roughness of PLA compared to smooth glass. As no difference between the sides and middle part of the channels in the biofilm was observed with an untreated biofilm that was growing at constant flow, the removal of the biofilm is due to the activity of ethanol/chlorhexidine. As the concentration of active ingredient increased, more biofilm was removed.

Removal of biofilms from the sides of the channels in the fabricated device is minor compared to the middle part. Those biofilms can be used for viability studies, shown by both ethanol and chlorhexidine.

The detachment of formed biofilm was not observed after the addition of ethanol or chlorhexidine to biofilms formed in static conditions or the drip-flow rector.

The structure of each biofilm grown by three different methods had unique forms, each different from the others. Static biofilm is flat and smooth. Continuous biofilm in a drip-flow reactor has a very uneven structure with flat and bumpy areas. Continuous biofilm in a fabricated device is dense on the sides of the channels and less dense in the middle, uniform in the structure due to continuous liquid flow in the channels. Because of this difference, the effect of antibacterial agents varied on each film.

Ethanol above 60% concentration kills cells in a static biofilm (61), which was shown by trypan blue staining. In a biofilm grown in a drip-flow reactor, there was no difference between the 40% and 70% concentrations of ethanol. This is due to the uneven, very rough structure of biofilm in a drip-flow reactor. Ethanol did not cause any removal of biofilm grown by these two methods. In a fabricated device, as a concentration of ethanol reached 70%, removal of biofilm was observed from 100% area of biofilm to 10% area. Biofilm was not present at 70% of ethanol; only small clusters of cells were visible. As has been shown previously (61), 60-80% of ethanol kills bacteria more effectively than lower or higher concentrations of ethanol.

With crystal violet staining, no such trends were observed due to the binding mechanism of crystal violet to EPS of biofilm. Both continuous biofilms had the same pattern in their pixel distributions across all concentrations of ethanol. Crystal violet staining cannot be used to determine viability of biofilm, but can be used to observe total biofilm mass, staining all bacterial cells and components of EPS (54). No removal of total biofilm mass was observed in a fabricated device with crystal violet staining. A change of the biofilm visual appearance was observed instead, which may result in binding of crystal violet to cell components released to EPS after lysis.

As the concentration of chlorhexidine increased, MGV of static biofilm decreased and this is reinforced by the pixel intensity distribution graph. Chlorhexidine was the most effective at a concentration of 0.12% at static biofilm (67) with trypan blue staining. The gradual decrease in MGV of biofilm was observed up to 0.12% chlorhexidine with crystal violet staining. Fluctuation in MGV of biofilm was observed due to no removal of biofilm from the slide.

Removal of biofilm mass was observed from the middle of the channels of the fabricated device. As the concentration of chlorhexidine increased, more biofilm was removed. With trypan blue

dye, as the concentration of chlorhexidine increased the MGV of biofilm decreased and the same was displayed by the pixel intensity distribution graph, hence the viability of cells within biofilm decreased with an increase in chlorhexidine concentration.

The opposite trend was observed with crystal violet staining: as concentration of chlorhexidine increased in a solution, the treated biofilms MGV increased in the fabricated device. Figure 6.20 demonstrates that as chlorhexidine concentration increased, biofilm was removed from the device and appeared thinner which contributed to this trend.

Biofilm in the drip-flow reactor had the same pixel intensity distribution profile throughout all concentrations of chlorhexidine with both staining methods.

Both ethanol and chlorhexidine antimicrobial agents performed as in literature, ethanol being most active against biofilm at 60% to 70% (58) and chlorhexidine – at 0.12% (63). Staining with trypan blue dye indicated a decrease in biofilm cell viability as the concentration of ethanol increased up to 70% and the concentration of chlorhexidine increased up to 0.12% by a static biofilm formation and in the fabricated device. No such trend was observed in a drip-flow reactor due to the uneven structure of the biofilm. Crystal violet staining of biofilm was useful to visualise the removal of biofilm from the middle of channels in the fabricated device at different concentration of antimicrobial agents.

Chapter 7 PROOF OF CONCEPT 2: DOSE-RESPONSE DATA FROM NATURALLY-DERIVED ACTIVES

7.1 WHAT IS THE EFFECT OF TANNIC ACID, GALLIC ACID AND ELLAGIC ACID ON THE *E. COLI* BIOFILM?

Polyphenols are a big family of naturally occurring compounds commonly found in plants, characterised by the presence of phenol units. It has been demonstrated that polyphenols exhibit biological activities, such as antibacterial and antioxidant activity (68). For example, tea polyphenols can inhibit the growth of *E. coli* biofilm (69). Tea polyphenols can also inhibit the growth of other bacterial biofilms and attenuate their formation (70), hence can potentially be used as anti-microbial compounds.

Tannic acid is an example of a polyphenol, consisting of numerous phenol groups. Tannic acid extracted from plant tissues has been reported to possess natural anti-microbial activity (71). The majority of studies have been conducted to investigate the effect of tannic acid concentrations during biofilm development stages and not the effect of tannic acid on a developed biofilm. Some mechanisms of action have been proposed based on those studies. It was suggested that tannic acid binds to the peptidoglycan of the cell walls and might inhibit the formation of biofilm structure (72). Cleavage of peptidoglycan reduces biofilm growth by altering the composition of proteins present in cell walls (3). It may also release signalling molecules that control biofilm gene expression and reduce biofilm formation.

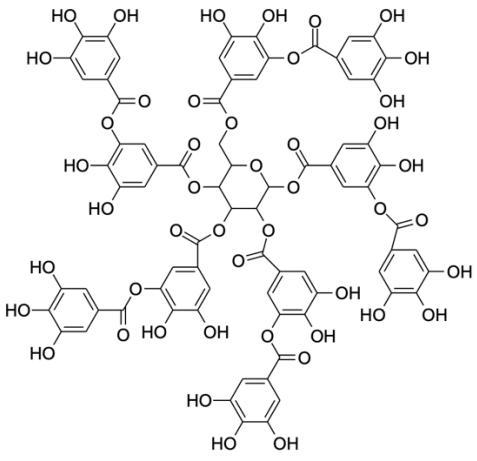

Figure 7.1 Tannic acid molecule.

Gallic acid is another example of a plant-derived phenolic compound with an anti-microbial effect. Its activity against biofilm formations is of particular interest to biofilm research. It has been shown that gallic acid added during biofilm formation causes a reduction in biofilm activity (73). It is proposed that gallic acid reduces cell motility and influences the adhesion of cells during the attachment phase of biofilm formation (74).

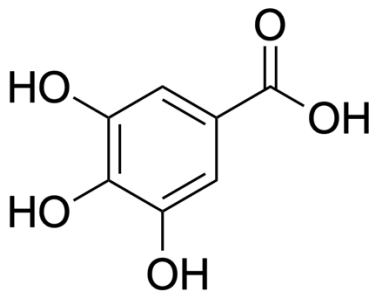

Figure 7.2 Gallic acid.

Ellagic acid is another polyphenol that possesses antimicrobial properties (75). It has been previously shown that ellagic acid acts as an anti-biofilm agent when added during the biofilm development stage (76). It is poorly soluble in water; hence DMSO is generally used as a solvent for ellagic acid.

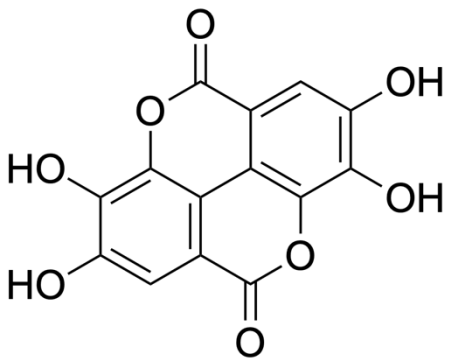

Figure 7.3 Ellagic acid molecule.

To validate the ability of the device to deliver dose-response studies, polyphenols and other plant-derived compounds were chosen. Their chemical diversity and complex action models provide a stringent assessment of device function to contribute to the compound discovery process.

7.1.1 Tannic and gallic acid effect on continuous *E. coli* biofilm in a fabricated device

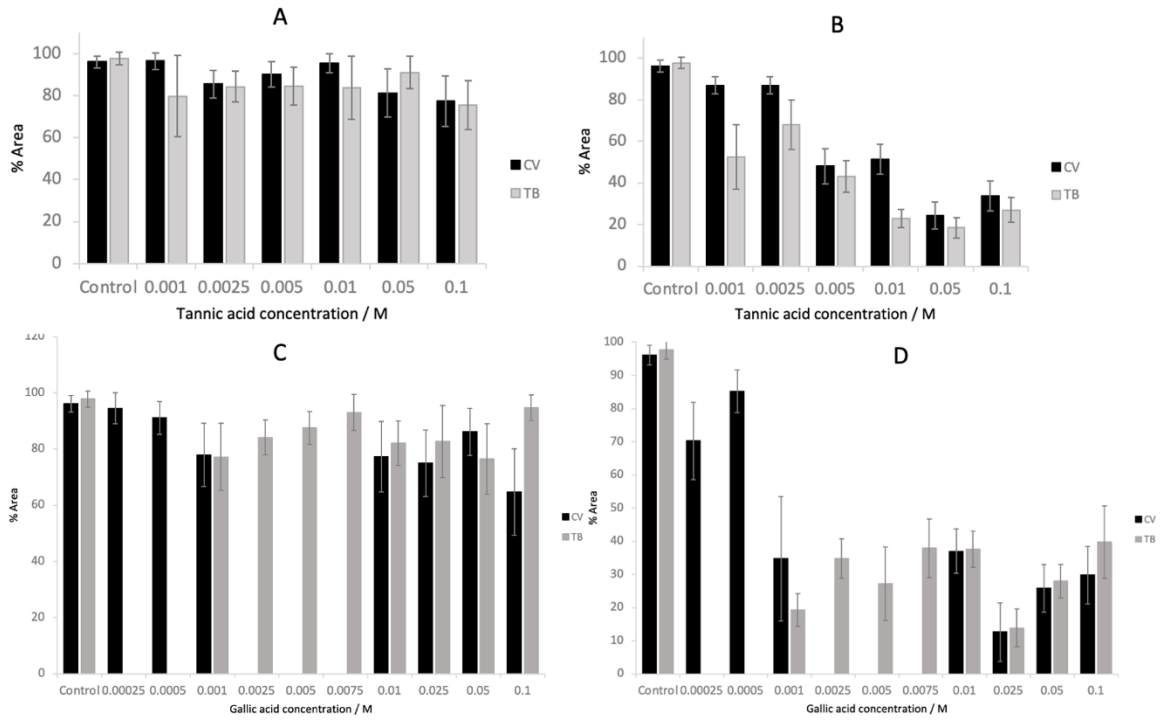

Figure 7.4 Graphs of % area occupied by biofilm in the fabricated device after the addition of different concentrations of tannic and gallic acid. A – tannic acid side of the channel, B – tannic acid middle of the channel, C – gallic acid side of the channel, D – gallic acid middle of the channel, N=9, error bars – SD.

In a fabricated device, the removal of biofilm from the middle of channels was observed. Two factors contribute to the removal of biofilm. The first factor is a constant flow of solution with different concentrations of the active ingredient, and the second factor – is the action of the active ingredient on the biofilm. Removal of biofilm from the sides of the channel is insignificant, and fluctuation in results is due to variation in biofilm formation – (Figure 7.4). An increase in tannic acid concentration caused biofilm removal from the channel's inner part. There is a gradual decrease in the %area occupied by biofilm with an increase in tannic acid concentration with both staining methods. Results for crystal violet staining are higher at all concentrations due to the mechanism of action of crystal violet, which binds to the entire biofilm mass. Trypan blue only binds to the dead cells; hence some of the biofilms are missed at low concentrations of tannic acid due to the lack of staining of trypan blue. The area occupied by biofilm drops from 87% at 0.001M of tannic acid to 30% at 0.1M of tannic acid, three times reduction in % area occupied by biofilm.

Gallic acid, the same as tannic acid, does not cause biofilm removal from the sides of the channels. However, instead of observing a gradual decrease in biofilm as the concentration of

gallic acid increases, there is minor removal of biofilm at low concentrations of gallic acid – 0.00025M and 0.0005M and then a sharp decrease in %area of biofilm with fluctuation in results at 25% area occupancy. Both staining methods show the same trend.

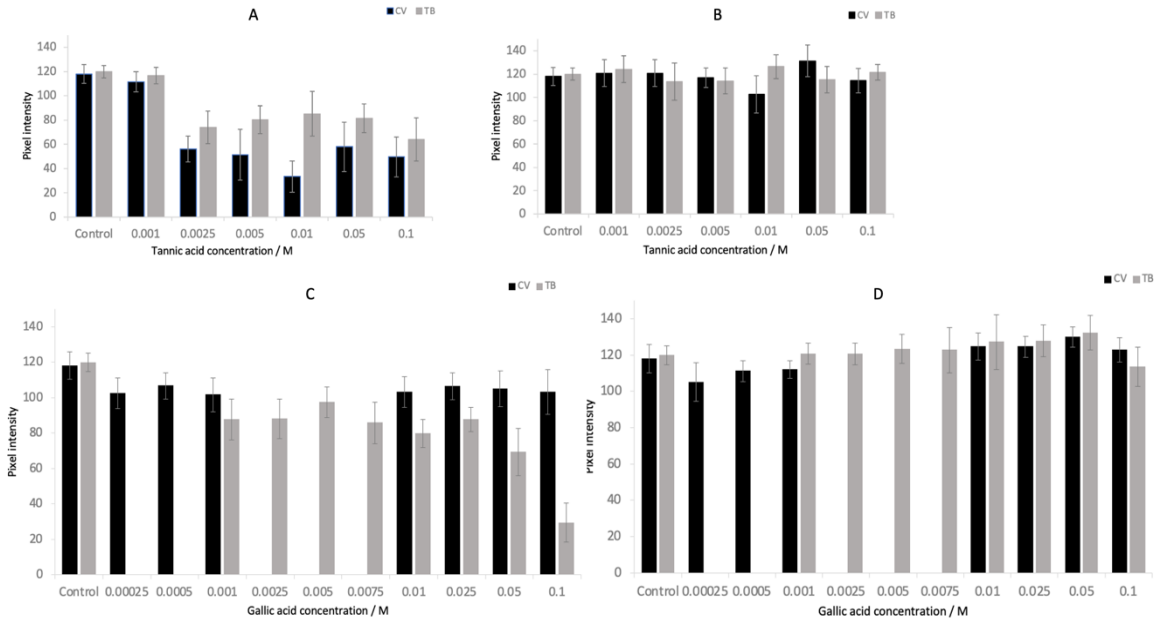

Figure 7.5 Graph of MGV of biofilm at different concentrations of tannic and gallic acid. A – tannic acid side of channels, B – tannic acid middle of channels, C – gallic acid side of channels, D – gallic acid middle of channels, N=9, error bars – SD.

MGV of biofilm does not change in the middle part of channels as the biofilm is removed from that area. As the concentration of tannic acid increased, the MGV of the biofilm decreased. At 0.001M, there is no difference compared to untreated biofilm – (Figure 7.5). As concentration increased from 0.0025M to 0.1M, results fluctuated at about 40 MGV with crystal violet staining and 80MGV with trypan blue. This is due to the removal of biofilm from the surface – (Figure 7.6). No effect on biofilm was observed at 0.001M of tannic acid with both dyes. As the concentration of tannic acid increased, more dye was binding to the biofilm, and more biofilm was removed from the surface with increases in tannic acid concentration.

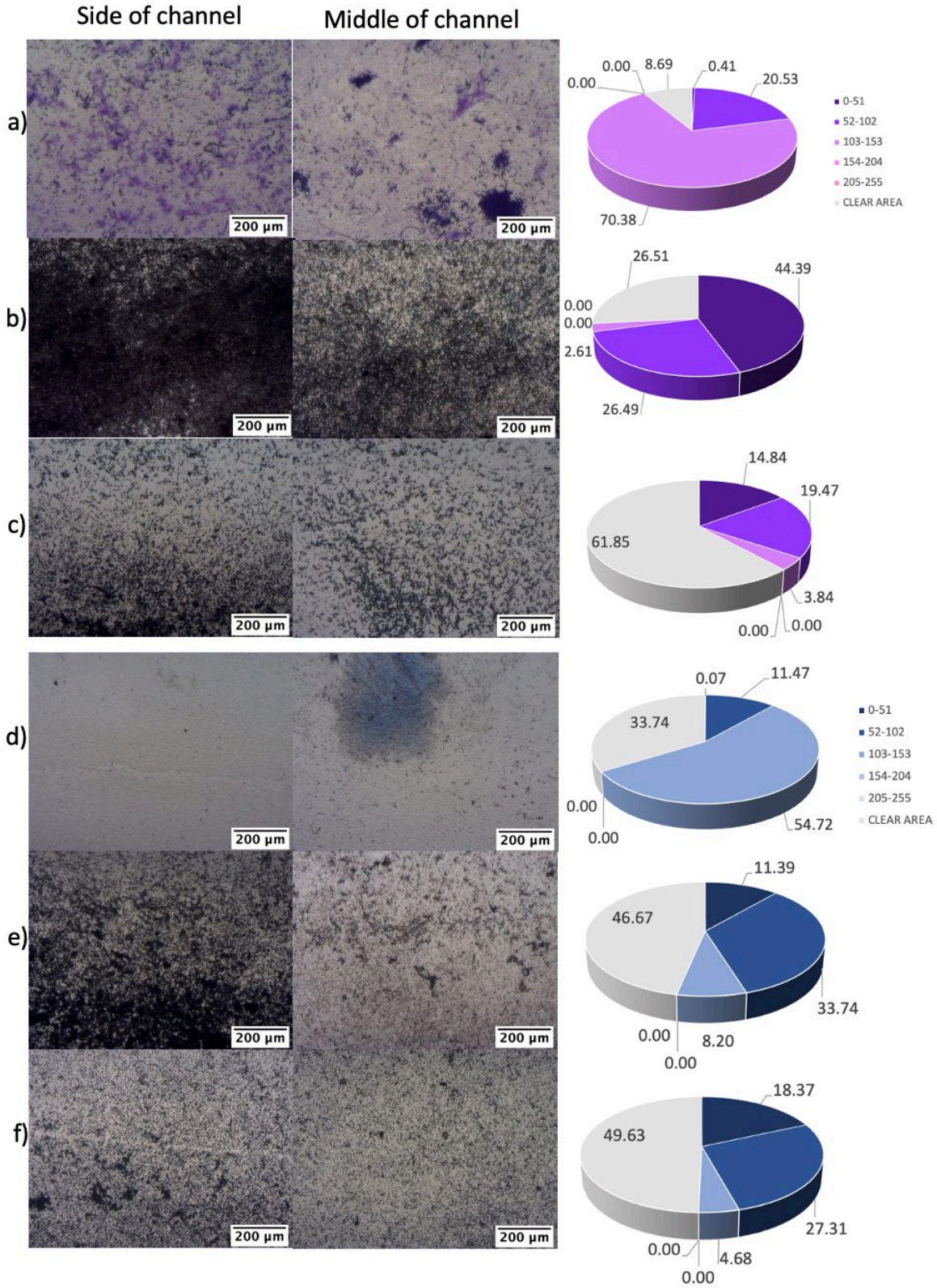

Figure 7.6 Images of biofilm inside fabricated device after addition of tannic acid, sides and middle of channels and pie charts of pixel distributions. a) – 0.001M, b) – 0.01 and c) -0.1M crystal violet, d) – 0.001M, e) – 0.01M, and f) – 0.1M trypan blue.

MGV of biofilm treated with gallic acid slightly decreased as the concentration of active ingredient increased to 0.025M with trypan blue dye. Sudden decreases in MGV were observed at 0.05M

and 1M of gallic acid – (Figure 7.5). Crystal violet staining displayed stable MGV across all concentrations of gallic acid. Images of biofilms at different concentrations of gallic acid illustrate more transformations to biofilms compared to MGV – (Figure 7.7). As the concentration of gallic acid increased, the biofilm appeared darker; hence more dye was absorbed. At 0.1M gallic acid with crystal violet staining, there is an unclear result to biofilm colour that does not fit any trend and cannot be explained by the results obtained.

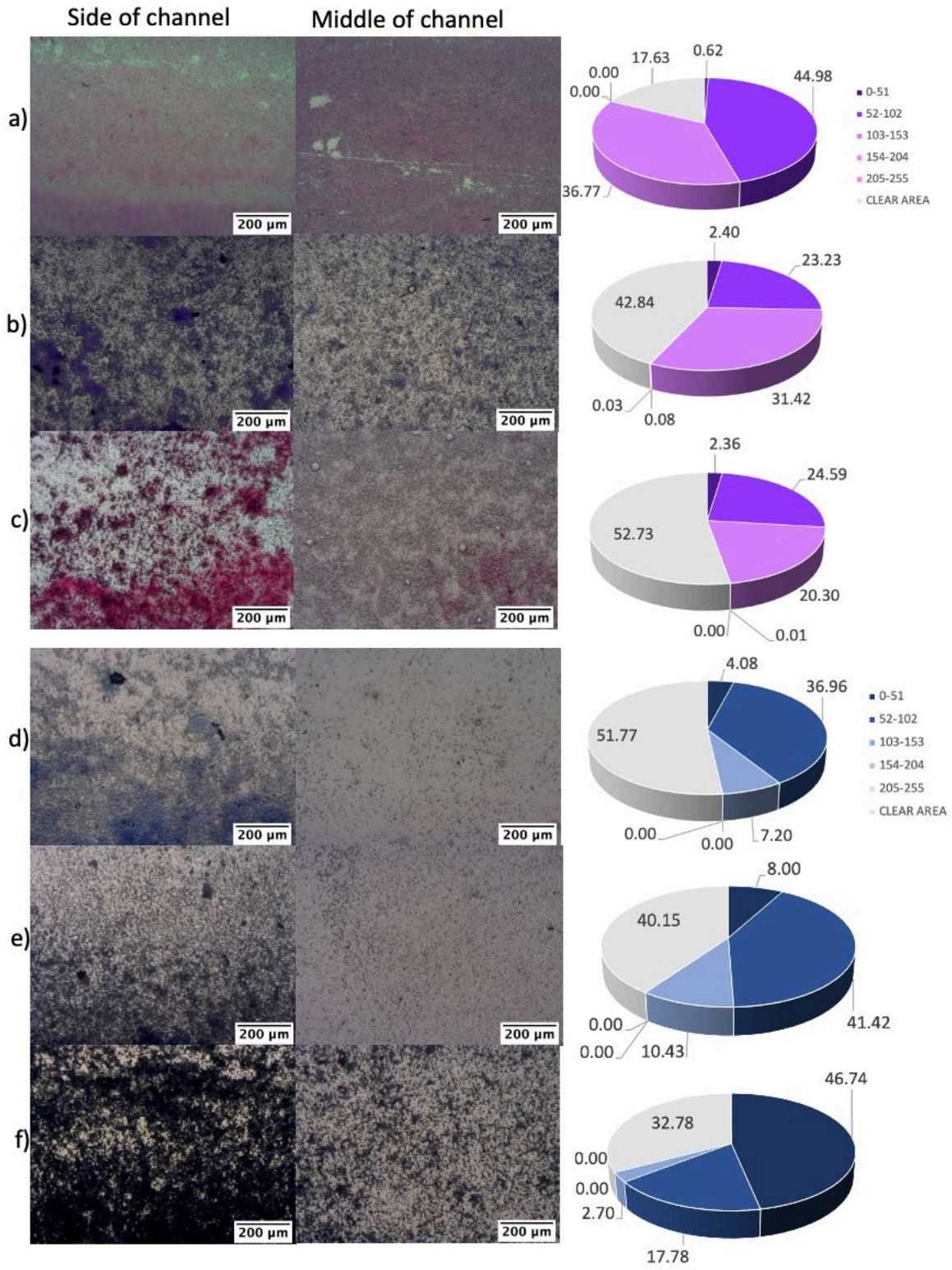

Figure 7.7 **Images of biofilm inside fabricated device after addition of gallic acid, sides and middle of channels and pie charts of pixel distributions. a) – 0.00025M, b) – 0.01 and c) -0.1M crystal violet, d) – 0.001M, e) – 0.01M, and f) – 0.1M trypan blue.**

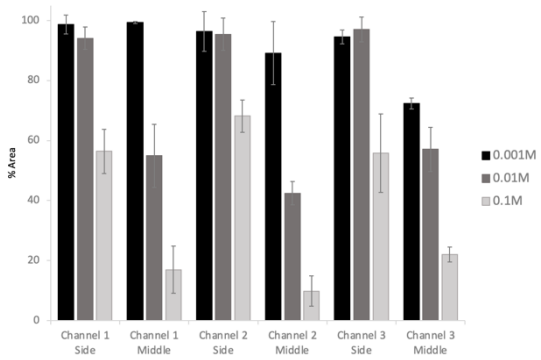

Figure 7.8 Graph showing biofilm distribution inside channels at different concentrations of tannic acid, N=9, error bars – SD.

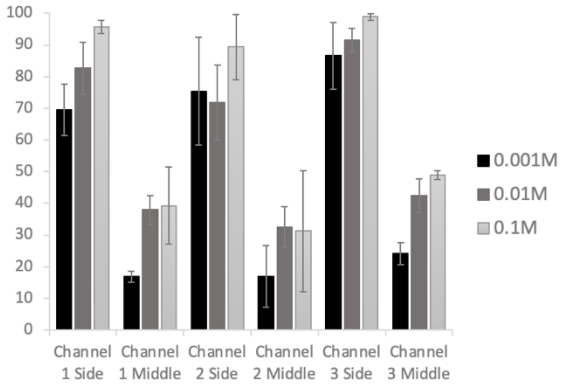

Figure 7.9 Graph showing the distribution of biofilm inside channels at different concentrations of gallic acid, N=9, error bars – SD.

Both phenolic compounds show an anti-microbial effect against formed biofilms. As the concentration of tannic and gallic acid increased, the MGV of biofilm decreased. Hence more binding of the staining agent occurs. Tannic acid removes more biofilm from the devices' surface than gallic acid. Tannic acid and gallic acid display the removal of biofilm by two staining methods from full channel coverage down to 30% and 40%, respectively. Figure 7.8 illustrates uniform biofilm distribution within and between channels and demonstrates biofilm removal as a concentration of tannic acid increases. A more significant % of biofilm is removed from the inner part of the device, but the same pattern is present in all channels. Biofilm distribution within and between channels is uniform when treated with gallic acid – (Figure 7.9). More biofilm is present on the sides of the channels. The effect of the concentration of gallic acid on the removal of biofilm from the surface is due to fluctuation in the %area occupied by biofilm after gallic acid treatment.

7.1.2 Investigating the effect of tannic and gallic acid on static *E. coli* biofilm

Static *E. coli* biofilm was treated with different concentrations of tannic and gallic acid. No biofilm removal from the surface was observed in Figure 8.22 and Figure 8.23. MGV of biofilm after exposure to different concentrations of tannic had little change across all concentrations compared to the control (Figure 7.10). The action of gallic acid on biofilm caused a more pronounced change than tannic acid. A gradual decrease in MGV was observed as the concentration of gallic acid increased with crystal violet staining – (Figure 7.11). A decrease from 114 MGV at control to 51 MGV at 0.1M of gallic acid was observed. A much lesser decrease in

MGV was observed with trypan blue staining, from 118 MGV at control to 110 at 0.1M of gallic acid.

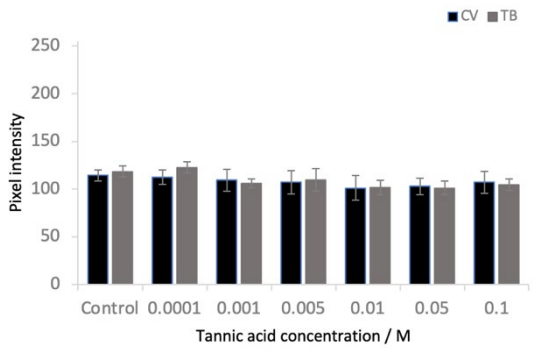

Figure 7.10 Graph showing MGV of biofilm when different concentrations of tannic acid were added, crystal violet and trypan blue staining, N=12, error bars – SD.

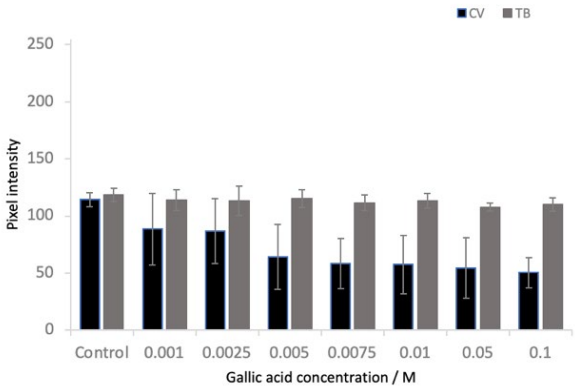

Figure 7.11 Graph showing MGV of biofilm when different concentrations of gallic acid were added, crystal violet and trypan blue staining, N=12, error bars – SD.

MGV and %area occupied by biofilm suggested no change to biofilm when treated with tannic acid. The addition of gallic acid to the formed biofilm affected the MGV of biofilms.

Pixel intensity distribution graphs present variation in pixel intensity distribution within biofilms with both polyphenols (Figure 7.12). Graph A shows pixel intensity distribution within biofilm after the addition of different concentrations of tannic acid with trypan blue staining. At 0.0001M, no change compared to untreated biofilm was observed. This is in the concentration range used for studies of tannic acid during biofilm development (77). As the concentration of tannic acid increases to 0.001M there is a distinct change in pixel intensity distribution, a trend that was not present in Figure 7.7. This could have been easily missed on a graph of MGV distributions. Pixel intensity Group 3 (103 – 153) decreases from 94% at 0.0001M to 59% at 0.001M, and Group 2 (52 – 102) increases ten times, from 4% at 0.0001M to 40% at 0.001M. As concentration continues to increase, the gradual decrease of pixel Group 3 and increase of pixel Group 2 was observed from 0.001M to 0.05M. Group 3 decreased from 59% to 36%, occupying 0.001M and 0.05M, respectively, and Group 2 increased from 40% to 54%. There is no change in biofilm viability at a low concentration of tannic acid. As concentration increases, the number of dead cells increases. Crystal violet shows a gradual decrease in pixel Group 3 (53 – 103) from 67% to 41% at 0.0001M and 0.01M, respectively, with a gradual increase in pixel intensity Group 2 (52 – 102) from 29% to 56% at 0.0001M and 0.01M. Above 0.01M, fluctuation in the pixel intensity groups is observed. Both staining methods display the same pattern in pixel intensity distribution within biofilm when

tannic acid is added to the developed biofilm, suggesting a minor effect on static biofilm at different tannic acid concentrations.

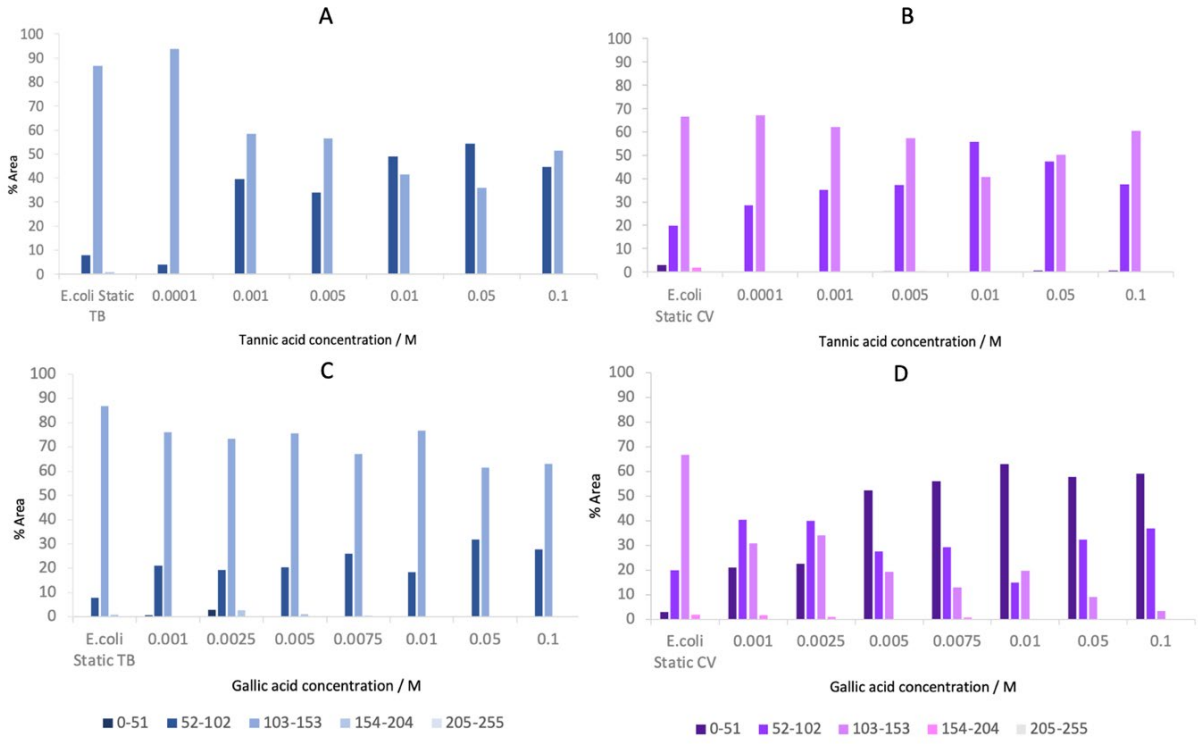

Figure 7.12 Graphs of the pixel intensity distribution in biofilms after exposure to different concentrations of tannic acid – A -trypan blue, B – crystal violet and gallic acid – C - trypan blue, D – crystal violet.

Graphs of pixel intensity distribution after the addition of gallic acid display a steady increase in pixel intensity Group 2 (52 – 102), indicating an increase in dead cells number as a concentration of gallic acid increases, with trypan blue staining. Although, the increase is much smaller compared to the tannic acid. Graph D displays pixel intensity distribution after the addition of gallic acid to the biofilm with crystal violet staining. The changes to pixel intensity distribution are very apparent. Pixel intensity Group 1 (0 -51) gradually increased from 3% at untreated biofilm to 58% at 0.05M gallic acid. Group 3 (103 – 153) steadily decreased from 67% *E. coli* biofilm to 3% at 0.1M of gallic acid. Group 2 (52 – 102) increased from 20% to 34% between untreated biofilm and 0.0025M gallic acid and was fluttered as Group 1 and 3 rose and fell – (Figure 7.12). As the gallic acid concentration increased, biofilm absorbed more crystal violet dye. It is unconfirmed why this trend was observed.

7.1.3 Action of tannic and gallic acid on continuous *E. coli* biofilm formed in a drip-flow reactor

A study of the tannic and gallic acid effect on biofilm in a drip-flow reactor was performed, and MGVs are presented in Figure 7.13. It needs to be taken into consideration that biofilm grown in a drip-flow reactor is rutted and uneven. This affects the results. Gallic acid effect on biofilm with crystal violet staining has the lowest reduction in MGV as the concentration of gallic acid increases. As shown in Figure 7.14A, there is a slight fluctuation in pixel distribution due to biofilm structure. When trypan blue is used as a staining agent, there is a sudden change in pixel intensity distribution between the control and 0.001M gallic acid concentration – (Figure 7.14B). Drop from 60% of Group 3 (103 – 153) in control biofilm to 8% when treated with 0.001M gallic acid. It is not reflected in (Figure 7.13). Fluctuation of results is observed from 0.001M to 0.025M of gallic acid concentration. As the concentration of gallic acid reached 0.5M, pixel Group 1 (0 – 51) drastically increased to 35% and, at 0.1M, almost doubled to 86% area within a biofilm. When concentrations from 0.001M to 0.025M are compared, there is no fluctuation in pixel distribution, but the effect on biofilm is the same. As concentration reaches 0.05M and above, more staining agent is absorbed by the biofilm, meaning more dead cells in a biofilm. Hence, gallic acid has an effect on the viability of bacteria cells.

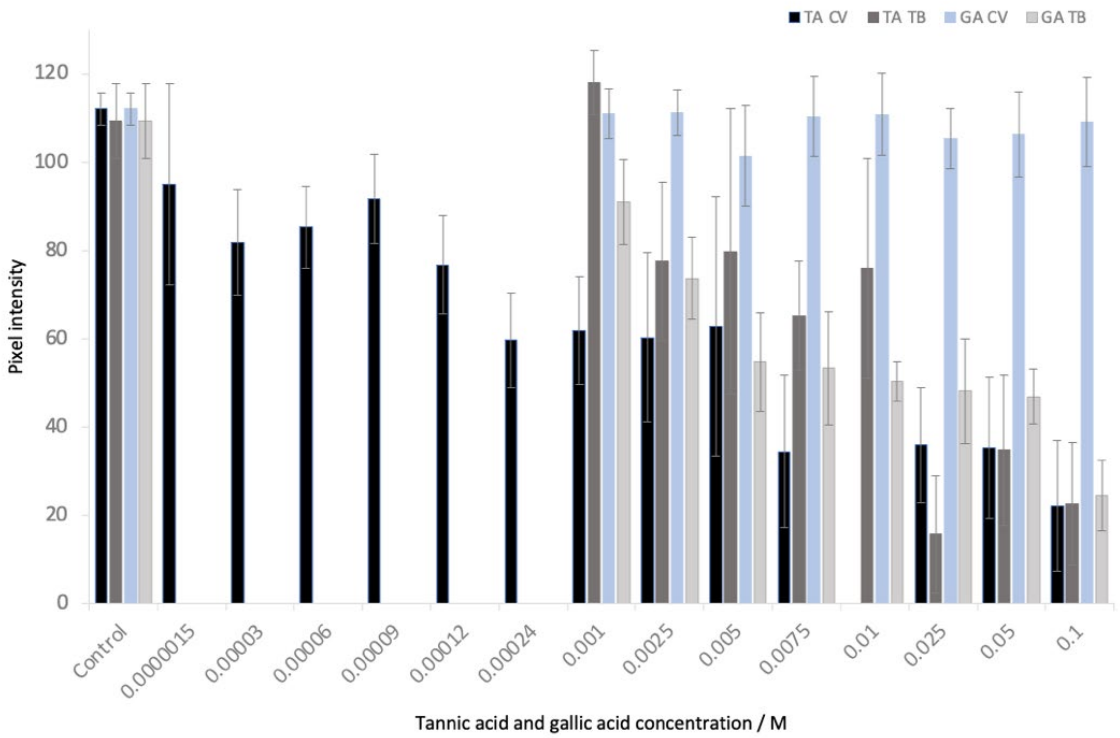

Figure 7.13 Graph of MGV of biofilms after addition of tannic acid and gallic acid concentrations, trypan blue and crystal violet staining, error bars – SD.

Investigation of low concentrations of tannic acid effect on biofilm was conducted in a drip-flow reactor. A decrease in biofilm MGV was observed as the concentration of tannic acid increased with both staining reagents – (Figure 7.13). As the concentration of tannic acid increased, biofilm absorbed more dye. This observation means that tannic acid has an antimicrobial effect on developed biofilm formed in a drip-flow reactor. Three distinct regions of pixel intensity distribution patterns can be identified in (Figure 7.14D). The first region is from 1.5μM to 90μM of tannic acid, the second between 120μM to 0.005M and the third from 0.0075M to 0.1M of tannic acid. A low concentration of tannic acid affects biofilm, and as concentration increases, the effect increases. Although, with the trypan blue reagent, which is only attached to dead cells, no change was detected at 0.001M of tannic acid - Figure 7.14C. As concentration continues to increase, more dye is absorbed, and after 0.025M, there is no difference in pixel intensity distribution.

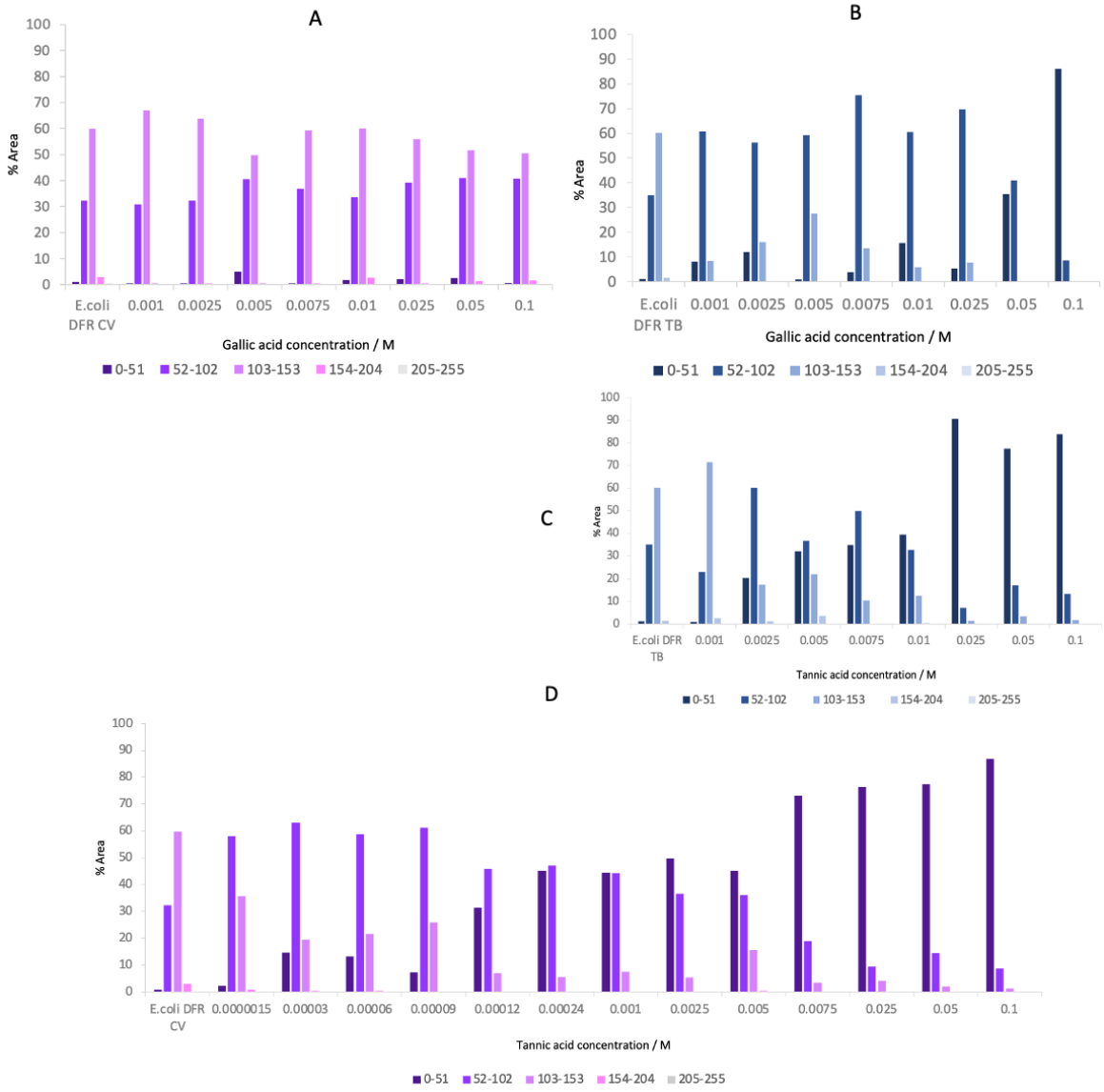

Figure 7.14 Graphs of pixel intensities distribution within biofilm after tannic and gallic acid addition, A – gallic acid, crystal violet staining, B – gallic acid, trypan blue staining, C – tannic acid, crystal violet staining, D – tannic acid, crystal violet staining.

Trypan blue staining indicates an increase in dead cells number as both tannic acid and gallic acid concentrations increase. As the concentration of gallic acid increases, there is a slow but constant increase in dead cells within the biofilm. Lower concentrations of tannic acid are required to achieve the same effect on biofilm as gallic acid – at 0.025M of tannic acid, 91% of biofilm consists of the darkest regions. In contrast, with gallic acid, 86% of biofilm consists of the darkest pixels at a concentration of 0.1M. Crystal violet dye does not indicate any changes in MGV of biofilm across all concentrations of gallic acid. With tannic acid, the MGV of biofilm decreases as concentration increases.

7.1.4 Effect of ellagic acid on *E. coli* biofilm

Ellagic acid in DMSO was added to developed biofilms in a drip-flow reactor and fabricated device. DMSO itself affects MGV of biofilm – (Figure 7.15). Thus, the effect of ellagic acid dissolved in DMSO is a combined effect of two. As the concentration of ellagic acid in DMSO increased, there was a reduction in the MGV of biofilm in the drip-flow reactor from 112 MGV of untreated biofilm to 6 MGV at 0.1M ellagic acid. A slight decrease in MGV was observed within a fabricated device.

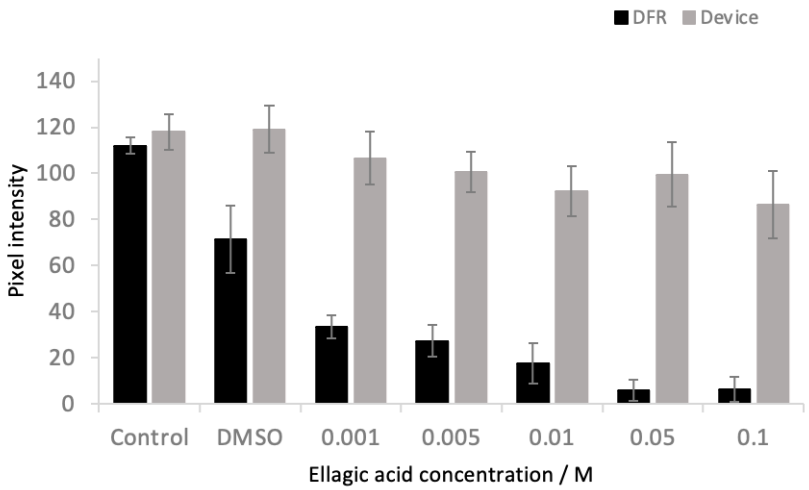

Figure 7.15 Graph showing MGV of biofilm in a drip-flow reactor and fabricated device after addition of DMSO and ellagic acid concentration, crystal violet staining, N=9, error bars – SD.

Pixel intensity distribution graphs - Figure 7.16 and Figure 7.17 illustrate no change in pixel intensity distribution across all concentrations of biofilm in a fabricated device. In a drip-flow reactor, pixel intensity Group 1 (0 – 51) increases from 90% to 96% at 0.001M and 0.1M, respectively, and Group 2 (51 – 102) decreases from 8% to 1% at those concentrations. These small changes in pixel intensity distribution have a substantial effect on the MGV of biofilms, from 33 MGV at 0.001M to 6 MGV at 0.1M.

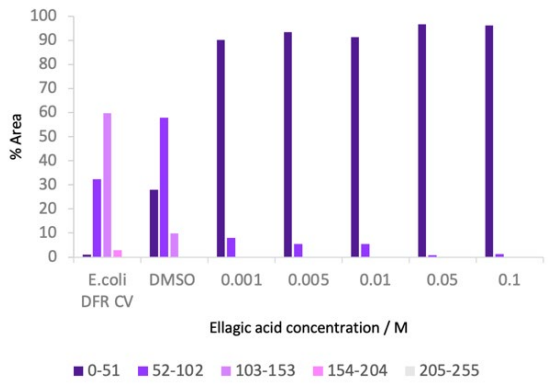

Figure 7.16 Graph showing pixel intensity distribution within biofilm after the addition of ellagic acid in a drip-flow reactor.

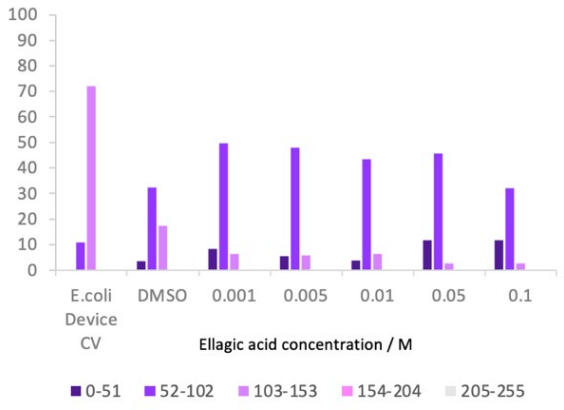

Figure 7.17 Graph of pixel intensity distribution within biofilm after the addition of ellagic acid in a fabricated device.

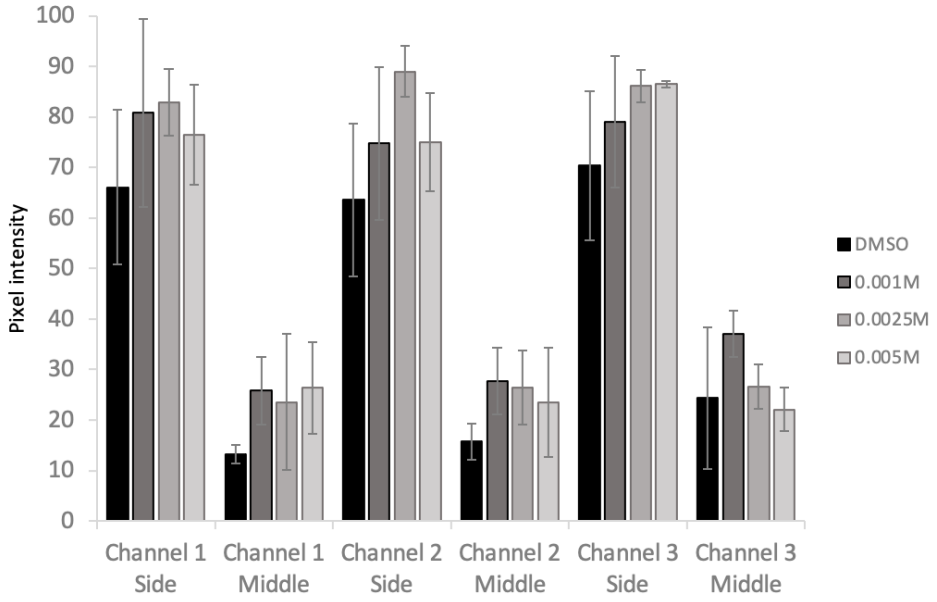

Figure 7.18 Graph showing the distribution of biofilm within and between each channel when treated with ellagic acid, N=9, error bars – SD.

The distribution of biofilm is presented in Figure 7.18. The fabricated device is efficient in supporting uniform biofilm. This is demonstrated by the distribution of biofilms after the addition of active compounds to the flow. The remaining biofilm has the same distribution between the three channels and between devices.

7.2 THE EFFECT OF NON-POLYPHENOL COMPOUNDS ON THE E. COLI BIOFILM

Berberine chloride is extracted from several plants. It is known for its antimicrobial, anti-inflammatory and antidiarrheal activities (78). Berberine inhibits biofilm development by interacting with the quorum sensing – communication system in biofilm (79). Berberine is slightly soluble in cold water, but the solubility of berberine increases as water temperature increases.

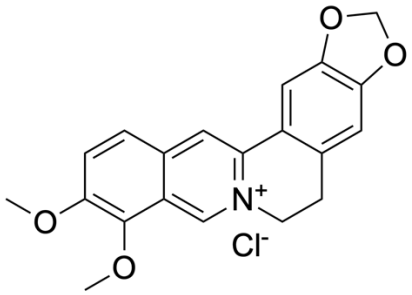

Figure 7.19 Berberine chloride molecule.

(+)-Usnic acid is extracted from lichens and is used in medicine due to its biological activities. Numerous studies present antimicrobial properties of (+)-usnic acid against planktonic bacteria (80). (+)-Usnic acid shows an inhibitory effect on some biofilms. While its mechanism is unclear, it is proposed that it occurs via inhibition of quorum sensing of biofilm (81). It is poorly soluble in water and primarily soluble in ethanol. Ethanol itself affects biofilms; hence very low concentrations of (+)-usnic acid activity dissolved in water were investigated.

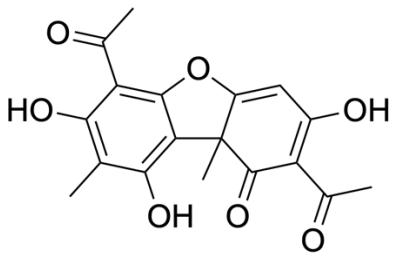

Figure 7.20 Usnic acid molecule.

Esculetin is another plant-derived molecule that targets quorum sensing in biofilm (82). Most of its activity was reported as antioxidant and anticancer agents, although some studies report the antibacterial properties of coumarins (83). It is poorly soluble in an aqueous solution; hence very low concentrations were used.

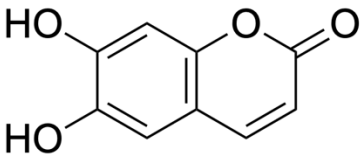

Figure 7.21 Esculetin molecule.

7.2.1 Effect of berberine on *E. coli* biofilm in the fabricated device

Biofilm was removed from the surface when solutions of different concentrations of berberine chloride were added to the biofilm in a fabricated device – (Figure 7.22). With trypan blue staining gradual decrease in the %area occupied by biofilm was observed from the sides and middle part of the channels. At the concentration of 0.0002M, 92% of the side area was occupied by biofilm and 47% in the middle of the channels. As concentration increased to 0.005M, 54% of the side area was covered by biofilm and 38% of the area at the inner part of the channels. With crystal violet, no removal of biofilm from the sides was observed, but the removal of biofilm in the middle part of channels was down to 15% at 0.005M berberine chloride.

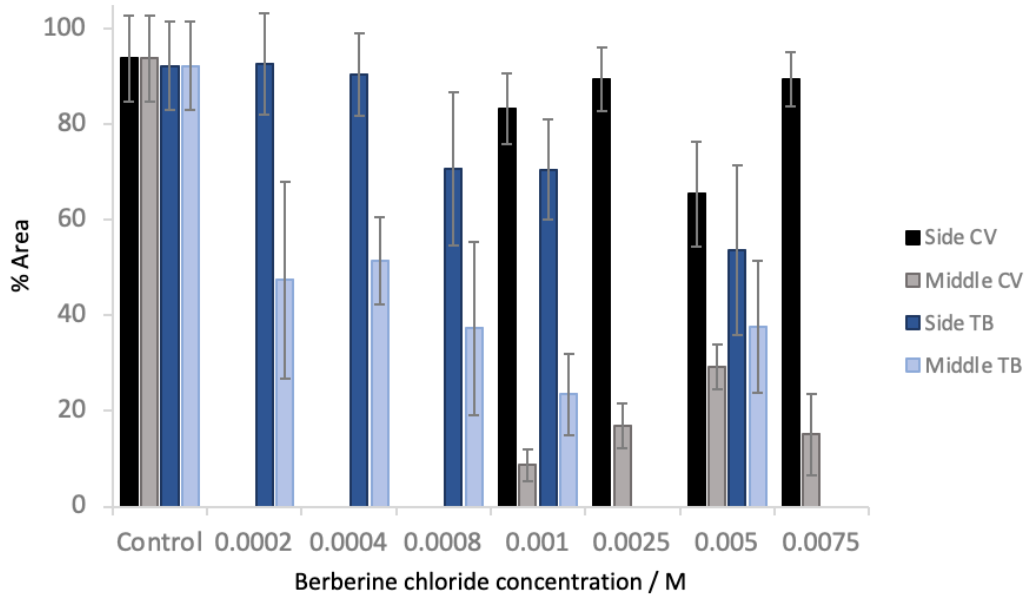

Figure 7.22 Graph of % area of biofilm inside channel after addition of berberine chloride, error bars – SD.

Removal of biofilm from the fabricated device is uniform between the side and middle parts between channels and between channels in devices – (Figure 7.23). The difference is present between staining agents. More biofilm was observed in the middle part of the channels when

stained with trypan blue. Although crystal violet stains bacteria live and dead cells and EPS in biofilm, trypan blue stains dead cells only. However, tiny clusters of cells were left in the middle of channels after berberine chloride addition, which might be the reason for those observations.

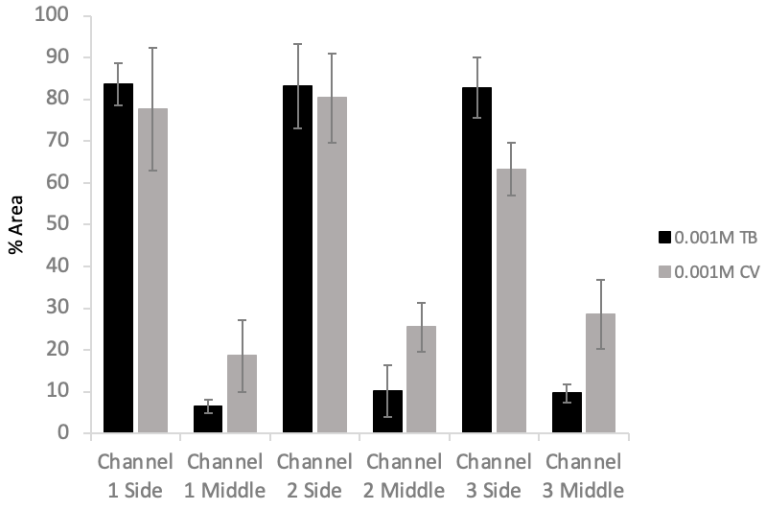

Figure 7.23 Distribution of biofilm inside channels and between channels at 0.001M of berberine chloride, N=9, error bars – SD.

No pixel distribution change at any berberine chloride concentration was observed with trypan blue – (Figure 7.24). The difference in pixel intensity distribution between untreated biofilm and biofilm after the addition of berberine chloride was observed. Pixel intensity Group 3 (103 – 153) dropped from 86% in untreated biofilm to 5% in treated biofilms, and Group 2 (52 – 102) increased from 6% to 60%, respectively. At low concentrations of berberine chloride with crystal violet staining gradual increase in pixel Group 2 (52 – 102) was observed from 11% within untreated biofilm to 50% at 0.001M and fluctuated around that percentage at other concentrations. Pixel Group 3 (103-153) decreases from 83% to 8% at 0.0025M. The reason for these observations is the effect of flow within channels.

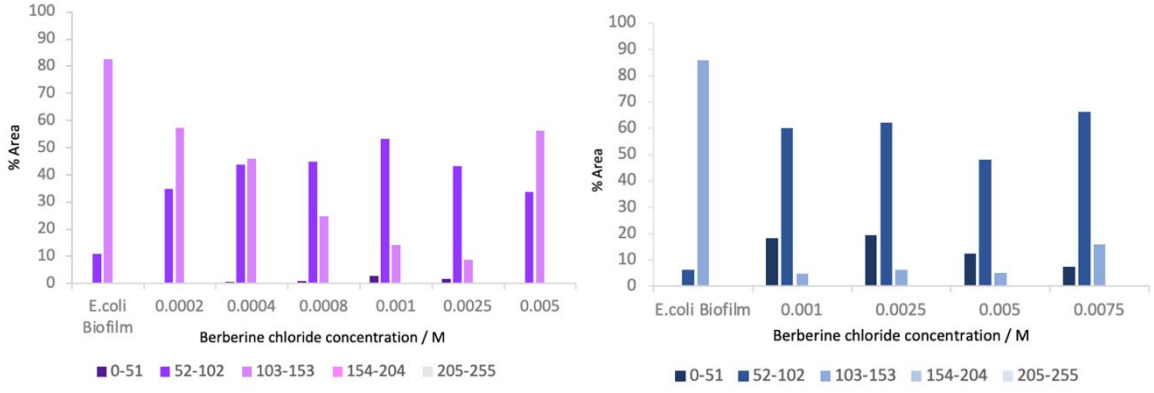

Figure 7.24 Graphs of pixel intensity distribution within biofilm in sides of channels after the addition of berberine chloride concentration. Left – crystal violet staining, right – trypan blue.

7.2.2 Effect of esculetin on *E. coli* biofilm in device

Trypan blue staining only was performed with esculetin in a fabricated device.

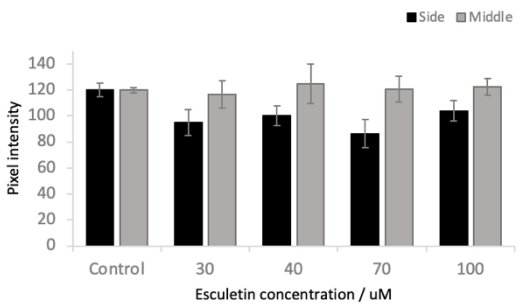

Figure 7.25 Graph of MGV of biofilm on the side and in the middle of the channel after addition of esculetin, trypan blue staining, N=9, error bars – SD.

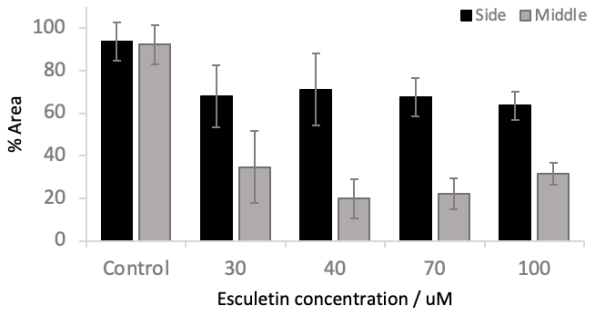

Figure 7.26 Graph of % biofilm area on the side and in the middle of the channel after the addition of esculetin, trypan blue staining, N=9, error bars – SD.

No difference between different concentrations of esculetin was observed. MGV of biofilm on the sides of the channels decreased compared to the untreated biofilm from 120 MGV to 100 MGV – (Figure 7.25). Removal of biofilm was observed from the middle of channels (Figure 7.26).

No effect of different concentrations of esculetin on biofilm was also confirmed by the pixel intensity distribution graph – (Figure 7.27). The distribution of pixels within a biofilm is not only the same in the %area they occupy, but also the total amount fluctuates by about 50%. Hence, an equal amount of biofilm was removed at all concentrations of esculetin, and all concentrations had the same effect on the biofilm. These results are similar to other studies performed with esculetin on biofilms (82) and other coumarins that have been studied to inhibit biofilm, formation (84). μM concentrations of esculetin have an antimicrobial effect not only on growing biofilms but also on developed biofilms as was shown in the present study. μM concentration of esculetin solutions was enough to change the pixel intensity distribution of biofilms compared to the control and cause the removal of biofilm from the surface.

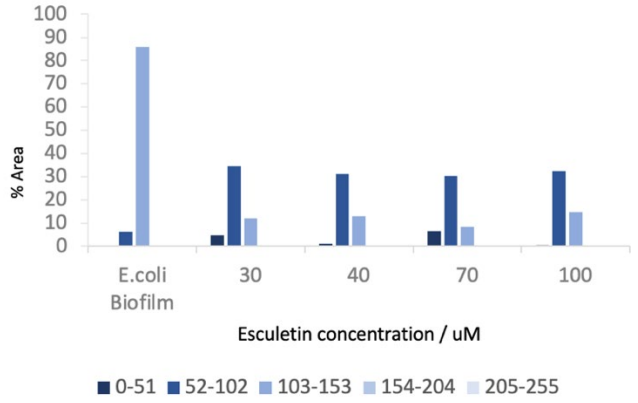

Figure 7.27 Graph of pixel intensity distribution within biofilm after addition of different concentrations of esculetin, device average, trypan blue staining.

7.2.3 Effect of (+)-usnic acid on continuous *E. coli* biofilm in the fabricated device

Lesser biofilm removal was observed with (+)-usnic acid compared to berberine chloride and esculetin, mainly in the middle part of channels – (Figure 7.28). As the concentration of (+)-usnic acid increases, the MGV of biofilm decreases. This trend is more visible with trypan blue staining when MGV decreases from 120 MGV of untreated biofilm to 69 MGV at 100μM on the sides of the channel, hence increasing cells death as the concentration of active ingredient increases.

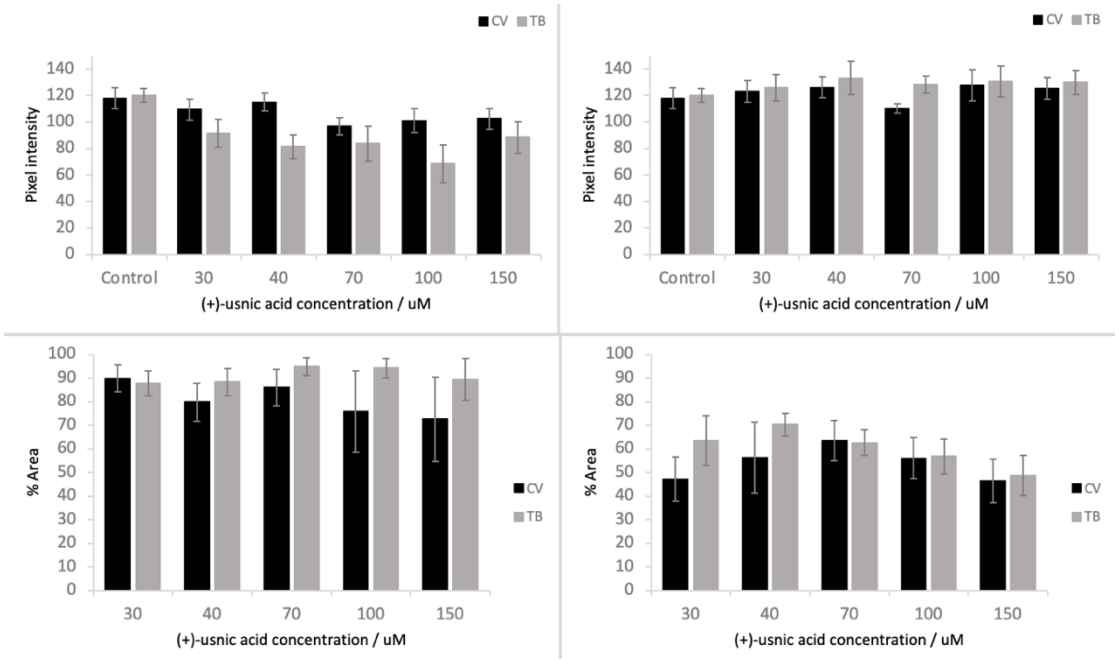

Figure 7.28 Graphs show the MGV of biofilm and the %area it occupied within the fabricated device. Top left – MGV of side biofilm, top right – MGV of biofilm in the inner part of channels, bottom left - % area on sides, bottom right - % area middle of channels, N=9, error bars – SD.

Crystal violet staining presents two groups of results. At 30μM and 40μM, MGV decreases to 110 MGV from 119 at untreated biofilm. As concentration continues to decrease, the MGV of biofilm drops to 100 MGV. This further supports observations obtained with trypan blue staining. As the concentration of (+)-usnic acid increased, more binding sites for crystal violet dye in the biofilm.

Pixel intensity distribution within biofilm illustrates the same pattern with both staining methods – (Figure 7.29) – lesser change in the pixel intensity distribution at 30μM and 40μM compared to the control biofilm, and greater change at higher concentrations. No change to pixel intensity distribution was observed in the middle part of the channel as a concentration of (+)-usnic acid changes. Both dyes also show the same pixel distribution between untreated biofilm and after the addition of active substance. However, after adding (+)-usnic acid, the number of pixels decreases due to the removal of biofilm. On the sides of the channels, two regions can be identified. The first region is between 30μM and 40μM, and the second is between 70μM and 150μM. In addition, trypan blue biofilm staining differs from untreated biofilm more than crystal violet. With trypan blue decrease in pixel group 3 (103 – 153) from 86% untreated biofilm to 20% of 30μM (+)-usnic acid is observed, while with crystal violet, the same pixel group decreases from 83% to 61%.

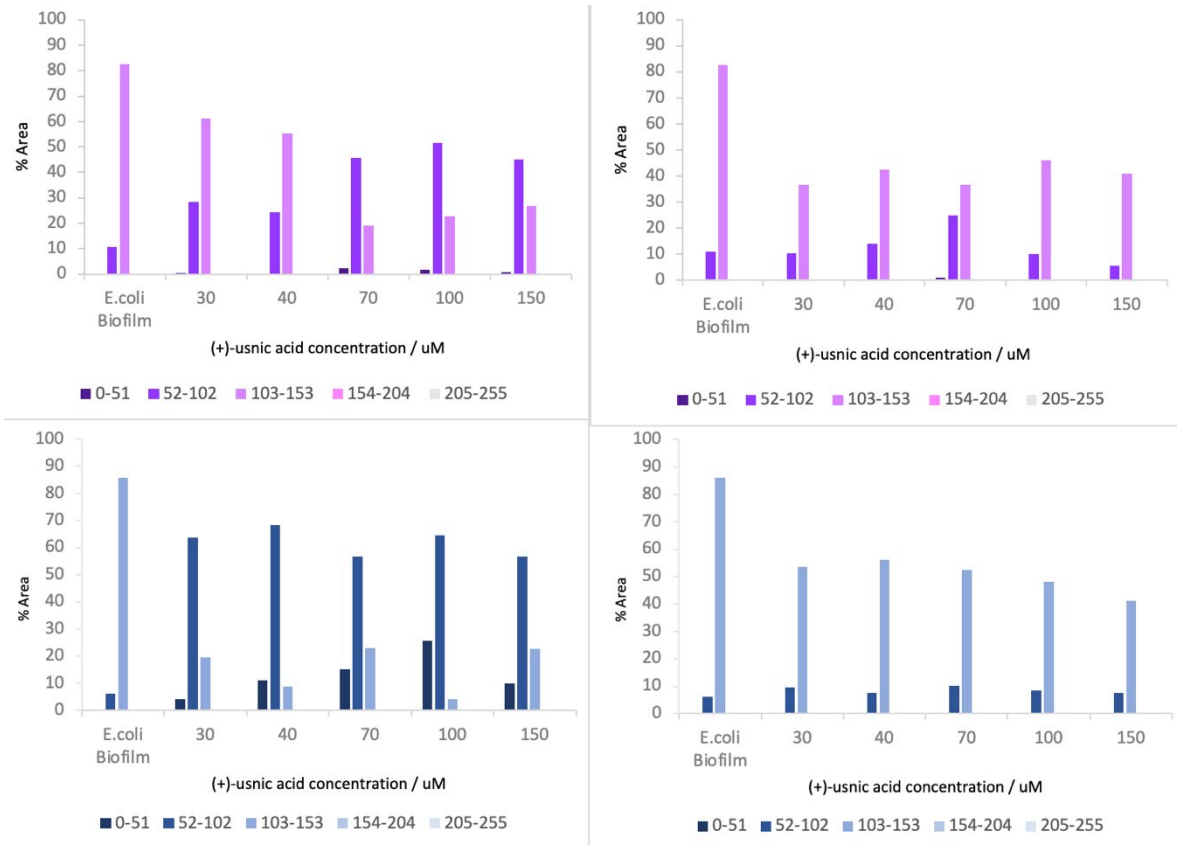

Figure 7.29 Graphs of pixel intensity distribution within biofilm after addition of (+)-usnic acid. Top left – biofilm in the side of the channel, crystal violet, top right – middle part, crystal violet, bottom left – side, trypan blue, bottom right – middle, trypan blue.

(+)-usnic acid causes lesser cell detachment compared to berberine chloride and esculetin. Because more biofilm is left on the surface, it is possible to observe some changes to biofilm MGV and pixel intensity distribution after treatment with (+)- usnic acid of different concentrations. With berberine chloride and esculetin, no change in pixel intensity distribution is observed, a big proportion of biofilm is removed from the channels, and pixel intensity distribution is the same for all concentrations. This might be due to the vigorous removal of biofilm.

7.2.4 Activity of berberine, esculetin and usnic acid on static E. coli biofilm

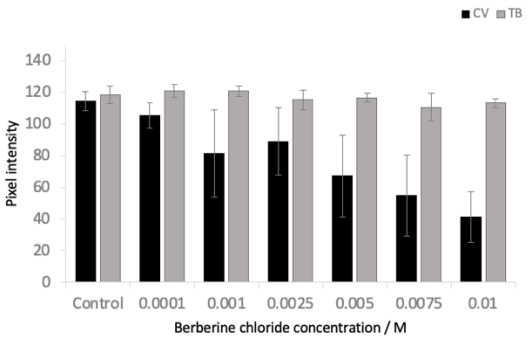

Figure 7.30 Graph showing MGV of static biofilm after addition of berberine chloride, N=12, error bars – SD.

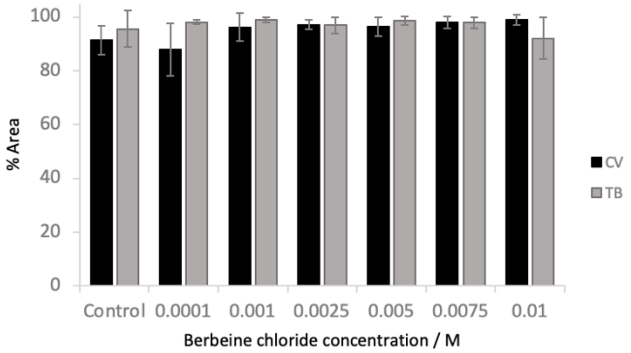

Figure 7.31 Graph of % area occupied by static biofilm after the addition of berberine chloride, N=12, error bars – SD.

Berberine chloride does not cause biofilm removal from the slide surface at any concentrations – (Figure 7.31). A decrease in MGV of biofilms is observed as the concentration of berberine chloride increases – (Figure 7.30). This is especially visible with crystal violet stain. As the concentration of berberine increases to 0.1M, there is a decrease from 114 MGV at control to 41 MGV. With trypan blue staining MGV stayed the same at all concentrations and did not change compared to untreated biofilm. Trypan blue staining suggested no changes to biofilm viability. At the same time, the binding of crystal violet increased with an increase in berberine concentration, suggesting more binding sites to crystal violet dye with increases in berberine. The reason for this trend is unclear and require further investigations.

Both (+)- usnic acid and esculetin are poorly soluble in water, but other solvents, DMSO and ethanol, affect biofilms. It was possible to dissolve these active compounds at very low concentrations to examine their effect on formed biofilm. None of them did cause the removal of biofilm from the surface – (Figure 7.33). Changes in MGV of biofilm were only observed with (+)-

usnic acid with crystal violet staining. Esculetin did not cause any changes to biofilm MGV at any concentrations – (Figure 7.32).

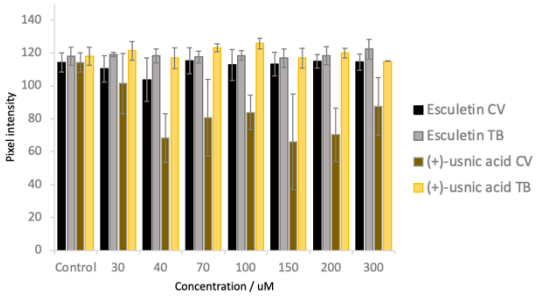

Figure 7.32 Graph showing MGV of static biofilm after addition of (+)-usnic acid and esculetin, N=12, error bars – SD.

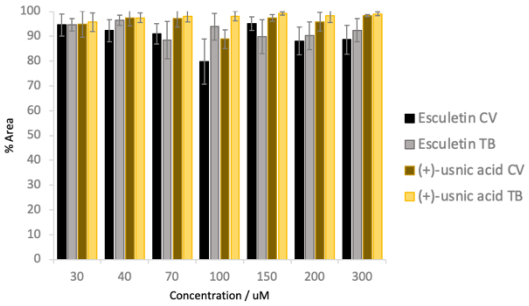

Figure 7.33 Graph showing % area occupied by static biofilm after the addition of (+)-usnic acid and esculetin, N=12, error bars – SD.

None of the three plant-derived compounds had an effect on the removal of biofilm from the surface of the glass slide. As with other antimicrobial agents and plant-derived compounds discussed in previous chapters, no biofilm removal was observed with a microtiter-plate assay. This assay cannot determine the ability of a compound to detach developed biofilm from the surface.

Trypan blue staining, which only binds to dead cells within the biofilm, showed no change in biofilm compared to control at any concentration of any of the three compounds. Crystal violet staining showed a decrease in MGV as the concertation of berberine chloride and (+)-usnic acid increased. With berberine chloride, a gradual decrease in MGV was observed, while with (+)-usnic acid, the results fluctuated at all concentrations. This suggests no effect on the viability of biofilm grown by static assay after the addition of active substances.

Most of the studies that present effectiveness of berberine chloride, (+)-usnic acid and esculetin have been conducted during biofilm development (79), (83), (85). In present studies, these compounds have been added to the developed biofilm. The effect observed is lesser compared to the effect of these compounds during the biofilm development stage due to the presence of EPS that prevents penetration of active compounds into the biofilm and quorum sensing.

7.2.5 Effect of berberine, esculetin and usnic acid on *E. coli* biofilm in DFR

After the addition of berberine to the biofilm formed in a drip-flow reactor, the same trend in MGV of biofilm as in static biofilm was observed - Figure 7.34 - no change to biofilm MGV stained with trypan blue staining and gradual decrease in MGV of biofilm stained with crystal violet. It is important to note that at a concentration of 0.0001M and 0.0025M, no change to biofilm MGV was observed with crystal violet staining.

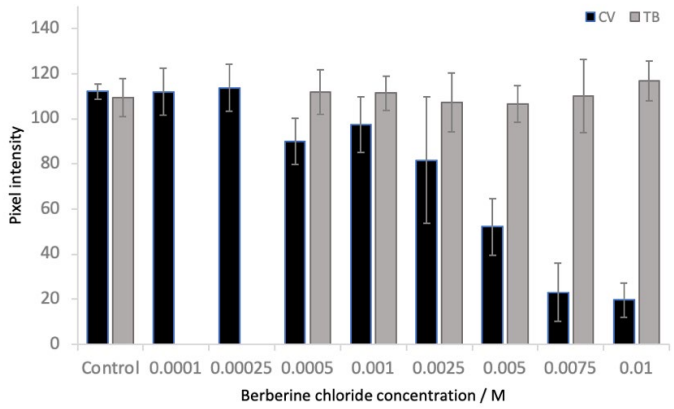

Figure 7.34 Graph showing MGV of biofilm formed in a drip-flow reactor after the addition of berberine chloride, crystal violet and trypan blue staining, N=9, error bars – SD.

At the concentration of 0.1mM and 0.25mM of berberine chloride, there is no change in pixel distribution within biofilm compared to untreated biofilm with crystal violet staining agent – (Figure 7.35). As concentration increases, pixel Group 3 (103 – 153) decreases to 22% and starts fluctuating, and Group 2 (52 – 102) increases from 0.0005M from 32% to 70% and gradually decreases to 4% at 0.01M. Pixel Group 1 (0 – 51) slowly increase from 0.0025M to 0.01M from 6% to 93%, respectively. No changes to pixel composite distribution compared to *E. coli* biofilm were observed with trypan blue staining.

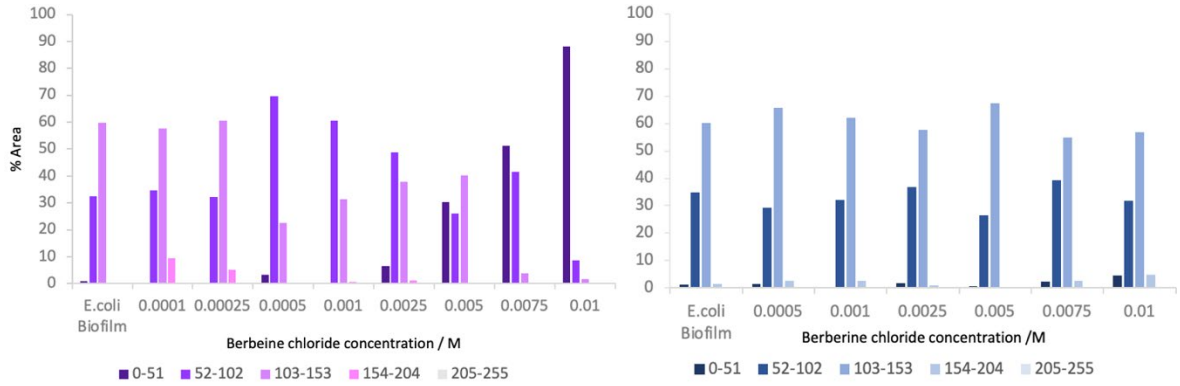

Figure 7.35 Graphs of pixel intensity distribution against % area they occupy in biofilm in a drip-flow reactor after addition of berberine chloride., left – crystal violet staining, right – trypan blue staining.

Esculetin has the same pattern in MGV of biofilm in a drip-flow reactor as in static biofilm – (Figure 7.36) – no change with both staining methods. On the other hand, (+)-usnic acid has the opposite pattern in MGV within biofilm in a drip-flow reactor compared to static biofilm. No change in MGV was observed with crystal violet staining, and a decrease in MGV of biofilm as a concentration of (+)-usnic acid increased with trypan blue dye – (Figure 7.37).

Due to the uneven structure of the biofilm formed in the drip-flow reactor, active ingredients cannot penetrate the biofilm uniformly and staining agents cannot bind to the biofilm homogeneously. This results in the observations above. Drip-flow reactor assay cannot be used to investigate the effect of active ingredients on biofilms in a dose-response manner because of the structure of biofilm formed in this method. This was proved by all antimicrobial agents used in this study.

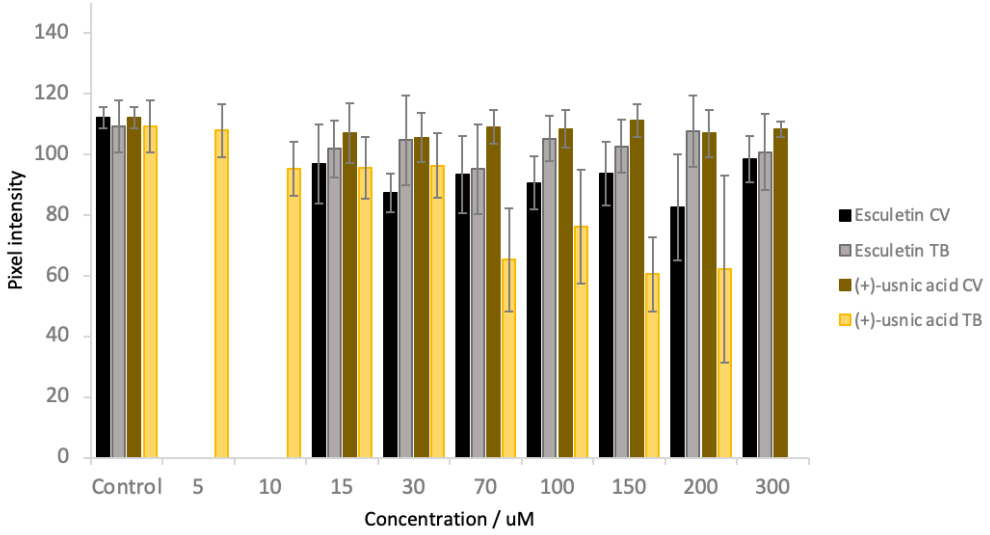

Figure 7.36 Graph showing MGV of biofilm after addition of esculetin and (+)-usnic acid, trypan blue and crystal violet staining, N=9, error bars – SD.

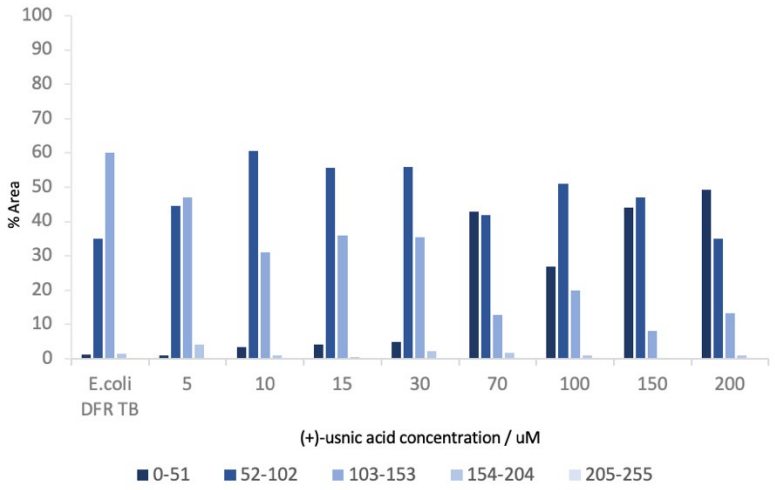

Figure 7.37 Graph showing the pixel intensity distribution of biofilm after the addition of different concentrations of (+)-usnic acid, trypan blue staining.

7.3 Conclusion

Biofilm information by static assay and in a drip-flow reactor does not allow subsequent investigations of biofilm detachment from the surface. This was possible to achieve in a fabricated device only. Not only viability of developed biofilm can be examined using a fabricated device, but also the effect of plant-derived compounds in a dose-response manner.

Both tannic and gallic acids caused the removal of biofilm from the middle of device channels as the concentration in a solution increased. The removal of biofilm mass was only observable in a fabricated device, unlike the static assay and the drip-flow reactor, which showed no removal of biofilm mass. Residual biofilm on the sides of the channel was used to test the effect of both compounds on the viability of the biofilm. Both showed a decrease in MGV as their concentration increased. This was not observed with a static biofilm. MGV remained the same across all concentrations except for gallic acid with crystal violet staining. Similar performance to the fabricated device was observed in a drip-flow reactor.

Berberine chloride showed the removal of biofilm from a fabricated device, mainly from the middle part of the channel. The viability of the remaining biofilm in a channel did not change across all concentrations but had different pixel intensity distributions compared to untreated biofilms. Esculetin only showed biofilm removal from the middle of the channel with trypan blue staining and no change to the viability of biofilm across all concentrations. (+)-Usnic acid also had no effect on developed biofilm by all methods.

Tannic, ellagic and gallic acids were more effective against developed biofilm by both – removal of biofilm from the surface and killing cells within biofilm compared to the other plant-derived compounds tested in this study.

Chapter 8 CONCLUSION AND FUTURE WORK

8.1 CONCLUSIONS

8.1.1 DESIGN AND FABRICATION OF A DEVICE FOR CONTINUOUS BIOFILM GROWTH

- A device that can be used for biofilm studies, designed and fabricated using 3D printing technology, has been successfully achieved.
- Production of the device is cheap and quick and requires little post-printing modifications. A method was developed to seal the 3D-printed part of the device between two glass pieces to produce a leakage-free assembly with a transparent observation area.
- Each device has three parallel channels that provide separate growth compartments allowing for triplicate repeats (statistical repeats). The channel area is transparent, which allows for the non-destructive observations of biofilms. All devices are produced to tight tolerances, enabling comparisons between biofilms grown in different devices.
- The device is versatile as its structure can be easily changed if required by the experiment.
- The device is robust.

8.1.2 PHYSICAL VALIDATION OF DEVICE PERFORMANCE

- Physical validation of device performance was made to prove the identical behaviour of each individual device. The evaluation of flow through the device channels was performed at different flow rates and demonstrated the same speed of liquid through each of the three channels. This provides a consistent and reliable starting point for the growth of reproducible biofilms.
- The flow rate can be reduced to 20ul/min without a change in flow uniformity via three parallel running channels, and the device can withdraw the flow rate of 10ml/min without leakage.
- Quantification of the inter-channel consistency of biofilm coverage was also used as the physical validation of the device performance. Uniform formation of biofilm between channels of one device and between devices was achieved. After 48 hours of growth, the uniform coverage of each channel was observed.

8.1.3 PROOF OF CONCEPT 1: DOSE-RESPONSE STUDIES FOR STERILISING AGENTS

- The fabricated devices were shown to yield does-response data on two known antimicrobial agents that are consistent with literature data.
- Uniform biofilm formation within three channels of a device and between devices was confirmed. The device allows for uniform delivery of active ingredients to all channels. The same patterns of remaining biofilms proved this after the addition of active ingredients.

8.1.4 PROOF OF CONCEPT 2: DOSE-RESPONSE DATA FROM NATURALLY DERIVED ACTIVES

8.2 The new devices were used to investigate the anti-biofilm properties of a range of polyphenols and other plant-derived molecules. The data obtained show that several of the compounds investigated contribute to the removal of biofilm from the surface and the viability of cells in a biofilm in a dose-response manner.

8.3 FURTHER WORK

The device that was developed is suitable for immediate use in studies on the effect of the addition of active ingredients during initial cell attachment or during biofilm development.

Modifications to the design of the device can be made easily, providing a versatile high-throughput data generation platform. For example, different surface topographies on the sides of channels can be printed to study the attachment of cells to the surface.

The design of the device can be extended further by incorporating a temperature sensor during production to allow accurate temperature control inside the device.

Appendix A Supplementary information

A.1 2.1 Design of a device

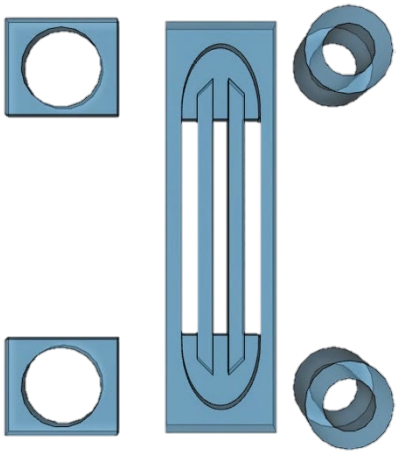

Figure 8.1 Separate parts of device design v.1

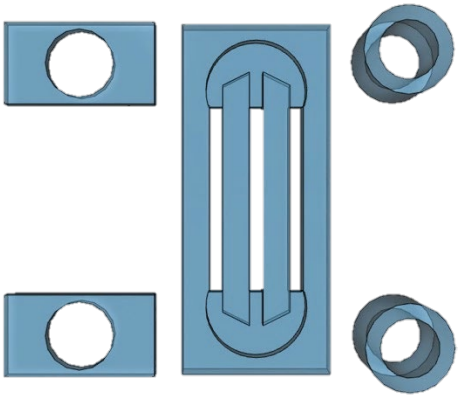

Figure 8.2 Separate parts of device design v.2

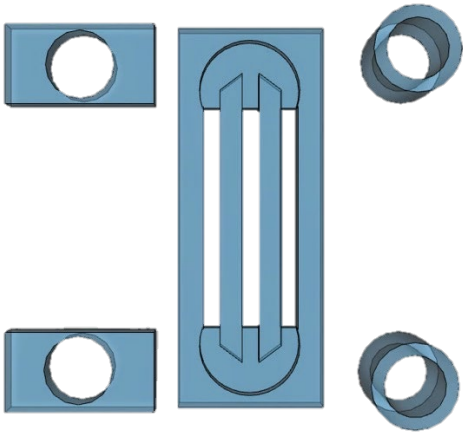

Figure 8.3 Separate parts of device design v.3

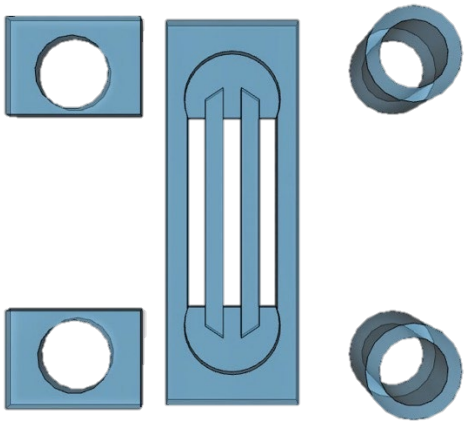

Figure 8.4 Separate parts of device design v.4

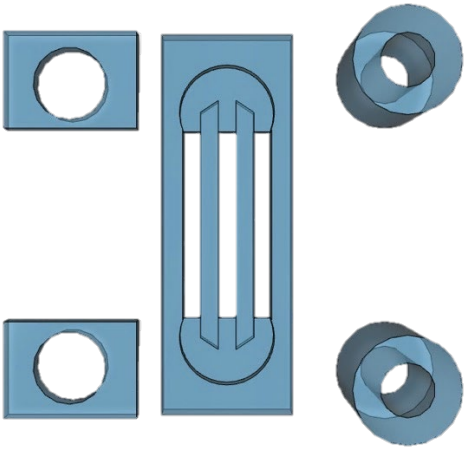

Figure 8.5 Separate parts of device design v.5

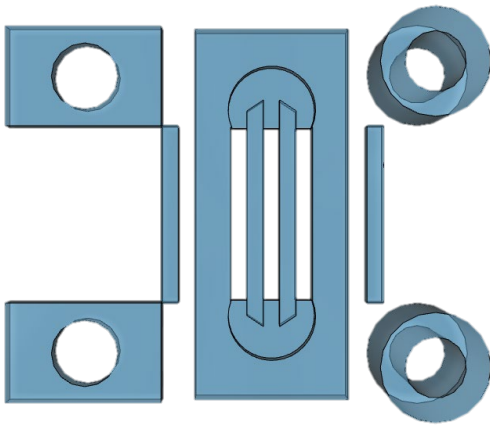

Figure 8.6 Separate parts of device design v.6

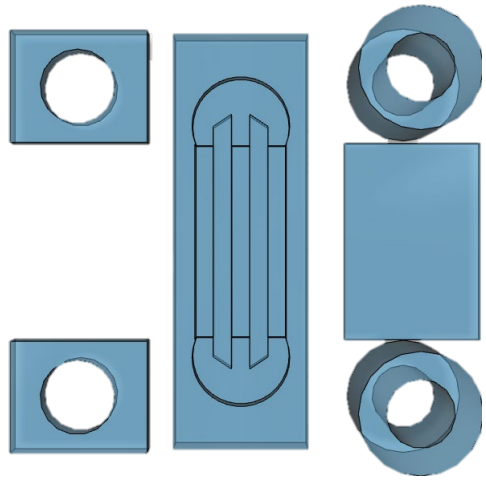

Figure 8.7 Separate parts of device design v.7

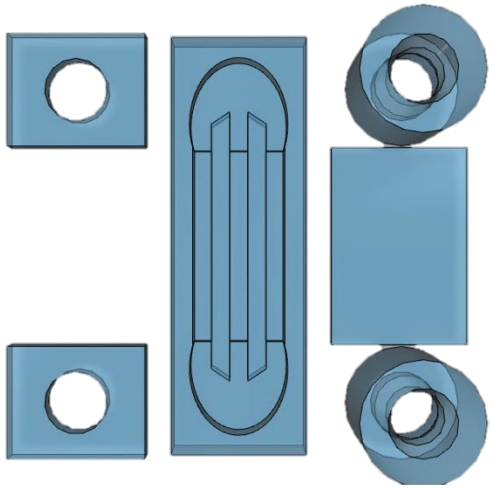

Figure 8.8 Separate parts of device design v.8

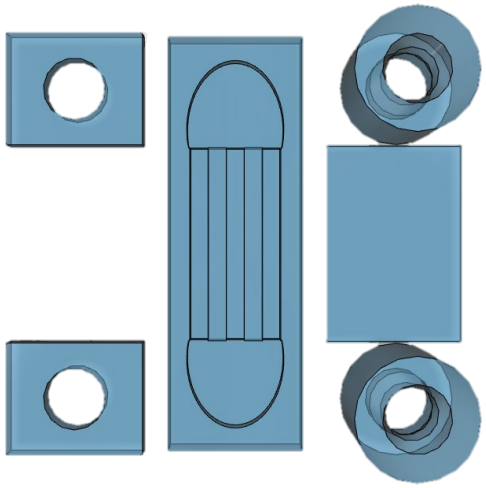

Figure 8.9 Separate parts of device design v.9

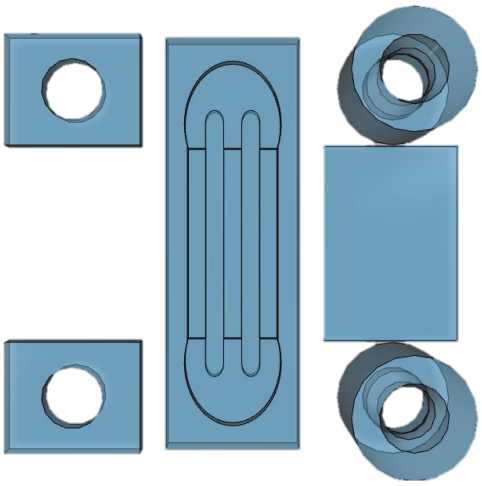

Figure 8.10 Separate parts of device design v.10

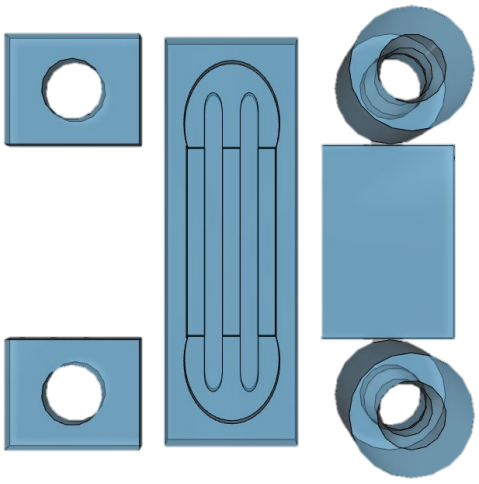

Figure 8.11 Separate parts of device design v.11

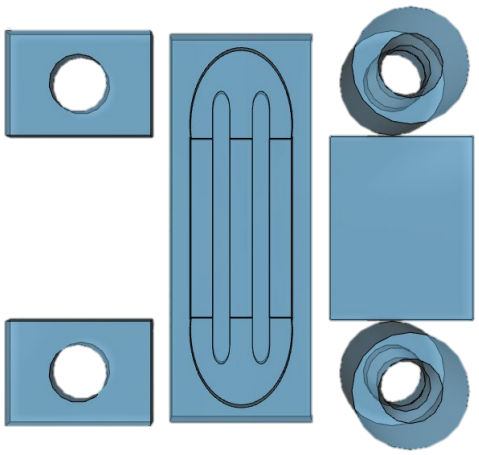

Figure 8.12 Separate parts of device design v.12

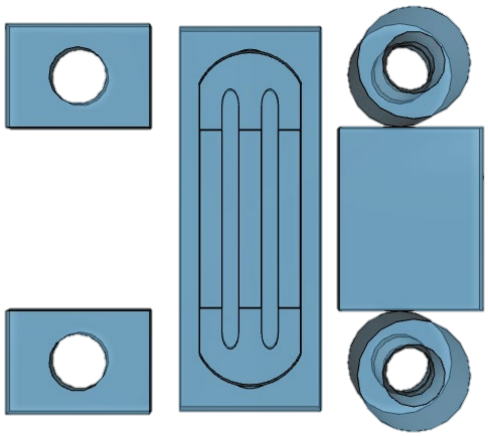

Figure 8.13 Separate parts of device design v.13

Figure 8.14 Separate parts of device design v.14

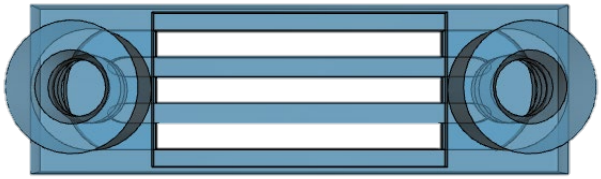

Figure 8.15 Separate parts of device design v.15

A.2 5.1.1 Effect of ethanol on static 24h *E. coli* biofilm

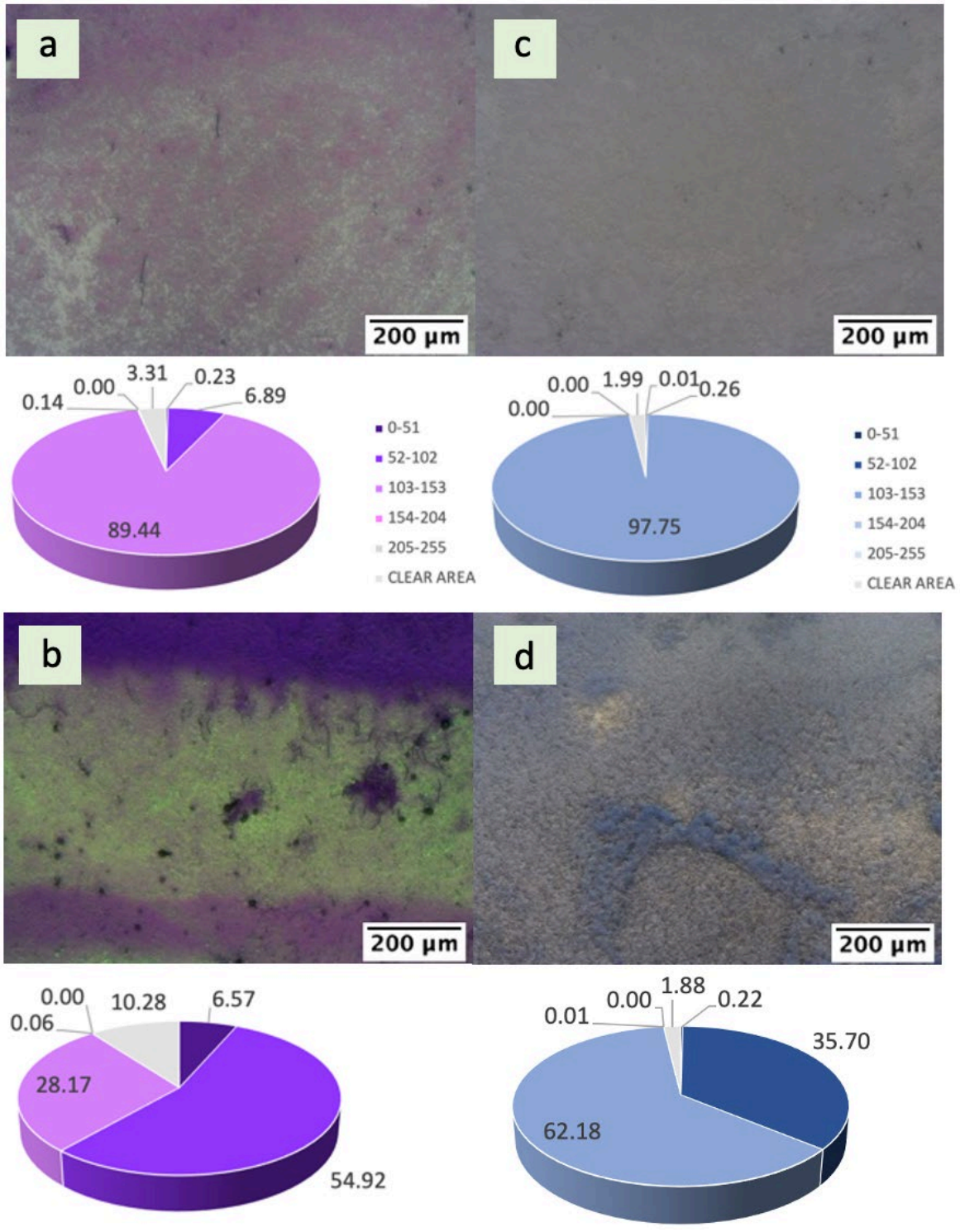

Figure 8.16 Images of static biofilm after ethanol treatment and pixel intensity distribution in pie charts. a – 10% ethanol, crystal violet, b – 70% ethanol, crystal violet, c – 10% ethanol, trypan blue, d – 70% ethanol, trypan blue, N=12.

A.3 5.1.2 The reaction of ethanol with continuous 48h E. coli biofilm in Drip-flow reactor

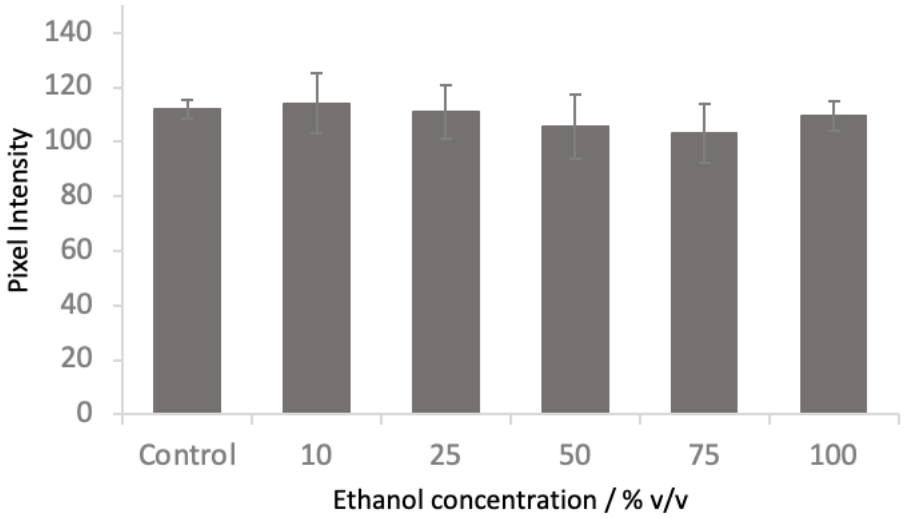

Figure 8.17 Graph showing the MGV of biofilm after exposure to different concentrations of ethanol, crystal violet staining, N=9.

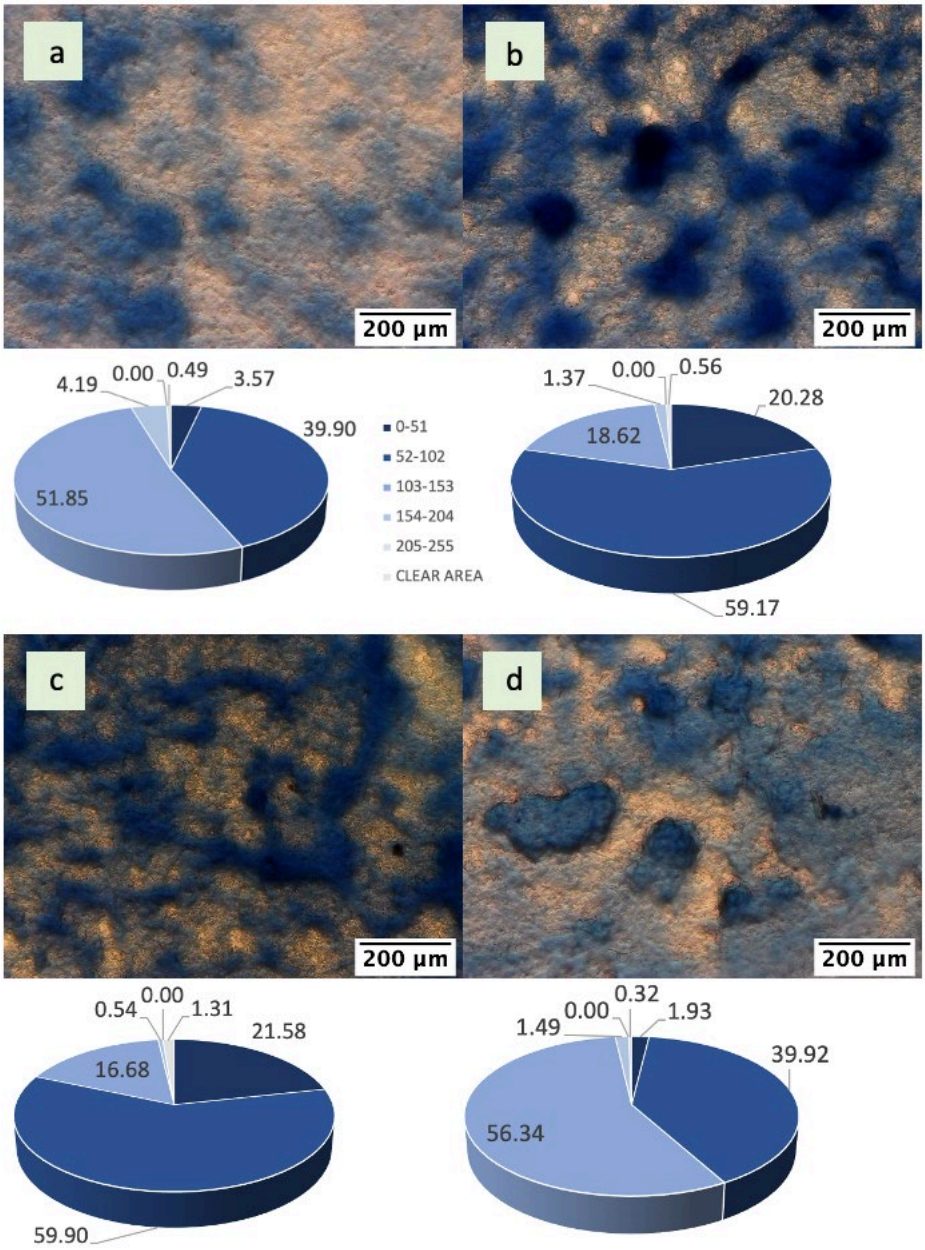

Figure 8.18 A graph showing the images of biofilm in a drip-flow reactor and their pixel intensity distribution – pie charts after exposure to different concentrations of ethanol. a – 10% ethanol, b – 40% ethanol, c – 70% ethanol, d – 100% ethanol.

A.4 5.2.2 Study of the effect of chlorhexidine on continuous 48h biofilm in Drip-flow reactor

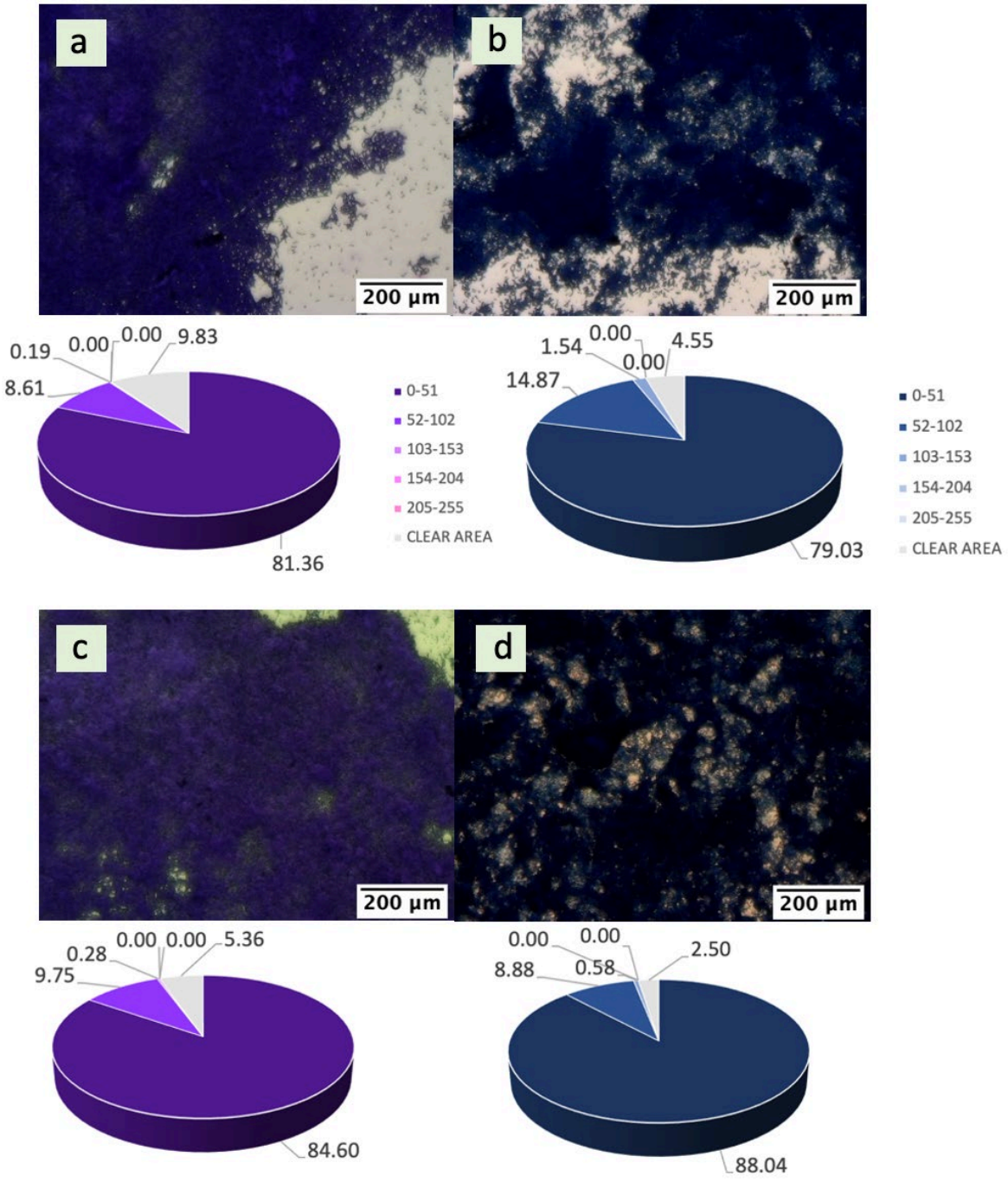

Figure 8.19 Images of continuous biofilm in a drip flow reactor after CHX treatment and pie charts of their pixel intensity distribution, a – 0.04% CHX crystal violet, b – 0.04% CHX trypan blue, c – 0.12% CHX crystal violet, d – 0.12% CHX trypan blue.

A.5 5.2.3 Testing the exposure of 72h E. coli biofilm to the chlorhexidine concentrations

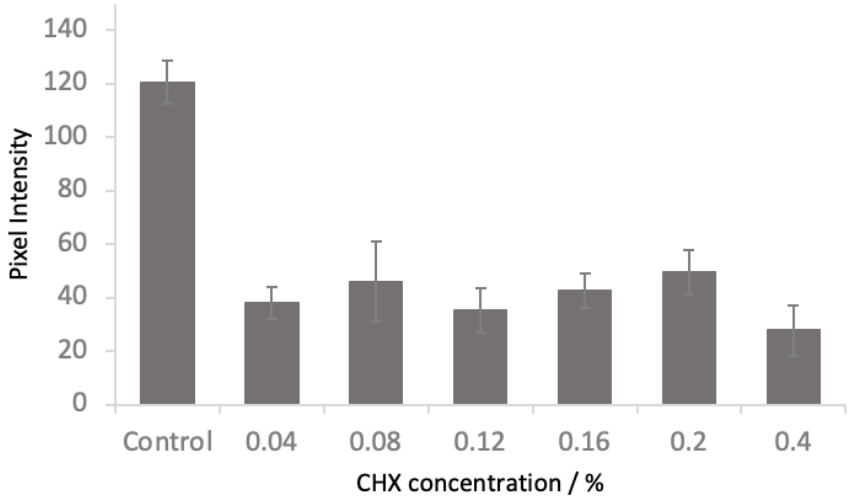

Figure 8.20 Graph showing the MGV of continuous 72h biofilm after CHX treatment.

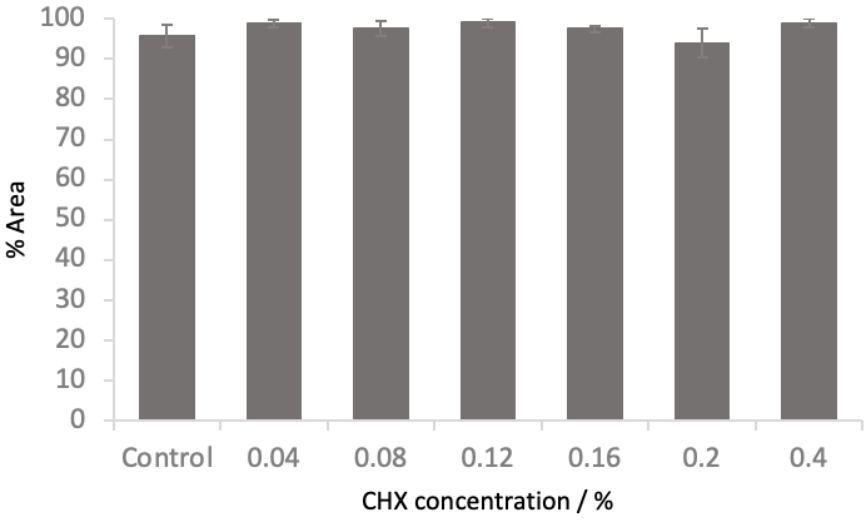

Figure 8.21 Graph showing the % area of continuous 72h biofilm after CHX treatment.

A.6 6.1.1 Investigating the effect of tannic and gallic acid on static *E. coli* biofilm

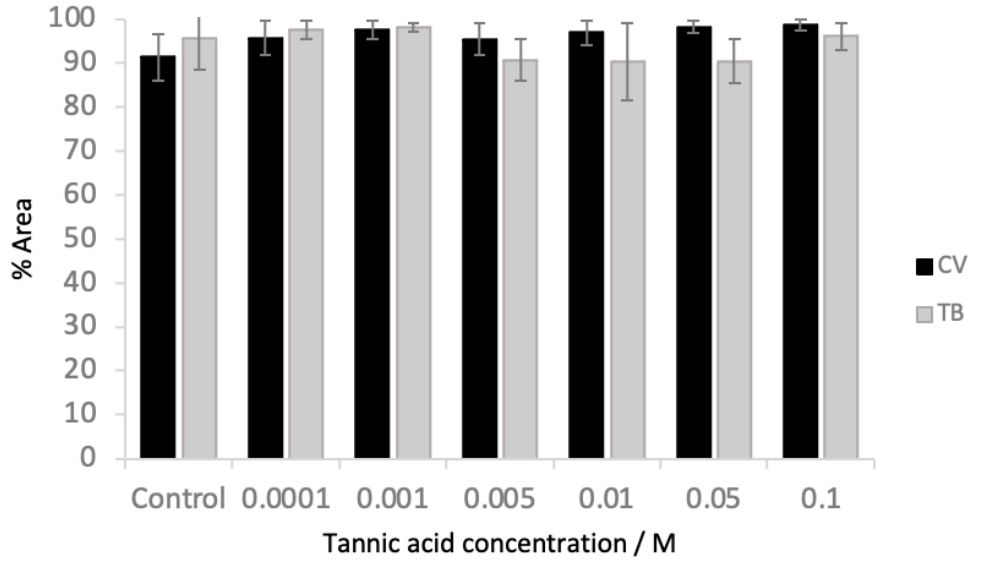

Figure 8.22 Graph showing the % area occupied by static biofilm after addition of different concentrations of tannic acid, crystal violet and trypan blue staining.

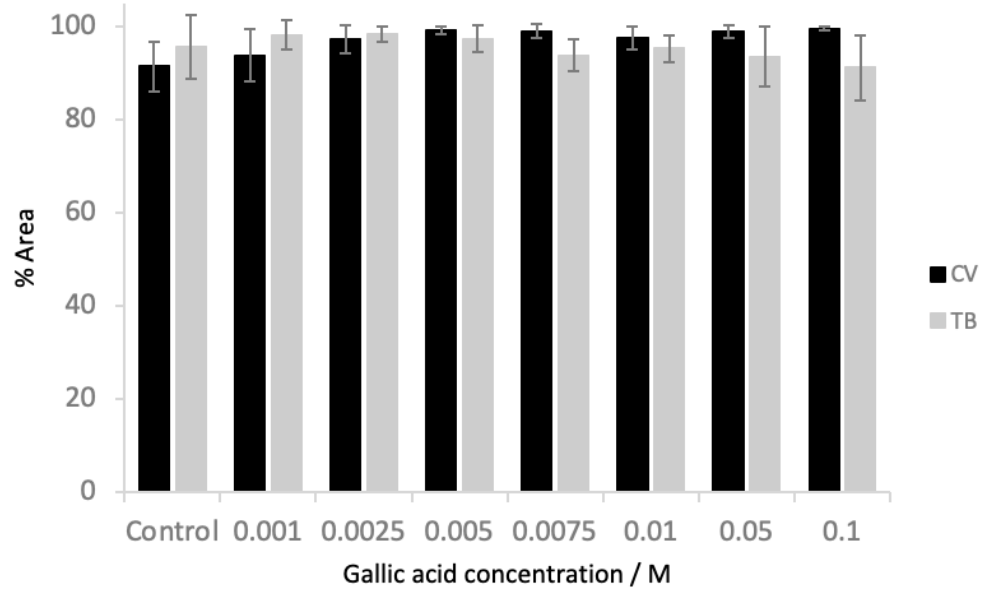

Figure 8.23 Graph showing the % area occupied by static biofilm after addition of different concentrations of gallic acid, crystal violet and trypan blue staining.

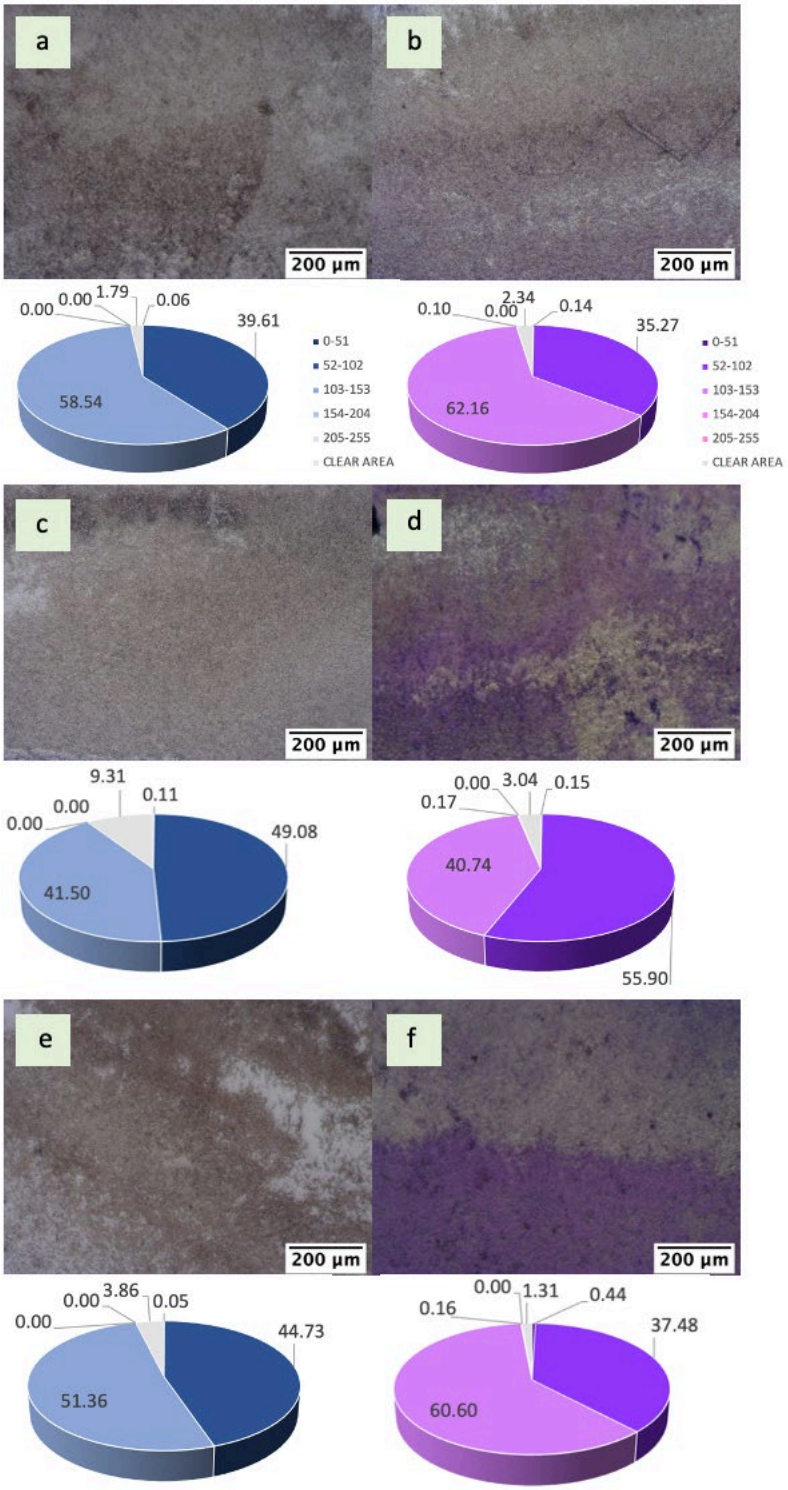

Figure 8.24 **Images of static biofilms after tannic acid addition and pie charts of their pixel intensities distribution. a – 0.001M trypan blue staining, b – 0.001M crystal violet, c – 0.01M trypan blue, d – 0.01M crystal violet, e – 0.1M trypan blue, f – 0.1M crystal violet.**

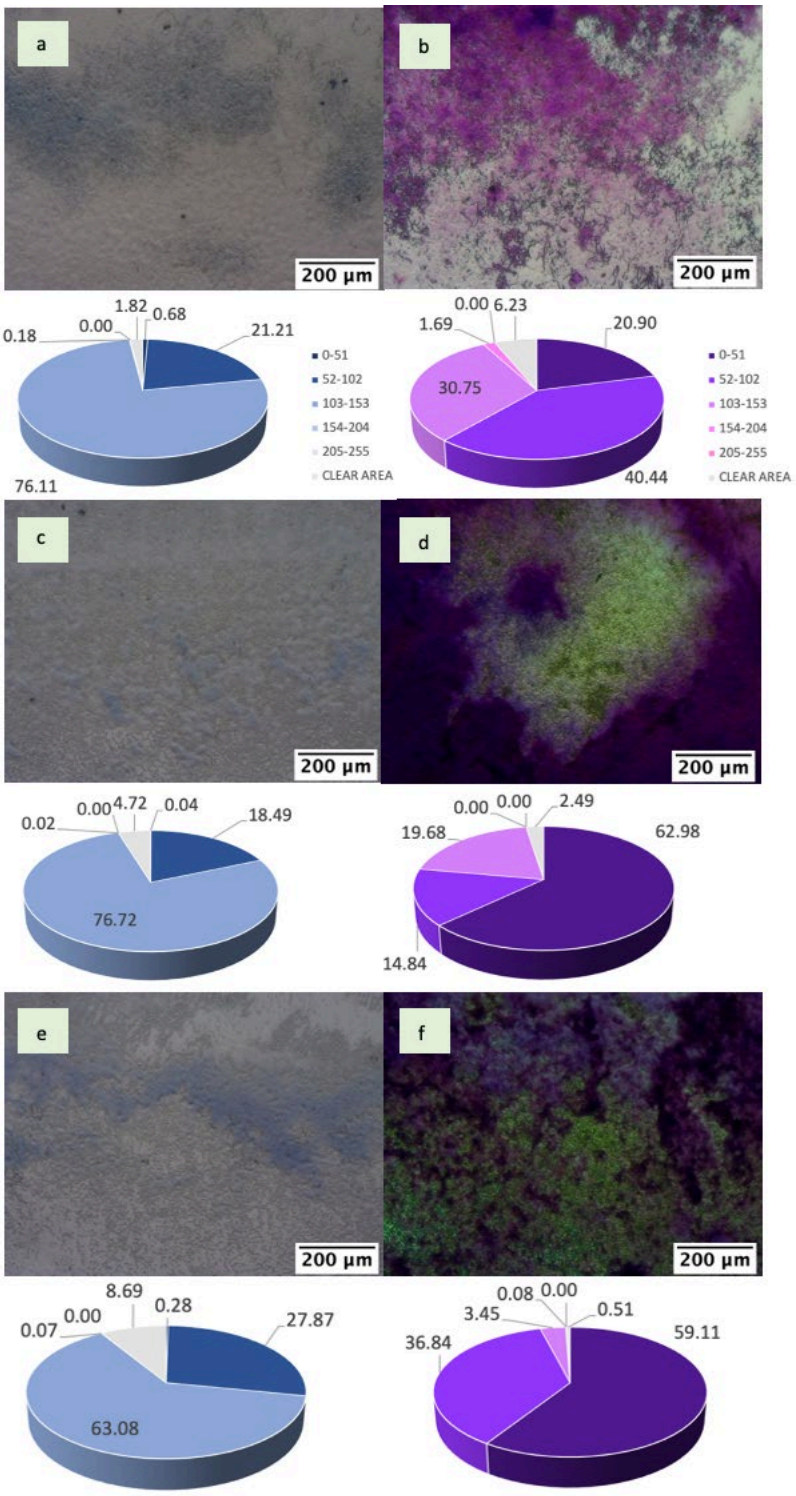

Figure 8.25 **Images of static biofilms after gallic acid addition and pie charts of their pixel intensities distribution. a – 0.001M trypan blue staining, b – 0.001M crystal violet, c – 0.01M trypan blue, d – 0.01M crystal violet, e – 0.1M trypan blue, f – 0.1M crystal violet.**

A.7 6.1.2 Action of tannic and gallic acid on continuous *E. coli* biofilm formed in a drip-flow reactor

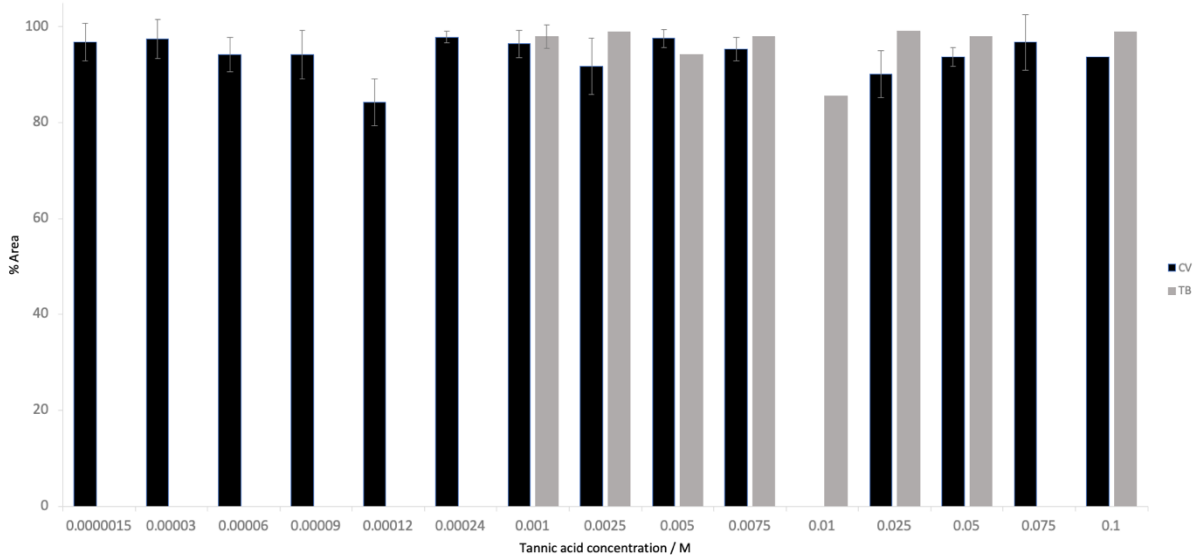

Figure 8.26 Graph of % area occupied by biofilm after addition of different concentrations of tannic acid to biofilm grown in a drip-flow reactor.

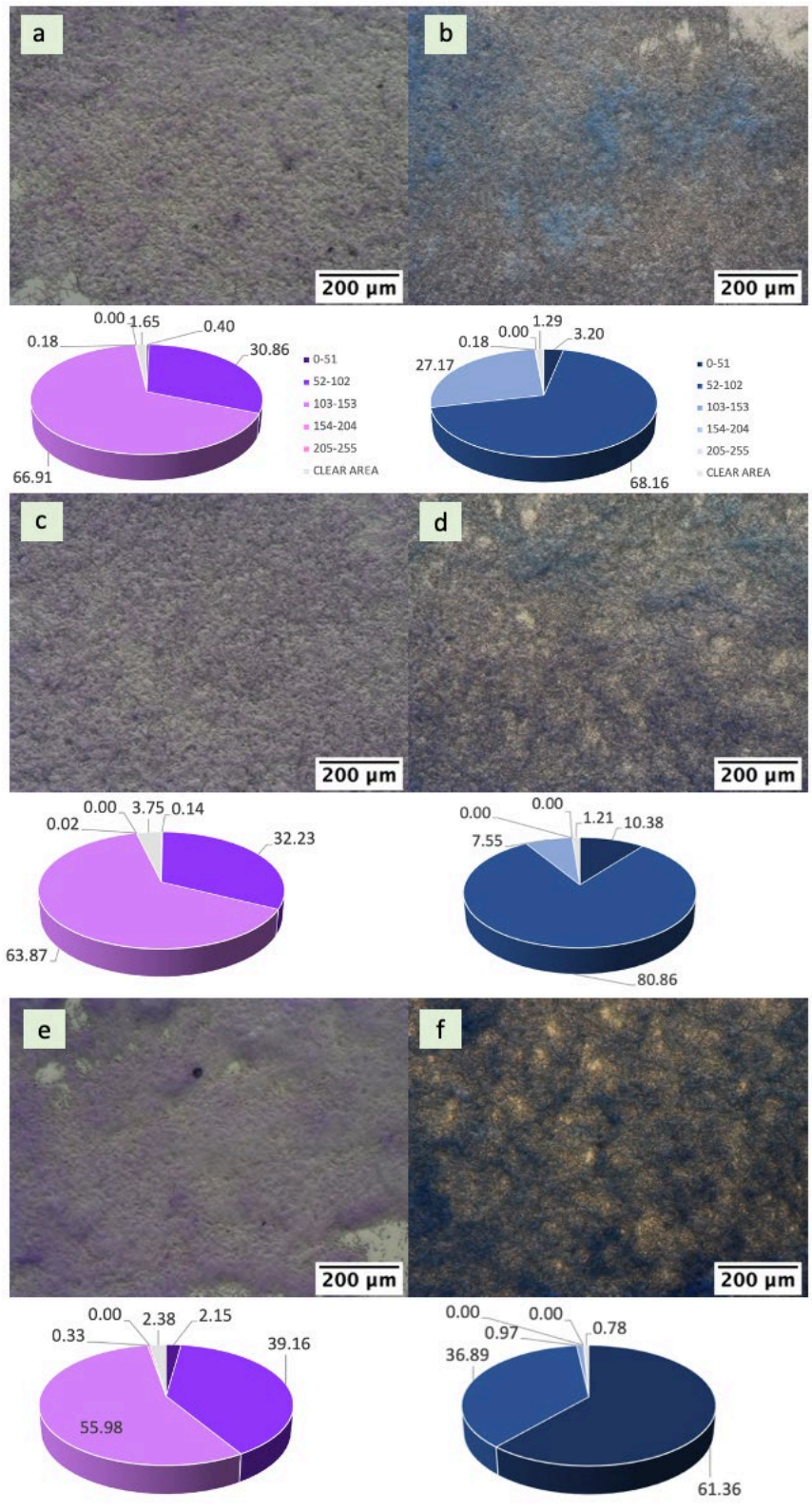

Figure 8.27 Images of biofilms in a drip-flow reactor after gallic acid addition and pie charts of their pixel intensities distribution. a – 0.001M crystal violet staining, b – 0.001M trypan blue, c – 0.0025M crystal violet, d – 0.0025M trypan blue, e – 0.025M crystal violet, f – 0.025m trypan blue.

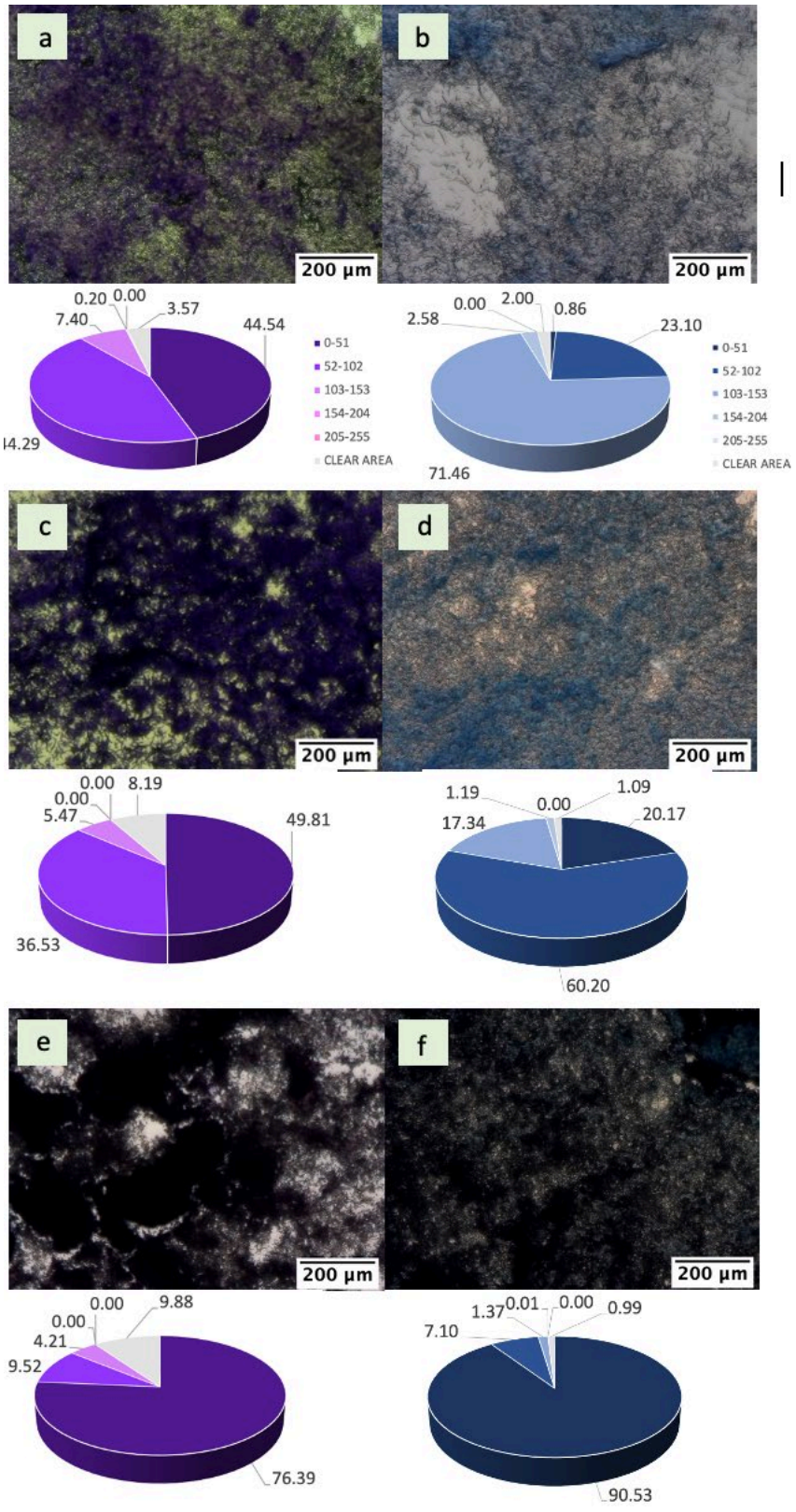

Figure 8.28 **Images of biofilms in a drip-flow reactor after tannic acid addition and pie charts of their pixel intensities distribution. a – 0.001M crystal violet staining, b – 0.001M trypan blue, c – 0.0025M crystal violet, d – 0.0025M trypan blue, e – 0.025M crystal violet, f – 0.025M trypan blue.**

A.8 6.2.1 The activity of berberine, esculetin and usnic acid on static E. coli biofilm

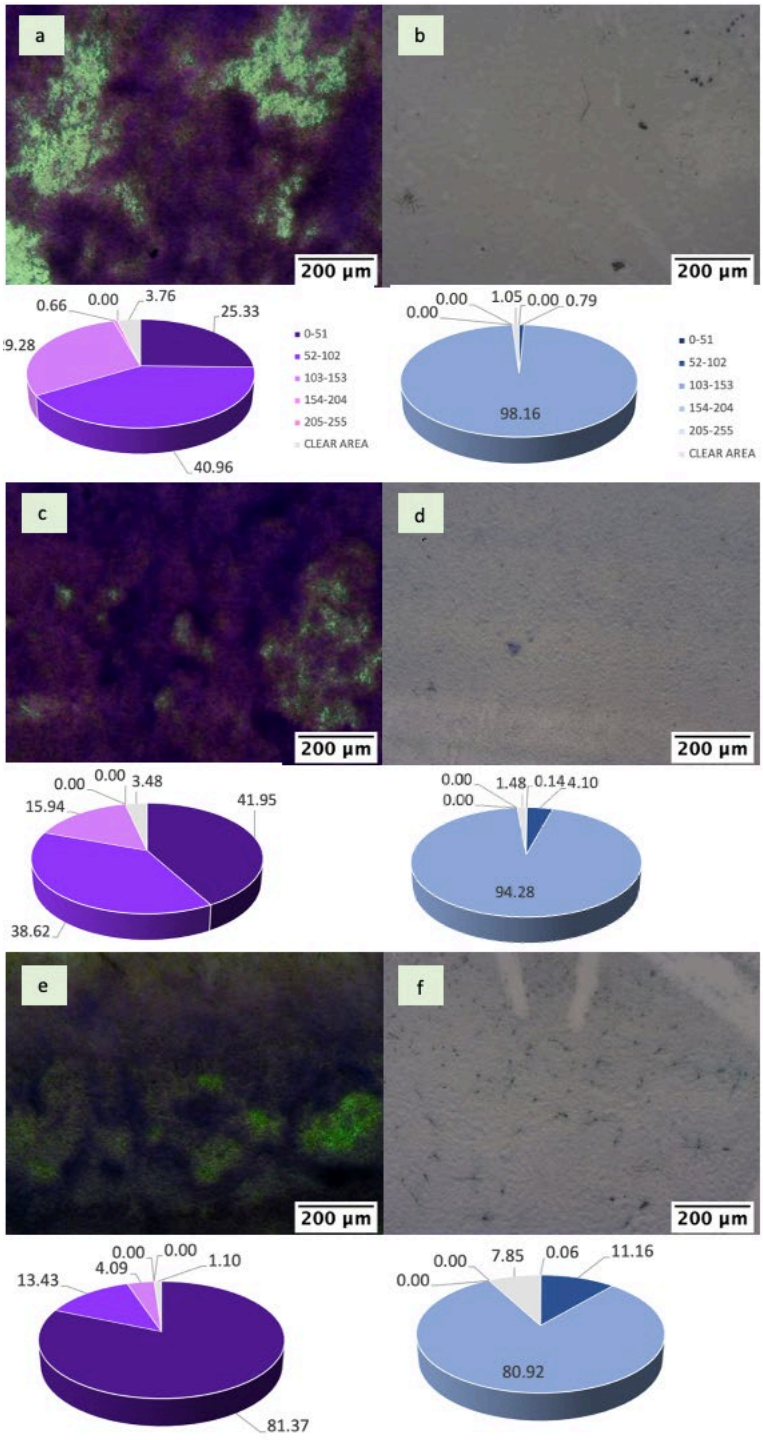

Figure 8.29 Images of static biofilm after addition if berberine chloride and pie charts of pixel distribution. a – 0.001M, crystal violet, b – 0.001M, trypan blue, c – 0.005M, crystal violet, d – 0.005M, trypan blue, e – 0.01M, crystal violet, f – 0.01M, trypan blue.

A.9 6.2.3 Effect of berberine on E. coli biofilm in fabricated device

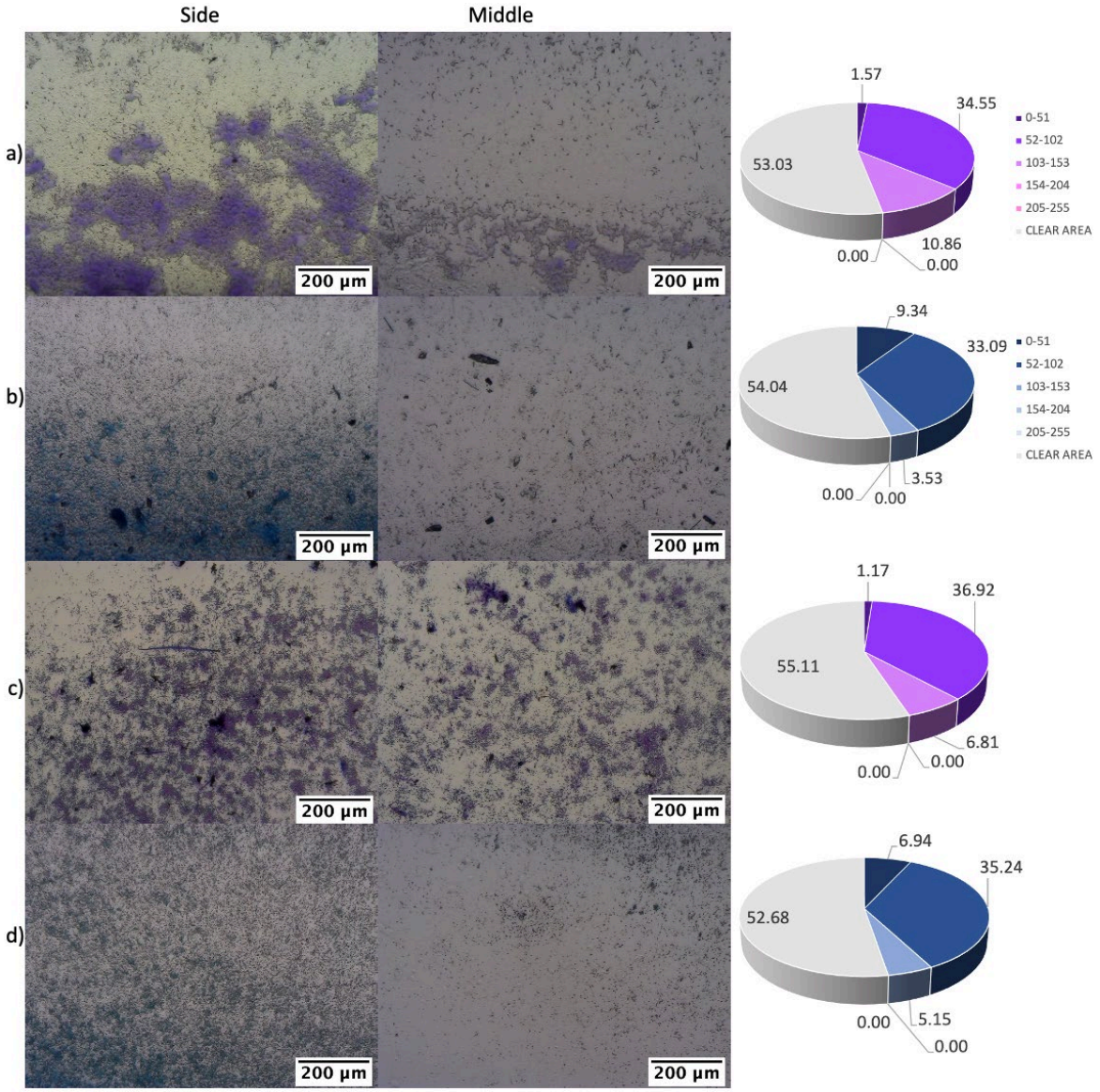

Figure 8.30 Images of biofilm in fabricated device side and middle part and pie chart of pixel intensity distribution, a) – 0.001M trypan blue, b) – 0.001M crystal violet, c) 0.005M crystal violet, d) – 0.005M trypan blue.

A.10 6.2.4 Effect of esculetin of E. coli biofilm in device

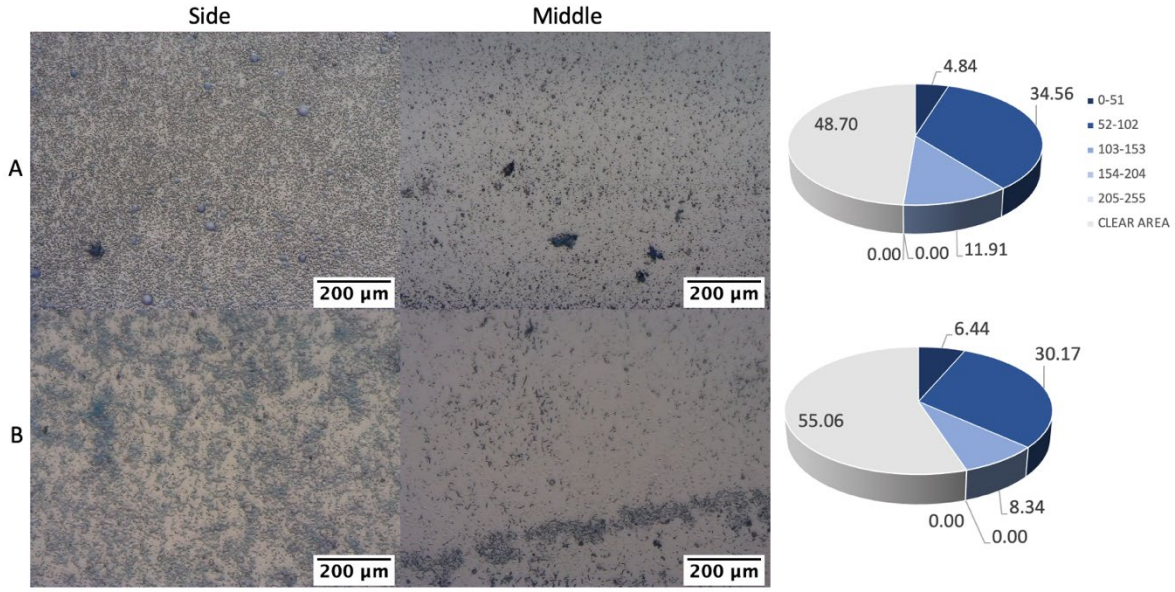

Figure 8.31 Images of biofilm after addition of esculetin and pie chart of pixel intensity distribution. A – 30uM, B – 100uM.

A.11 6.2.5 Effect of usnic acid on continuous E. coli biofilm in fabricated device

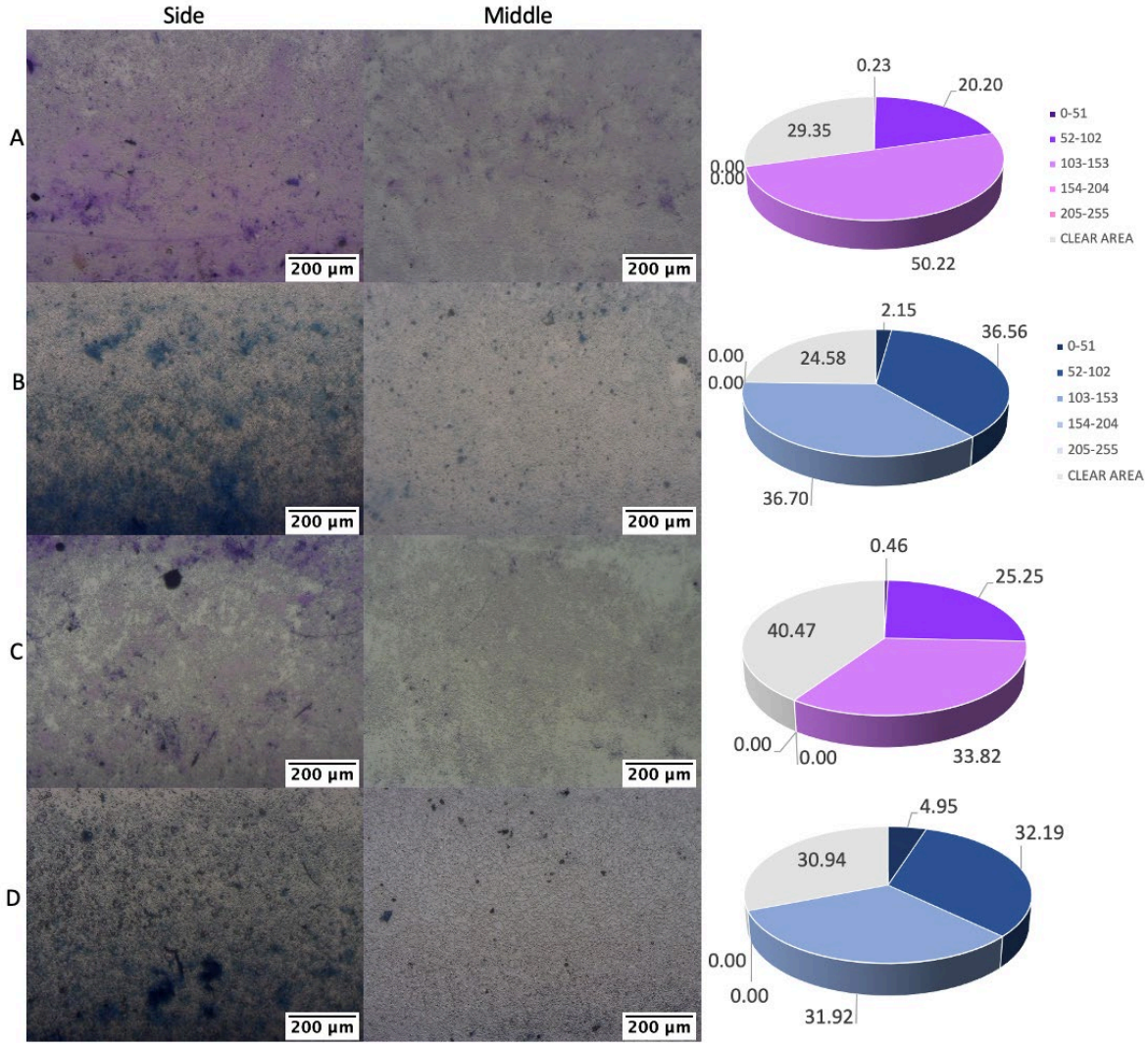

Figure 8.32 Images of biofilm after addition of (+)-uscnic acid concentrations and pie charts of their pixel intensity distribution. A – 30uM crystal violet, B – 30uM trypan bluer, C – 100uM crystal violet, D – 100uM trypan blue.

A.12 Negative controls

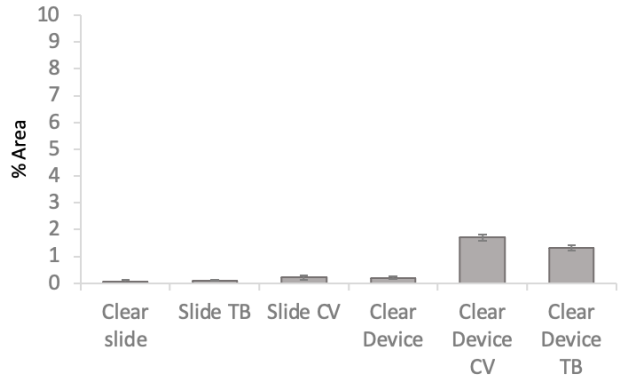

Figure 8.33 Graph of % area in empty device and slide, and after staining with trypan blue and crystal violet.

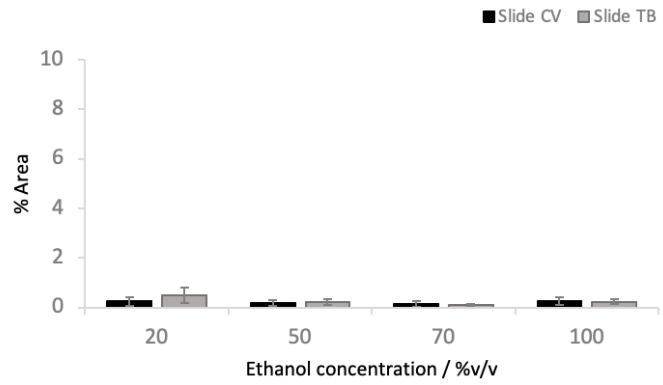

Figure 8.34 Graph of % area on clear slide after contact with ethanol concentrations.

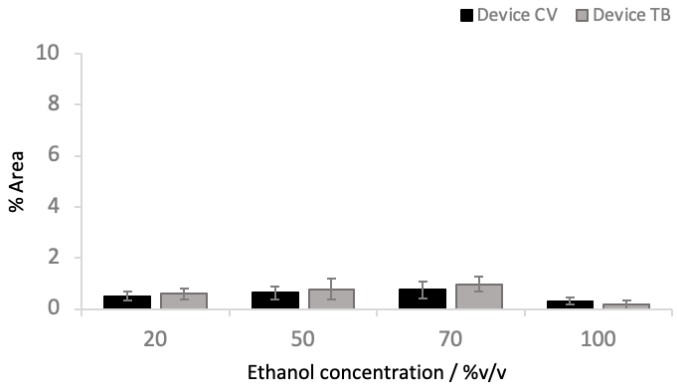

Figure 8.35 Graph of % area in clear device after contact with ethanol concentrations.

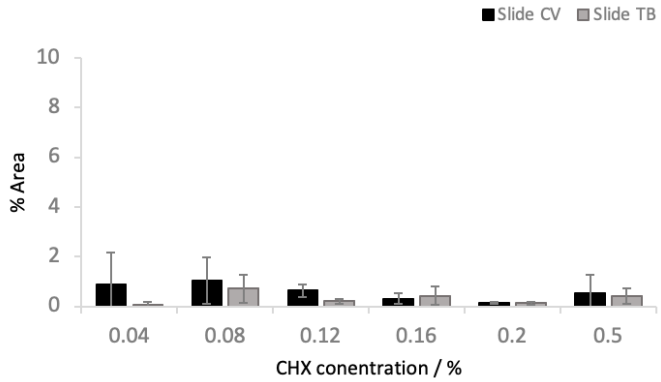

Figure 8.36 Graph of % area on clear slide after contact with chlorhexidine concentrations.

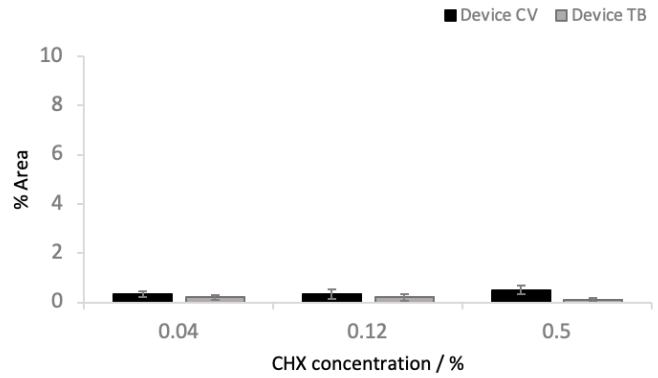

Figure 8.37 Graph of % area in clear device after contact with chlorhexidine concentrations.

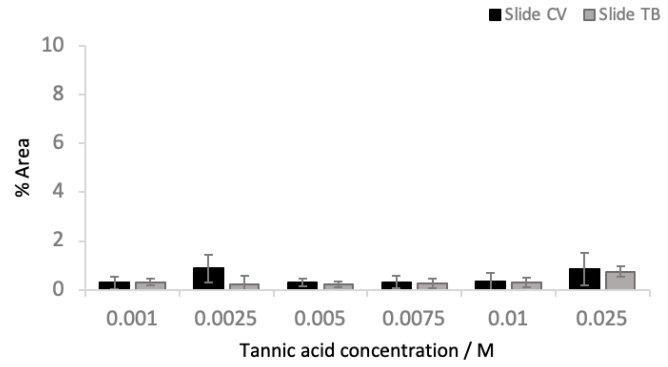

Figure 8.38 Graph of % area on clear slide after contact with tannic acid concentrations.

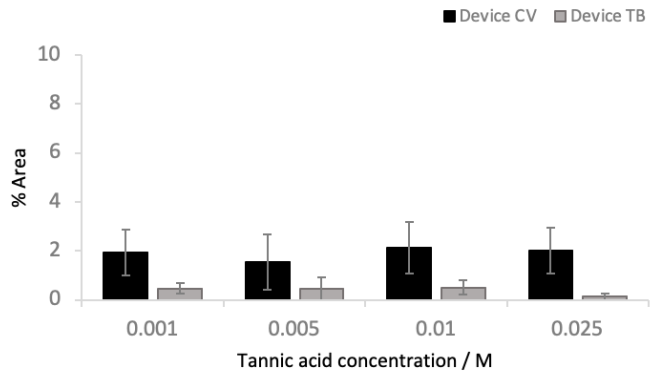

Figure 8.39 Graph of % area in clear device after contact with tannic acid concentrations.

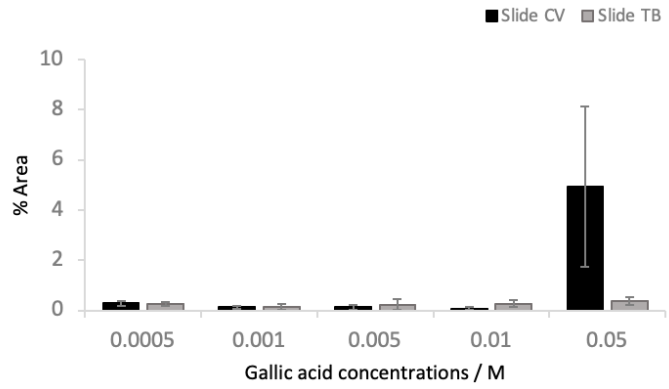

Figure 8.40 Graph of % area on clear slide after contact with gallic acid concentrations.

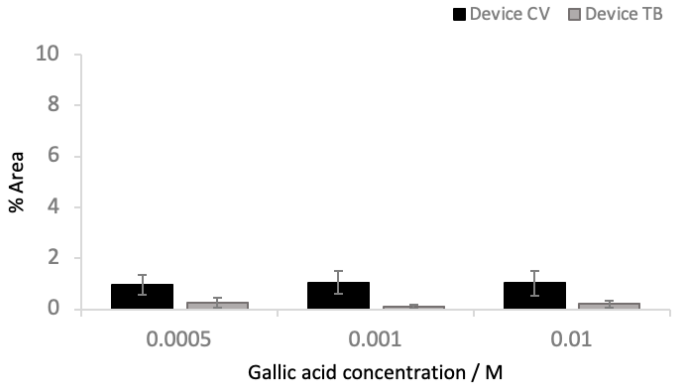

Figure 8.41 Graph of % area in clear device after contact with gallic acid concentrations.

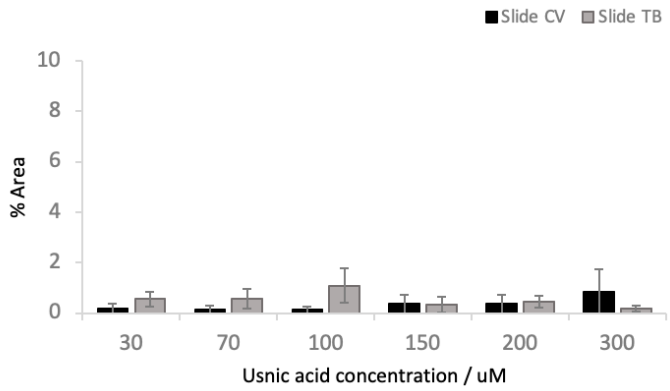

Figure 8.42 Graph of % area on clear slide after contact with usnic acid concentrations.

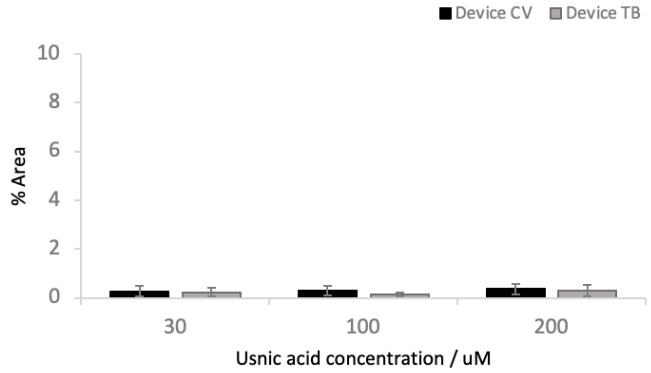

Figure 8.43 Graph of % area in clear device after contact with usnic acid concentrations.

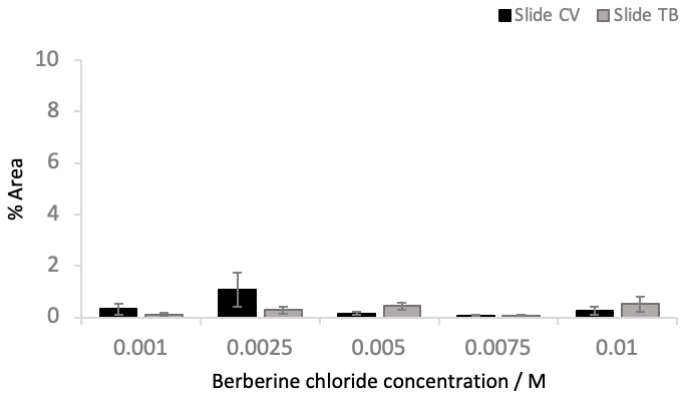

Figure 8.44 Graph of % area on clear slide after contact with berberine chloride concentrations.

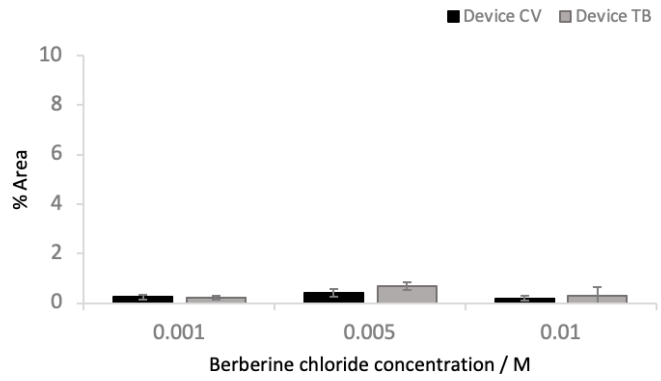

Figure 8.45 Graph of % area in clear device after contact with berberine chloride concentrations.

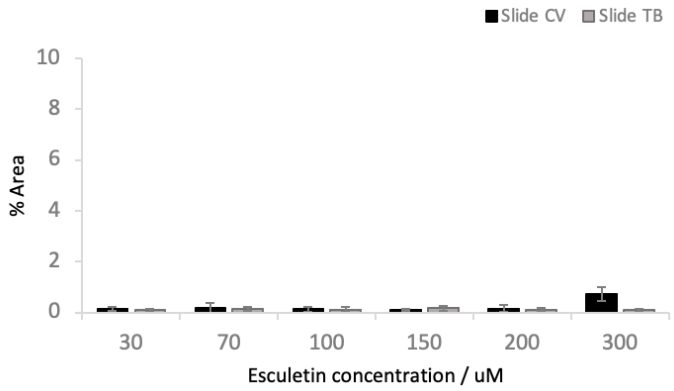

Figure 8.46 Graph of % area on clear slide after contact with esculetin concentrations.

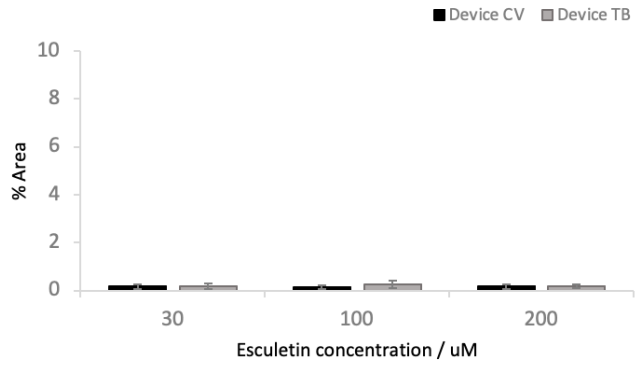

Figure 8.47 Graph of % area in clear device after contact with esculetin concentration.

Appendix B 3D printer settings

Table 8.1 MakerBot Replicator 2X printer settings for PLA filament.

Extruder Temperature	215°C	Platform Temperature	110°C
Travel Speed	150 mm/s	Z-axis Travel Speed	23 mm/s
Infill Print Speed	90 mm/s	Inserts Print Speed	90 mm/s
Outlines Print Speed	40 mm/s	Raft Print Speed	90 mm/s
Raft Base Print Speed	10 mm/s	Bridges Print Speed	40 mm/s
First Layer Print Speed	30 mm/s	Infill Density	80%
Infill Pattern	Linear	Layer Height	0.15 mm
Infill Layer Height	0.2 mm	Number of Shells	2
Roof Thickness	0.80 mm	Floor Thickness	0.80 mm
Coarseness	0.0001 mm	Raft-Model Spacing	0.35 mm
Raft Margin	4.0 mm	Support	Off
Bridging	Off	Filament Diameter	1.75 mm
Retraction Distance	1.3 mm	Retraction Speed	25 mm/s
Restart Speed	25 mm/s	Extra Restart Distance	0.0 mm

Table 8.2 MakerBot Replicator 2X printer settings for T-glase filament.

Extruder Temperature	230°C	Platform Temperature	60°C
Travel Speed	150 mm/s	Z-axis Travel Speed	23 mm/s
Infill Print Speed	90 mm/s	Inserts Print Speed	90 mm/s
Outlines Print Speed	40 mm/s	Raft Print Speed	90 mm/s
Raft Base Print Speed	10 mm/s	Bridges Print Speed	40 mm/s
First Layer Print Speed	30 mm/s	Infill Density	80%
Infill Pattern	Linear	Layer Height	0.2 mm
Infill Layer Height	0.2 mm	Number of Shells	2

Roof Thickness	1 mm	Floor Thickness	0.80 mm
Coarseness	0.0001 mm	Raft-Model Spacing	0.35 mm
Raft Margin	4.0 mm	Support	Off
Bridging	Off	Filament Diameter	1.75 mm
Retraction Distance	1.3 mm	Retraction Speed	25 mm/s
Restart Speed	25 mm/s	Extra Restart Distance	0.0 mm

Table 8.3 MakerBot Replicator 2X printer settings for HDGlase filament.

Extruder Temperature	220°C	Platform Temperature	60°C
Travel Speed	150 mm/s	Z-axis Travel Speed	23 mm/s
Infill Print Speed	90 mm/s	Inserts Print Speed	90 mm/s
Outlines Print Speed	40 mm/s	Raft Print Speed	90 mm/s
Raft Base Print Speed	10 mm/s	Bridges Print Speed	40 mm/s
First Layer Print Speed	30 mm/s	Infill Density	80%
Infill Pattern	Linear	Layer Height	0.2 mm
Infill Layer Height	0.2 mm	Number of Shells	2
Roof Thickness	1 mm	Floor Thickness	0.80 mm
Coarseness	0.0001 mm	Raft-Model Spacing	0.35 mm
Raft Margin	4.0 mm	Support	Off
Bridging	Off	Filament Diameter	1.75 mm
Retraction Distance	1.3 mm	Retraction Speed	25 mm/s
Restart Speed	25 mm/s	Extra Restart Distance	0.0 mm

Bibliography

1. Stepanovic S, Vukovic D, Hola V, Di Bonaventura G, Djukic S, Cirkovic I, et al. Quantification of biofilm in microtiter plates: overview of testing conditions and practical recommendations for assessment of biofilm production by staphylococci. Apmis. 2007;115(8):891-9.

2. Donlan RM, Costerton JW. Biofilms: Survival mechanisms of clinically relevant microorganisms. Clinical Microbiology Reviews. 2002;15(2):167-+.

3. Roy R, Tiwari M, Donelli G, Tiwari V. Strategies for combating bacterial biofilms: A focus on anti-biofilm agents and their mechanisms of action. Virulence. 2018;9(1):522-54.

4. Zhou MX, Yang Y, Chen PL, Hu HJ, Hardwidge PR, Zhu GQ. More than a locomotive organelle: flagella in Escherichia coli. Applied Microbiology and Biotechnology. 2015;99(21):8883-90.

5. Palmer RJ, White DC. Developmental biology of biofilms: implications for treatment and control. Trends in Microbiology. 1997;5(11):435-40.

6. Crawford RJ, Webb HK, Truong VK, Hasan J, Ivanova EP. Surface topographical factors influencing bacterial attachment. Advances in Colloid and Interface Science. 2012;179:142-9.

7. O'Toole G, Kaplan HB, Kolter R. Biofilm formation as microbial development. Annual Review of Microbiology. 2000;54:49-79.

8. Waters CM, Bassler BL. Quorum sensing: Cell-to-cell communication in bacteria. Annual Review of Cell and Developmental Biology. 2005;21:319-46.

9. Tsuneda S, Aikawa H, Hayashi H, Yuasa A, Hirata A. Extracellular polymeric substances responsible for bacterial adhesion onto solid surface. Fems Microbiology Letters. 2003;223(2):287-92.

10. Costa OYA, Raaijmakers JM, Kuramae EE. Microbial Extracellular Polymeric Substances: Ecological Function and Impact on Soil Aggregation. Frontiers in Microbiology. 2018;9.

11. Bassler BL. How bacteria talk to each other: regulation of gene expression by quorum sensing. Current Opinion in Microbiology. 1999;2(6):582-7.

12. Nadell CD, Xavier JB, Foster KR. The sociobiology of biofilms. Fems Microbiology Reviews. 2009;33(1):206-24.

13. Juhasz AL, Naidu R. Bioremediation of high molecular weight polycyclic aromatic hydrocarbons: a review of the microbial degradation of benzo a pyrene. International Biodeterioration & Biodegradation. 2000;45(1-2):57-88.

14. Davies JC, Bilton D. Bugs, Biofilms, and Resistance in Cystic Fibrosis. Respiratory Care. 2009;54(5):628-38.

15. Post JC. Direct Evidence of Bacterial Biofilms in Otitis Media. Laryngoscope. 2015;125(9):2003-14.

16. Wagenlehner FME, Pilatz A, Bschleipfer T, Diemer T, Linn T, Meinhardt A, et al. Bacterial prostatitis. World Journal of Urology. 2013;31(4):711-6.

17. Paju S, Scannapieco FA. Oral biofilms, periodontitis, and pulmonary infections. Oral Diseases. 2007;13(6):508-12.

18. Vlassova N, Han A, Zenilman JM, James G, Lazarus GS. New horizons for cutaneous microbiology: the role of biofilms in dermatological disease. British Journal of Dermatology. 2011;165(4):751-9.

19. Qureshi N. Beneficial biofilms: wastewater and other industrial applications. Biofilms in the Food and Beverage Industries. 2009(181):474-98.

20. Wolcott R. Disrupting the biofilm matrix improves wound healing outcomes. Journal of Wound Care. 2015;24(8):366-71.

21. Beech WB, Sunner J. Biocorrosion: towards understanding interactions between biofilms and metals. Current Opinion in Biotechnology. 2004;15(3):181-6.

22. Martin M, Dragos A, Otto SB, Schafer D, Brix S, Maroti G, et al. Cheaters shape the evolution of phenotypic heterogeneity in Bacillus subtilis biofilms. Isme Journal. 2020;14(9):2302-12.

23. Popat R, Crusz SA, Messina M, Williams P, West SA, Diggle SP. Quorum-sensing and cheating in bacterial biofilms. Proceedings of the Royal Society B-Biological Sciences. 2012;279(1748):4765-71.

24. Wood TK, Knabel SJ, Kwan BW. Bacterial Persister Cell Formation and Dormancy. Applied and Environmental Microbiology. 2013;79(23):7116-21.

25. Fong JNC, Yildiz FH. Biofilm Matrix Proteins. Microbiology Spectrum. 2015;3(2).

26. Khatoon Z, McTiernan CD, Suuronen EJ, Mah TF, Alarcon EI. Bacterial biofilm formation on implantable devices and approaches to its treatment and prevention. Heliyon. 2018;4(12).

27. Stewart PS, Franklin MJ. Physiological heterogeneity in biofilms. Nature Reviews Microbiology. 2008;6(3):199-210.

28. Allison DG. The biofilm matrix. Biofouling. 2003;19(2):139-50.

29. Thibeaux R, Kainiu M, Goarant C. Biofilm Formation and Quantification Using the 96-Microtiter Plate. LEPTOSPIRA SPP: Methods and Protocols. 2020;2134:207-14.

30. Walters MC, Roe F, Bugnicourt A, Franklin MJ, Stewart PS. Contributions of antibiotic penetration, oxygen limitation, and low metabolic activity to tolerance of Pseudomonas aeruginosa biofilms to ciprofloxacin and tobramycin. Antimicrobial Agents and Chemotherapy. 2003;47(1):317-23.

31. Crusz SA, Popat R, Rybtke MT, Camara M, Givskov M, Tolker-Nielsen T, et al. Bursting the bubble on bacterial biofilms: a flow cell methodology. Biofouling. 2012;28(8):835-42.

32. Manner S, Goeres DM, Skogman M, Vuorela P, Fallarero A. Prevention of Staphylococcus aureus biofilm formation by antibiotics in 96-Microtiter Well Plates and Drip Flow Reactors: critical factors influencing outcomes. Scientific Reports. 2017;7.

33. Christensen GD, Simpson WA, Younger JJ, Baddour LM, Barrett FF, Melton DM, et al. ADHERENCE OF COAGULASE-NEGATIVE STAPHYLOCOCCI TO PLASTIC TISSUE-CULTURE PLATES - A QUANTITATIVE MODEL FOR THE ADHERENCE OF STAPHYLOCOCCI TO MEDICAL DEVICES. Journal of Clinical Microbiology. 1985;22(6):996-1006.

34. De Rosa S, Sconza F, Volterra L. Biofilm amount estimation by fluorescein diacetate. Water Research. 1998;32(9):2621-6.

35. Boulos L, Prevost M, Barbeau B, Coallier J, Desjardins R. LIVE/DEAD (R) BacLight (TM): application of a new rapid staining method for direct enumeration of viable and total bacteria in drinking water. Journal of Microbiological Methods. 1999;37(1):77-86.

36. Ramalingam B, Sekar R, Boxall JB, Biggs CA. Aggregation and biofilm formation of bacteria isolated from domestic drinking water. Water Science and Technology-Water Supply. 2013;13(4):1016-23.

37. Kalmbach S, Manz W, Szewzyk U. Dynamics of biofilm formation in drinking water: Phylogenetic affiliation and metabolic potential of single cells assessed by formazan reduction and in situ hybridization. Fems Microbiology Ecology. 1997;22(4):265-79.

38. Mariscal A, Lopez-Gigosos RM, Carnero-Varo M, Fernandez-Crehuet J. Fluorescent assay based on resazurin for detection of activity of disinfectants against bacterial biofilm. Applied Microbiology and Biotechnology. 2009;82(4):773-83.

39. Pantanella F, Valenti P, Frioni A, Natalizi T, Coltella L, Berlutti F. BioTimer Assay, a new method for counting Staphylococcus spp. in biofilm without sample manipulation applied to evaluate antibiotic susceptibility of biofilm. Journal of Microbiological Methods. 2008;75(3):478-84.

40. Pernthaler A, Pernthaler J, Amann R. Fluorescence in situ hybridization and catalyzed reporter deposition for the identification of marine bacteria. Applied and Environmental Microbiology. 2002;68(6):3094-101.

41. Wallace PK, Arey B, Mahaffee WF. Subsurface examination of a foliar biofilm using scanning electron- and focused-ion-beam microscopy. Micron. 2011;42(6):579-85.

42. Alhede M, Qvortrup K, Liebrechts R, Hoiby N, Givskov M, Bjarnsholt T. Combination of microscopic techniques reveals a comprehensive visual impression of biofilm structure and composition. Fems Immunology and Medical Microbiology. 2012;65(2):335-42.

43. Merod RT, Warren JE, McCaslin H, Wuertz S. Toward automated analysis of biofilm architecture: Bias caused by extraneous confocal laser scanning microscopy images. Applied and Environmental Microbiology. 2007;73(15):4922-30.

44. Sandt C, Smith-Palmer T, Pink J, Brennan L, Pink D. Confocal Raman microspectroscopy as a tool for studying the chemical heterogeneities of biofilms in situ. Journal of Applied Microbiology. 2007;103(5):1808-20.

45. Broach JR, Thorner J. High-throughput screening for drug discovery. Nature. 1996;384(6604):14-6.

46. du Plessis A, le Roux SG, Steyn F. Quality Investigation of 3D Printer Filament Using Laboratory X-Ray Tomography. 3d Printing and Additive Manufacturing. 2016;3(4):262-7.

47. Hutmacher DW, Schantz T, Zein I, Ng KW, Teoh SH, Tan KC. Mechanical properties and cell cultural response of polycaprolactone scaffolds designed and fabricated via fused deposition modeling. Journal of Biomedical Materials Research. 2001;55(2):203-16.

48. Beloin C, Roux A, Ghigo JM. Escherichia coli biofilms. Bacterial Biofilms. 2008;322:249-89.

49. Peeters E, Nelis HJ, Coenye T. Comparison of multiple methods for quantification of microbial biofilms grown in microtiter plates. Journal of Microbiological Methods. 2008;72(2):157-65.

50. Wang HZ, Hoiby N, Ciofu O. Pharmacokinetics and Pharmacodynamics of Antibiotics in Biofilm Infections of Pseudomonas aeruginosa In Vitro and In Vivo. Microbial Biofilms: Methods and Protocols. 2014;1147:239-54.

51. Buckingham-Meyer K, Goeres DM, Hamilton MA. Comparative evaluation of biofilm disinfectant efficacy tests. Journal of Microbiological Methods. 2007;70(2):236-44.

52. Benoit MR, Conant CG, Ionescu-Zanetti C, Schwartz M, Matin A. New Device for High-Throughput Viability Screening of Flow Biofilms. Applied and Environmental Microbiology. 2010;76(13):4136-42.

53. Chan LLY, Rice WL, Qiu J. Observation and quantification of the morphological effect of trypan blue rupturing dead or dying cells. Plos One. 2020;15(1).

54. Ommen P, Zobek N, Meyer RL. Quantification of biofilm biomass by staining: Non-toxic safranin can replace the popular crystal violet. Journal of Microbiological Methods. 2017;141:87-9.

55. Hajdu S, Lassnigg A, Graninger W, Hirschl AM, Presterl E. Effects of Vancomycin, Daptomycin, Fosfomycin, Tigecycline, and Ceftriaxone on Staphylococcus epidermidis Biofilms. Journal of Orthopaedic Research. 2009;27(10):1361-5.

56. Hassanpourfard M, Sun XH, Valiei A, Mukherjee P, Thundat T, Liu Y, et al. Protocol for Biofilm Streamer Formation in a Microfluidic Device with Micropillars. Jove-Journal of Visualized Experiments. 2014(90).

57. Liao Y, Zhao H, Lu XL, Yang ST, Zhou JF, Yang RY. Efficacy of Ethanol against Trichosporon asahii Biofilm in vitro. Medical Mycology. 2015;53(4):396-404.

58. Park HS, Ham Y, Shin K, Kim YS, Kim TJ. Sanitizing Effect of Ethanol Against Biofilms Formed by Three Gram-Negative Pathogenic Bacteria. Current Microbiology. 2015;71(1):70-5.

59. Rodgers N, Murdaugh A. Chlorhexidine-induced elastic and adhesive changes of Escherichia coli cells within a biofilm. Biointerphases. 2016;11(3).

60. Vitkov L, Hermann A, Krautgartner WD, Herrmann M, Fuchs K, Klappacher M, et al. Chlorhexidine-induced ultrastructural alterations in oral biofilm. Microscopy Research and Technique. 2005;68(2):85-9.

61. Sauerbrei A. Bactericidal and virucidal activity of ethanol and povidone-iodine. Microbiologyopen. 2020;9(9).

62. Emilson CG. SUSCEPTIBILITY OF VARIOUS MICROORGANISMS TO CHLORHEXIDINE. Journal of Dental Research. 1976;55:D188-D.

63. Zanatta FB, Antoniazzi RP, Rosing CK. Staining and calculus formation after 0.12% chlorhexidine rinses in plaque-free and plaque covered surfaces: a randomized trial. Journal of Applied Oral Science. 2010;18(5):515-21.

64. Thangavelu A, Kaspar S, Kathirvelu R, Srinivasan B, Srinivasan S, Sundram R. Chlorhexidine: An Elixir for Periodontics. Journal of Pharmacy and Bioallied Sciences. 2020;12:57-9.

65. Kuyyakanond T, Quesnel LB. THE MECHANISM OF ACTION OF CHLORHEXIDINE. Fems Microbiology Letters. 1992;100(1-3):211-5.

66. Willis L. FINAL REPORT ON THE SAFETY ASSESSMENT OF CHLORHEXIDINE CHLORHEXIDINE DIACETATE CHLORHEXIDINE DIHYDROCHLORIDE CHLORHEXIDINE DIGLUCONATE. Journal of the American College of Toxicology. 1993;12(3):201-23.

67. MH N. Comparative study of 0.2% and 0.12% digluconate chlorhexidine mouth rinses on the level of dental staining and gingival indices. In: Taheri M MM, et al., editor.: Dental research journal; 2012. p. 305-8.

68. Sajilata MG, Bajaj PR, Singhal RS. Tea polyphenols as nutraceuticals. Comprehensive Reviews in Food Science and Food Safety. 2008;7(3):229-54.

69. Xiong LG, Chen YJ, Tong JW, Huang JA, Li J, Gong YS, et al. Tea polyphenol epigallocatechin gallate inhibits Escherichia coli by increasing endogenous oxidative stress. Food Chemistry. 2017;217:196-204.

70. Guo L, Guo J, Liu HS, Zhang J, Chen XB, Qiu YS, et al. Tea polyphenols suppress growth and virulence-related factors of Haemophilus parasuis. Journal of Veterinary Medical Science. 2018;80(7):1047-53.

71. von Martius S, Hammer KA, Locher C. Chemical characteristics and antimicrobial effects of some Eucalyptus kinos. Journal of Ethnopharmacology. 2012;144(2):293-9.

72. Dong GF, Liu HY, Yu X, Zhang XX, Lu H, Zhou TL, et al. Antimicrobial and anti-biofilm activity of tannic acid against Staphylococcus aureus. Natural Product Research. 2018;32(18):2225-8.

73. Borges A, Saavedra MJ, Simoes M. The activity of ferulic and gallic acids in biofilm prevention and control of pathogenic bacteria. Biofouling. 2012;28(7):755-67.

74. Luis A, Silva F, Sousa S, Duarte AP, Domingues F. Antistaphylococcal and biofilm inhibitory activities of gallic, caffeic, and chlorogenic acids. Biofouling. 2014;30(1):69-79.

75. Chambers SA, Gaddy JA, Townsend SD. Synthetic Ellagic Acid Glycosides Inhibit Early Stage Adhesion of Streptococcus agalactiae Biofilms as Observed by Scanning Electron Microscopy. Chemistry-a European Journal. 2020;26(44):9923-8.

76. Hancock V, Dahl M, Vejborg RM, Klemm P. Dietary plant components ellagic acid and tannic acid inhibit Escherichia coli biofilm formation. Journal of Medical Microbiology. 2010;59(4):496-8.

77. Lee JH, Park JH, Cho HS, Joo SW, Cho MH, Lee J. Anti-biofilm activities of quercetin and tannic acid against Staphylococcus aureus. Biofouling. 2013;29(5):491-9.

78. Wang XQ, Yao X, Zhu ZA, Tang TT, Dai KR, Sadovskaya I, et al. Effect of berberine on Staphylococcus epidermidis biofilm formation. International Journal of Antimicrobial Agents. 2009;34(1):60-6.

79. Sun T, Li XD, Hong J, Liu C, Zhang XL, Zheng JP, et al. Inhibitory Effect of Two Traditional Chinese Medicine Monomers, Berberine and Matrine, on the Quorum Sensing System of Antimicrobial-Resistant Escherichia coli. Frontiers in Microbiology. 2019;10.

80. Francolini I, Norris P, Piozzi A, Donelli G, Stoodley P. Usnic acid, a natural antimicrobial agent able to inhibit bacterial biofilm formation on polymer surfaces. Antimicrobial Agents and Chemotherapy. 2004;48(11):4360-5.

81. Shang XF, Miao XL, Lv HP, Wang DS, Zhang JQ, He H, et al. Acaricidal activity of usnic acid and sodium usnic acid against Psoroptes cuniculi in vitro. Parasitology Research. 2014;113(6):2387-90.

82. Sun B, Luo HZ, Jiang H, Wang ZN, Jia AQ. Inhibition of Quorum Sensing and Biofilm Formation of Esculetin on Aeromonas Hydrophila. Frontiers in Microbiology. 2021;12.

83. He ZY, Jiang W, Jiang YT, Dong JC, Song ZC, Xu JR, et al. Anti-biofilm activities of coumarin as quorum sensing inhibitor for Porphyromonas gingivalis. Journal of Oral Microbiology. 2022;14(1).

84. Lee JH, Kim YG, Cho HS, Ryu SY, Cho MH, Lee J. Coumarins reduce biofilm formation and the virulence of Escherichia coli O157:H7. Phytomedicine. 2014;21(8-9):1037-42.

85. Dasgupta Q, Madras G, Chatterjee K. Controlled Release of Usnic Acid from Biodegradable Polyesters to Inhibit Biofilm Formation. Acs Biomaterials Science & Engineering. 2017;3(3):291-303.